CHALMERS

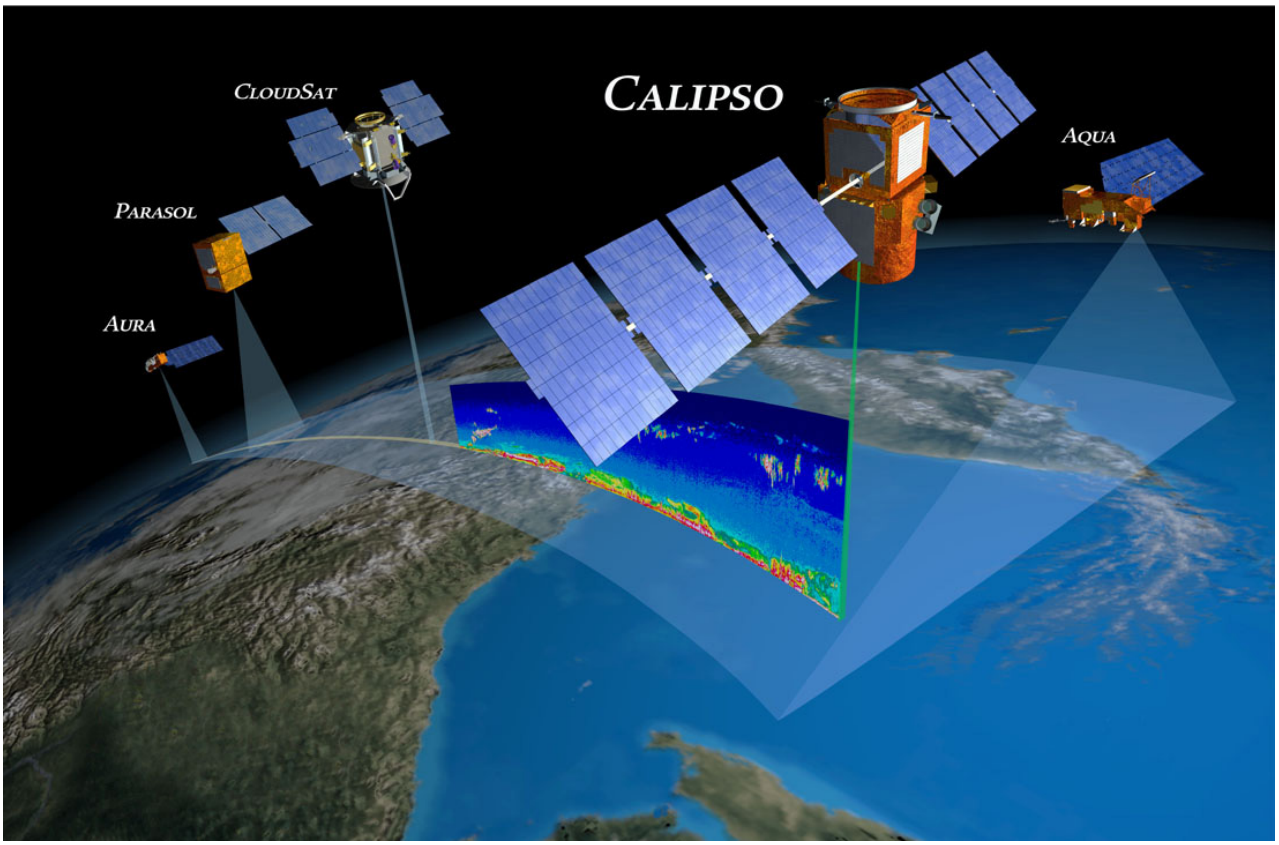


# Use of CALIOP satellite data to explore the distribution and sources of organic aerosols in the troposphere

*Master's thesis in Earth and Space Sciences*

SYLVAIN PETIOT

Department of Earth and Space Sciences
*Global Environmental Measurements and Modelling*
CHALMERS UNIVERSITY OF TECHNOLOGY
Gothenburg, Sweden 2012
Master's thesis 2012

MASTER'S THESIS IN EARTH AND SPACE SCIENCES

# Use of CALIOP satellite data to explore the distribution and sources of organic aerosols in the troposphere

SYLVAIN PETIOT

Department of Earth and Space Sciences
*Global Environmental Measurements and Modelling*
CHALMERS UNIVERSITY OF TECHNOLOGY

Gothenburg, Sweden 2012

Use of CALIOP satellite data to explore the distribution and sources of organic aerosols in the troposphere
SYLVAIN PETIOT



Master's thesis 2012
ISSN 1652-8557
Department of Earth and Space Sciences
Global Environmental Measurements and Modelling
Chalmers University of Technology
SE-412 96 Gothenburg
Sweden
Telephone: +46 (0)31-772 1000

Cover:
The satellite CALIPSO part of the constellation "A-train" with the satellites Aqua, Aura, CloudSat and Parasol.

Chalmers Reproservice
Gothenburg, Sweden 2012

Use of CALIOP satellite data to explore the distribution and sources of organic aerosols in the troposphere
Master's thesis in Earth and Space Sciences
SYLVAIN PETIOT
Department of Earth and Space Sciences
Global Environmental Measurements and Modelling
Chalmers University of Technology

## Abstract

Aerosols have been identified as a contributor to the Earth's radiative budget. Aerosol emissions from human activities play a role at least as important as for the greenhouse gases. Their role is even more important that their global effect is opposite to the one of greenhouse effects: aerosols tend to cool down the atmosphere. Given that little scientific attention has been put on the topic, many uncertainties remain. That is why many instruments have been developed these last years to improve our understanding on aerosols. One of them, the satellite Calipso has onboard the instrument Caliop providing unique measurements of the vertical distribution of aerosols.

The aim of this thesis was to look at the spatial and vertical distribution across the globe of one specific type of aerosols: the organic aerosols. Combining observations from Caliop and model predictions, through different algorithms written in MatLab, led to estimations on organic aerosol contribution to the total optical depth, as well as vertical profiles of extinction coefficients.

What came out of this work is a good representation of the contribution of organic aerosols to the total optical depth around the world. Moreover contrary to what was expected, no recurrent seasonal pattern, nor similarity in the extinction vertical distribution were identified. However, it was also showed that the Emep aerosol model, used as the unique source of information about organic aerosols, can be improved as regarding the satellite data. Furher investigation in this direction could therefore lead to more accurate information on organic aerosol in terms of spatial and vertical distribution.

Keywords: CALIPSO, CALIOP, EMEP, organic aerosols, vertical distribution.

## Acknowledgements

First of all, I would like to thank Patrick Eriksson without whom I would not have had the opportunity to realize this work within the Earth and Space Sciences department.
I would like to acknowledge the Norwegian Meteorological Institute MET.NO for allowing me to use their resources, and especially Michael Schulz who provided a great help and Svetlana Tsyro who gave me precious information as regarding the EMEP model.
I would like to thank Abdulla Sakalli, working at the Global Environmental Measurements and Modelling group, who greatly helped me to adapt myself in this new working environment.
I would also like to thank Abhay Devasthale from the Swedish Meteorological and Hydrological Institute, who devoted time and shared his knowledge increasing greatly the quality of my work.
Eventually, I would dedicate a special thank to my supervisor, David Simpson. He always supported me and made his best to make my work go as good as possible. Thanks to him, I gained experience and broader knowledge from a new environment and new people.

# Contents

# 1 Introduction

The Earth's *Global Warming* effect due to increasing emissions and concentrations of greenhouse gases in the atmosphere has been the subject of intense research and controversies for the last twenty years. But it also became apparent that aerosols play a major role on the Earth's radiative budget. This phenomenon is even more important given that the radiative forcing due to aerosols would be the same order of magnitude as the one due to greenhouse gases but opposite in sign. This *cooling effect* likely counterbalances to some extent the so well-known *Global Warming* (Charlson et al. 1992).

However, the influence of aerosols has received much less scientific -and media- attention than greenhouse gases. An important research effort has therefore been put on aerosols during the last decade, especially because the word *aerosol* encompasses a wide range of species and involves a multitude of chemical reactions. Thus models have been developed in order to improve our knowledge on aerosols. However the relevancy of model predictions is easily questionable due to the high uncertainties related to the emissions of aerosols and their precursors. Only few species, like $SO_4$, are indeed reasonably well-known. Observations are therefore of high relevance, that is why instruments were also designed and are now in operation to measure aerosol properties. One of them, the Cloud-Aerosol Lidar with Orthogonal Polarisation (Caliop) onboard the satellite CALIPSO, launched in 2006, provides unique measurements of the vertical distribution of aerosols.

This thesis aims at using these satellite data to get a better understanding of organic aerosols (OA) in terms of vertical distribution. More precisely, the goal is to look at:

- The distribution of organic aerosols across the globe and their temporal evolution over the year. It is expected to identify seasonal trends according to their sources, both anthropogenic and biogenic. More preceisely, biogenic organic aerosols have a strong seasonal dependence (see section 2.1.4), so that forest areas, for example, are expected to experience a greater influence from organic aerosols during the "summertime". The figure 1.0.1 below shows the time evolution of the optical depth in 2009 in Amazonia[1] computed by the Emep mode[2]: the optical depth increase during the months of June, July and August is clearly due to organic aerosols.

- The consistency of these satellite-derived data with other observations. Thus, the available data considered for comparison were from the ground-based sunphotometer network, Aeronet, and from the Moderate Resolution Imaging Spectrometers (MODIS) onboard satellites.

- The consistency of the EMEP aerosol model with these data.

However, since the data provided by CALIOP are unique, the comparison with other observations could not be made in terms of vertical profile, but only in terms of optical depth, which in one way do not ensure the quality of the Caliop data.

Furthermore, looking at organic aerosols from satellite data assumes to define a spatial resolution. Thus the world was divided into $5° \times 5°$ areas. A few number of them were selected to be representative of different aerosol contributions. In these areas, the optical depth evolution as well as the vertical distribution were looked at. Therefore a wider analysis, performed in more areas and on a different spatial resolution, should be done to confirm the conclusions drawn in this thesis.

[1] see section 4.1 for more information about the area under study.
[2] see section 3.4 for more information about the Emep model.

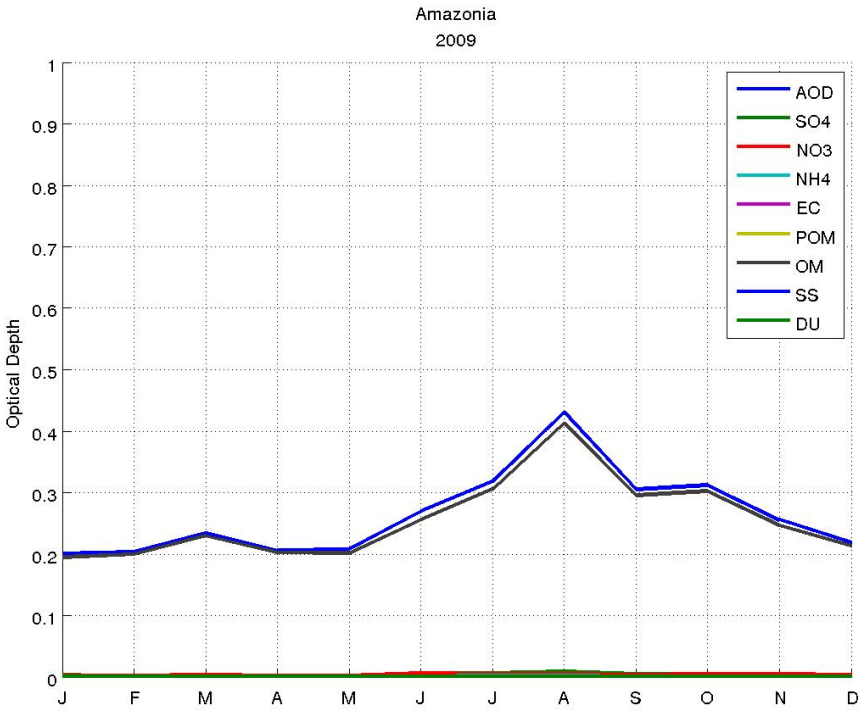


Figure 1.0.1: *Temporal evolution of the optical depth and aerosol contributions along the year 2009 in Amazonia according to the EMEP model.*

# 2 Theoretical Background

## 2.1 Aerosols Properties

### 2.1.1 Definition

An aerosol is generally defined as a suspension of liquid or solid particles in a gas, with particle diameters ranging from $10^{-9}$ m to $10^{-4}$ m (Poschl 2005). Clouds are examples of aerosols, they mainly consist of condensed water with particle diameters in the range of $10\mu$m. However, in atmospheric science, clouds are considered as a separated phenomena from aerosols.

The main parameter charecterizing aerosols is their size. The size classification is simplified if a spherical shape is assumed; therefore the "size" of an aerosol corresponds to its aerodynamical radius. The classification is divided into two modes:

- The coarse mode: $d_{particle} > 1\ \mu$m
- The fine mode: $d_{particle} < 1\ \mu$m

In the troposphere, the total particle number and mass concentration typically vary in the range of about $10^2$-$10^5$ cm$^{-3}$ and 1-100 $\mu$g m$^{-3}$, respectively.

Aerosols are usually divided into eight categories: sulfate, nitrate, ammonium, sea salt, mineral dust, organic compounds, and black or elemental carbon.

### 2.1.2 Aerosol Sources

Atmospheric aerosols originate from both natural and anthropogenic sources.

Mineral dust comes from the wind erosion of soils that occur when the wind speed exceeds a threshold value. However only particles with a radius smaller than 100 $\mu$m remain airborne, the others are quickly removed by gravitation.

Sea salts come either from the wind force at the sea surface lifting up particles, in a similar way as dust aerosols, or from bubbles bursting at the surface. The airborne particles have the same sea salt content as the sea water, that is to say 3.5% of which 85% is NaCl. As the sea water particles are lifted up, they dry until their water content is in equilibrium with the surrounding environment.

A wide and complex chemistry of gas to particle conversion engenders a multitude of aerosol compounds. The atmospheric gas phase reactions lead to the formation of condensable products. The oxidation of $SO_2$ to $H_2SO_4$ is one predominant reaction occuring in the gas phase:

$$\begin{gathered} OH + SO_2 = HOSO_2 \\ HOSO_2 + O_2 = SO_3 + HO_2 \\ SO_3 + H_2O = H_2SO_4 \end{gathered}$$

Thus the huge amounts of $SO_2$ released by volcanoes are oxidised into $H_2SO_4$.

Forest fires is one of the main sources of organic aerosols. The combustion process is made of three steps (Thunman 2012):

- The drying phase during which the fuel is dried.
- The devolatilisation phase during which volatiles, held in the fuel, are released.
- The char combustion.

Finally the char residue is exposed to wind erosion leading to additional carbonaceous material in the atmosphere. Production rates of smoke particles range from 5 to 50 g/kg depending on the type of fire and the smoke particle size is in the submicrometer range.

Biogenic particles are also released from plants (seeds, pollen, spores, leaf waxes, resins) with a size range of 1 to 250 $\mu$m.

### 2.1.3 Aerosol sinks

Different removal processes of aerosols from the atmosphere exist depending on their physical behavior. Such a process is called a *sink*.

Coagulation occurs when particles collide and produce a new larger particle. Fine particles are mainly removed by coagulation, depending on their mobility. The lifetime of a fine particle is proportionnal to its radius at the power of two.

Condensation is the deposition of vapors on particulate matter whether it is water of volatile organic compounds. If there is no preexisting particle, condensation leads to new fine particles.

Deposition is the main sink of atmospheric aerosol particles. Wet deposition occurs when aerosols are removed from the atmosphere with precipitation. 0.1 to 10 $\mu$m particles are mainly removed by wet precipitation. Dry deposition corresponds to transport, diffusion, and adhesion to the Earth's surface. This latter phenomenon is less important on a global scale, but is highly relevant with respect to local air pollution, health effects and the soiling of buildings and cultural monuments.

Sedimentation is the downward motion resulting from gravitationnal settling. It is predominant for particles whose size is greater than 10 $\mu$m. However mineral dust deposited on continental soils remains subjected to resuspension in the atmosphere by wind erosion contrary to mineral dust deposited on ocean surfaces which is irretrievably lost and forms deep-sea sediments.

The atmospheric residence times of aerosols can vary from hours to weeks, depending on their size (Poschl 2005).

### 2.1.4 Carboneceous Aerosol Components

Carbonaceous aerosol components account for a large fraction of air particulate matter, exhibit a wide range of molecular structures, and have a strong influence on the physicochemical, biological, climate- and health-related properties, and effects of atmospheric aerosols.

Traditionally the total carbon (TC) content of air particulate matter is defined as the sum of all the carbon contained in the particles, except in the form of inorganic carbonates. TC is usually divided into an organic carbon (OC) fraction and a black carbon (BC) - or elemental carbon (EC) - fraction, such as: TC = OC + BC.

The BC - or EC - is a substance consisting of polymeric carbonaceous materials formed by the incomplete hydrocarbon combustion or pyrolysis. Black or elemental carbon accounts for most of the light absorption by atmospheric aerosols and is therefore of crucial importance for the direct radiative effect of aerosols on climate (Poschl 2005).

#### Primary and Secondary Organic Aerosol Components

The sum of organic aerosol (OA) components, is usually estimated by multiplication the organic carbon by a factor of about 1.5/2 depending on the assumed average molecular composition and accounting for the contribution of elements other than carbon contained in organic substances (H, O, N, S...).

Depending on their origin, OA components can be classified as primary or secondary. Primary organic aerosol (POA) components are directly emitted in the condensed phase (liquid or solid particles) or as semivolatile vapors, which are condensable under atmospheric conditions.

The main sources of POA particles and components are natural and anthropogenic biomass burning (forest fires, slashing and burning, domestic heating), fossil-fuel combustion (domestic, industrial, traffic), and wind-driven or traffic-related suspension of soil and road dust, biological materials (plant and animal debris, microorganisms, pollen, spores, etc.), sea spray, and spray from other surface waters with dissolved organic compounds.

Secondary organic aerosol (SOA) components are formed by chemical reactions and gas-to-particle conversions of volatile organic compounds (VOCs) in the atmosphere.

The principal parameters governing secondary particle formation are temperature, relative humidity and the concentrations of organic and inorganic nucleating and condensing vapors which depend on atmospheric transport, local sources as well as sinks such as photochemistry and preexisting oxidants. In particular, biogenic emissions increase exponentially with temperature. Thus they have a strong **seasonal dependence**.

Depending on local sources, meteorological conditions, and atmospheric transport and thus on location, season, and time of day, the composition of organic matter can be dominated by POA or SOA components.

However, the reaction mechanisms involved in atmospheric chemistry, especially for aerosol formation, are numerous and complex. Reaction mechanisms and kinetics have been elucidated and fully characterized only for a small number of model reaction systems and components. Therefore, the current aerosol distribution models have difficulties to fit with current observations (Poschl 2005).

## 2.2 Radiation theory

### 2.2.1 Black Body Radiation

#### The Planck's law

A black body is an idealized physical body that absorbs all incident electromagnetic radiation, regardless of frequency or angle of incidence.

A black body in thermal equilibrium, that is to say at a constant temperature, emits an electromagnetic radiation called black-body radiation defined by the Planck's law:

$$B(\lambda, T) = \frac{2hc^2}{\lambda^5}[\exp(\frac{hc}{\lambda k_B T}) - 1]^{-1} \tag{2.2.1}$$

Different quantities can be derived from the Planck function, especially the Wien's displacement law and the Stefan-Boltzmann law.

The Wien's displacement law characterizes the wavelength of the peak of emission, $\lambda_{max}$, as a function of the temperature:

$$\lambda_{max} = \frac{A}{T} \tag{2.2.2}$$

with A $\approx 2.9 \cdot 10^{-3}$ Km, so that the peak of emission of a black-body in thermal equilibrium at 5800 K is reached for $\lambda = 0.5$ $\mu$m.

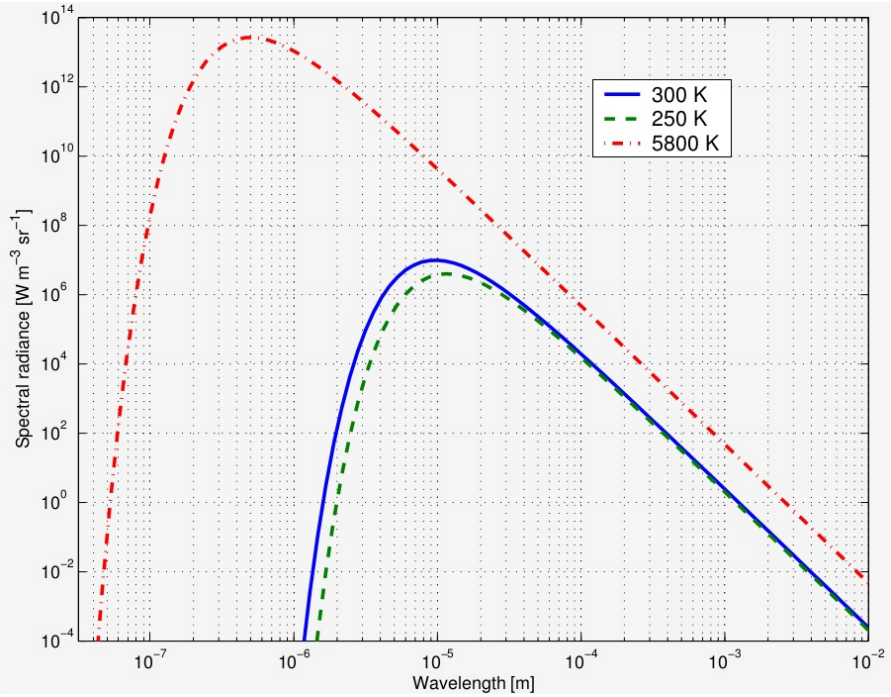


Figure 2.2.1: *Radiation of a black body in thermal equilibrium at three different temperatures (Eriksson 2012).*

The Stefan-Boltzmann law characterizes the outgoing power of a black body, M, as a function of the temperature such as:

$$M = \sigma \cdot T^4 \tag{2.2.3}$$

$$\sigma = 5.67 \cdot 10^{-8}\ \mathrm{Js^{-1}m^{-2}K^{-4}}$$

**Other Definitions**

As previously said, a black body is an *idealized* physical body. However, most physical objects, including the Sun, the Earth, can be approached by a "grey body" whose spectral emission differs from the black-body radiation by a factor $\epsilon(\lambda)$ called emissivity such as:

$$I(\lambda, t) = \epsilon(\lambda) \cdot B(\lambda, t) \tag{2.2.4}$$

The brightness temperature of a "grey body", $T_b$, is defined as the temperature of the equivalent blackbody that would emit the same radiation $I(\lambda)$ as the "grey body" that is to say $I(\lambda, T) = B(\lambda, T_b)$. Two different versions exist:

- The Planck's law leads to:

$$T_b = \frac{hc}{\lambda k_B ln(\frac{2hc^2}{\lambda^5 I} + 1)} \tag{2.2.5}$$

- The Rayleigh-Jeans approximation, valid when $\mathrm{hc}/\lambda k_B \mathrm{T} \ll 1$, is:

$$T_b = \frac{\lambda^4 I(\lambda)}{2k_B c} \Rightarrow T_b = \epsilon \cdot T \tag{2.2.6}$$

Finally the Kirchhoff's law of radiation sets that a body at thermodynamic equilibrium has an emissivity, $\epsilon$, equals to its absorptivity, $\alpha$:

$$\alpha = 1 - r = \epsilon \tag{2.2.7}$$

where r is the reflectivity.

**Characteristics of the solar radiation**

With an effective temperature of 5800 K and an emissivity of 0.99 the Sun's radiant exitance, integrated over all the wavelengths, is:

$$\mathrm{M} = \sigma\ \mathrm{T}^4 = 6.35 \cdot 10^7\ \mathrm{Wm}^{-2}$$

The total power radiated by the Sun is obtained by multiplying this quantity by the Sun's surface area:

$$\mathrm{P} = 4\pi\ \mathrm{r}^2\sigma\ \mathrm{T}^4 = 3.87 \cdot 10^{26}\ \mathrm{W}$$

Considering a sphere of radius D, corresponding to the distance Sun-Earth, centred on the Sun, the irradiance at the top of the Earth's atmosphere is:

$$\mathrm{E} = \frac{P}{4\pi D^2} = 1.37 \cdot 10^3\ \mathrm{Wm}^{-2}$$

This value is often called the *mean exoatmospheric irradiance*. With geometric considerations, it can be deduced that this value is divided by a factor of 4 at the ground level if the solar radiation is assumed to be equally distributed. So that the average solar radiation irrading the Earth's surface is $\mathrm{E}_{\mathrm{surface}} = 340\ \mathrm{Wm}^{-2}$.

### 2.2.2 Radiative transfer theory

**Absorption and Scattering**

The particles in the atmosphere interfere with the incoming solar radiation in two different ways: absorption and scattering.

Scattering is characterized by the size parameter, x:

$$x = \frac{\pi \cdot d}{\lambda} \tag{2.2.8}$$

where d is the particle diameter.

The range of x determines the kind of scattering occuring and the approach to follow for calculations:

- $\mathrm{x} \ll 1$ refers to Rayleigh Scattering
- $\mathrm{x} \approx$ refers to Mie Scattering
- $\mathrm{x} \gg 1$ refers to Geometrical Scattering

The efficiencies to scatter and to absorb depend on the scattering regime considered. For visible wavelengths, aerosols are mainly found in the Mie regime.

Thus, as a main result the solar radiation coming to the Earth is attenuated by these two phenomena.

**Radiative Transfer Equation**

The attenuation of the spectral radiance along the propagation path is given by the radiative transfer equation:

$$\frac{dI}{dl} = -(\gamma_a + \gamma_s)I + S \tag{2.2.9}$$

where $I$ is the spectral radiance [$\mathrm{Wm}^{-2}\mathrm{Hz}^{-1}\mathrm{sr}^{-1}$], $l$ is the length along the propagation path [m], $\gamma_a$ is the absorption coefficient [$\mathrm{m}^{-1}$], $\gamma_s$ is the scattering coefficient [$\mathrm{m}^{-1}$], $S$ is the total source including both emission and scattering [$\mathrm{Wm}^{-3}\mathrm{Hz}^{-1}\mathrm{sr}^{-1}$]

The integral of the extinction coefficient along the propagation path between the altitudes $\mathrm{z}_0$ and z is called the **optical depth**, $\tau$ such as:

$$\tau(\lambda, z_0, z) = \int_{z_0}^{z} \gamma(\lambda, l)\mathrm{d}l \tag{2.2.10}$$

where $\gamma$ is the total **extinction coefficient**, $\gamma = \gamma_a + \gamma_s$.

The absorption, (resp. scattering), coefficient is the product of the absorption, (resp. scattering) cross-section, $\sigma_a$ (resp. $\sigma_s$) , times the number of particles, $N$:

$$\begin{aligned} \gamma_a &= N\sigma_a \\ \gamma_s &= N\sigma_s \end{aligned} \tag{2.2.11}$$

Derived from the optical depth, the transmission, $t$ is defined as:

$$t = e^{-\tau} \tag{2.2.12}$$

The equation (2.2.9) can be easily solved for specific cases. For instance, assuming no scattering, that is to say $\gamma_s = 0$ and assuming that $z_0 = 0$, then (2.2.9) becomes:

$$\frac{dI}{dl} = \gamma_a(B - I) \Rightarrow I_z = I_0 \cdot e^{-\tau} + \int_0^z \gamma_a(l) \cdot B(l) \cdot e^{-\tau(\lambda,0,l)} \mathrm{d}l \tag{2.2.13}$$

where $\gamma_a(l)B(l)$ is the emission at point $l$, $\tau = \tau(\lambda, 0, z)$ and $e^{-\tau(\lambda,0,l)}$ is the transmission between the point $l$ and the observation points.

### 2.2.3 Models for surface observations

With the previous definitions, it is possible to define and characterize simple models for surface observations from an "active" instrument, like Caliop.

One example of such a model is depicted on the sketch (2.2.2).

In this model, the radiation emitted by the instrument is the only one considered, neglecting the solar radiation, the atmospheric radiation and the Earth radiation. So that, the atmosphere, considered as a single layer, is only characterized by an optical depth, $\tau_a$ and the surface is only characterized by a reflection coefficient, $r_E$.

The instrument (Caliop) will therefore measure the backscattered radiation, that is to say the radiation emitted and reflected from the Earth. Assuming a brightness temperature, $T_{sat}$, of the radiation emitted by the instrument, with the Rayleigh-Jeans approximation, the backscattered radiation measured is:

$$T_{back-scattered} = T_{sat} e^{-2\tau_a} r_E \tag{2.2.14}$$

From the backscattered radiation, it is therefore possible to retrieve the reflection coefficient, $r_E$, and the optical depth, $\tau_a$, if two measurements are performed at two different wavelengths.

## 2.3 Aerosols and Radiative Forcing

According to the IPCC (Climate Change 2007: Synthesis Report), "radiative forcing is a measure of the influence a factor has in altering the balance of incoming and outgoing energy in the Earth-atmosphere system and is an index of the importance of the factor as a potential climate change mechanism".

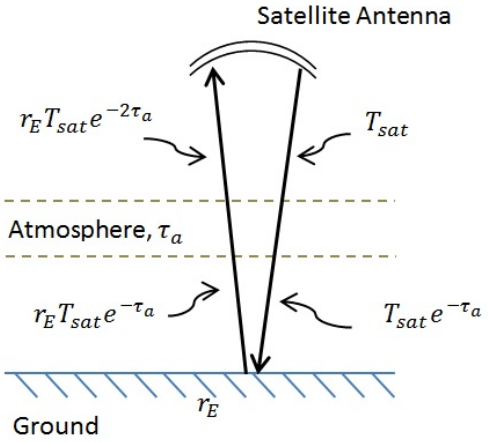


Figure 2.2.2: *Example of a model that can be used for surface observations.*

From the anthropogenic radiative forcing, $\Delta F$, it is possible to estimate the global mean surface temperature change due to human activities, $\Delta T$, calculated as:

$$\Delta F = \frac{\Delta T}{\lambda} \tag{2.3.1}$$

where $\lambda$ is the climate sensitivity with a typical value of 0.8 $\mathrm{KW}^{-1}\mathrm{m}^2$.

Aerosols have been identified as having an important -direct and indirect- influence on the Earth's radiative budget. The direct radiative influence refers to scattering and absorption while the indirect effect refers especially to the influence of aerosols on cloud radiative properties. More precisely, the figure (2.3.1) illustrates the distinction between direct and indirect aerosol effects as well as some major feedback loops in the climate system (Poschl 2005).

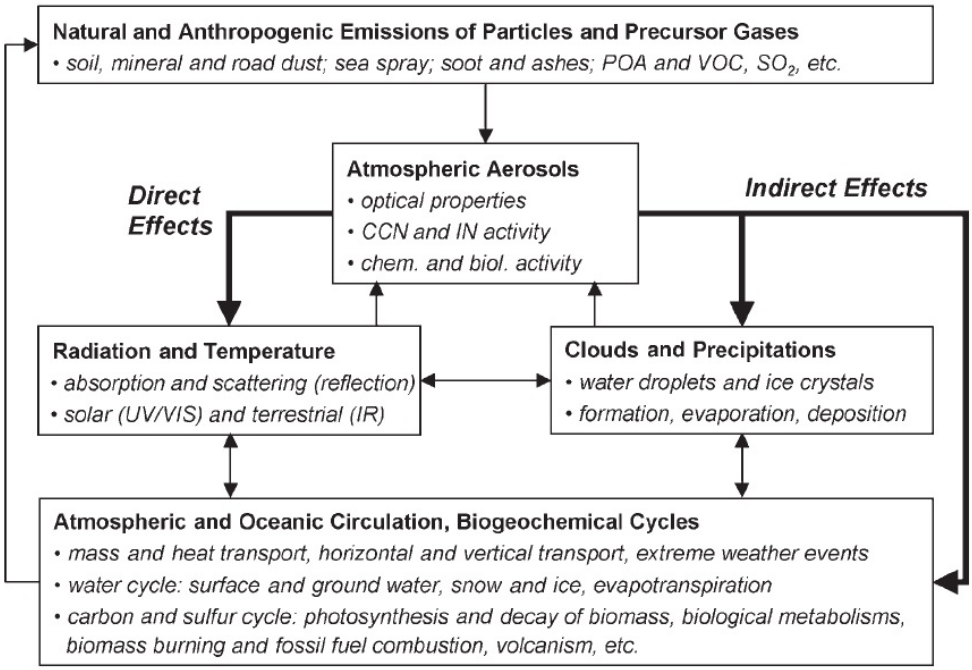


Figure 2.3.1: *Direct and indirect aerosol effects and major feedback loops in the climate system (Poschl 2005).*

The feedback loops involve the interaction of aerosols with solar and terrestrial radiations, clouds and precipitation, general circulation and hydrological cycle. On microscopic and molecular scales, each of the interactions outlined in figure (2.3.1) encompasses a multitude of physiochemical processes that depend on atmospheric composition and meteorological conditions that are largely not quantitatively characterized. Thus the natural climate system responses and feedbacks to natural and anthropogenic emissions are highly uncertain so that in many cases, the direction of the feedbacks is not even known.

The uncertainties of aerosol, cloud and precipitation interactions and feedback effects are among the main reasons for the high uncertainty of climate sensitivities and for the projected global mean surface temperature increase over the next century.

### 2.3.1 Direct Radiative Influence

Aerosol particles influence the Earth's radiative balance by reflecting directly back to space and absorbing shortwave solar radiation. Longwave radiation is also absorbed but the resulting effect remains small.

Charlson et al. (1992) showed that the aerosol direct radiative forcing, $\Delta F_{aer}$, is a function of the perturbation in the planetary mean albedo due to enhanced aerosol, $\Delta R_{aer}$, such as:

$$\Delta F_{aer} = -\frac{1}{4} E (1 - \alpha_C) \Delta R_{aer} \tag{2.3.2}$$

where $E$ is the irradiance at the top of the atmosphere [$\mathrm{Wm}^{-2}$], $\alpha_C$ is the cloud coverage [%].

And the perturbation in the planetary mean albedo cen expressed as a function of the aerosol optical depth, $\delta_{aer}$, such as:

$$\Delta R_{aer} = 2t^2(1 - R_S)^2\beta\delta_{aer} \tag{2.3.3}$$

where $t$ is the transmission of the atmosphere layer above the aerosol layer; $R_S$ is the mean albedo of the underlying surface: $\beta$ is the fraction of the radiation scattered upward by the aerosol

Combining the equations (2.3.2) and (2.3.3) leads to the following expression of the aerosol radiative forcing:

$$\Delta F_{aer} = -\frac{1}{2}Et^2(1 - \alpha_C)(1 - R_S)^2\beta\delta_{aer} \tag{2.3.4}$$

The aerosol radiative forcing depends therefore linearly on the aerosol optical depth.

The negative sign denotes that the forcing represents a cooling tendency opposite to the *global warming*. The current estimates of the aerosol radiative forcing directly derived from the equation (2.3.4) are about -1 $\mathrm{Wm}^{-2}$, uncertain to a factor 2. According to the equation (2.3.1), this radiative forcing leads to a temperature change of about -0.8°C.

### 2.3.2 Indirect Radiative Influence

In the lower part of the atmosphere, cloud droplets form on existing aerosol particles. The physical and chemical properties of the aerosols on which cloud droplets are formed directly influence the concentration and the size of the droplets which affect the shortwave radiative properties of the clouds despite the absence of any influence on the macroscopic and thermodynamic properties of the clouds.

Furthermore, a decrease in the mean droplet size combined with an increase of the cloud-droplet concentration tends to increase the cloud lifetime which associated with the resultant increase of the cloud cover leads to an increase of the short and longwave radiative influence of clouds.

However, since additional phenomena have also to be taken into account, the total indirect effect is difficult to quantify. The review article by Lohmann and Feichter (2005) estimates the total indirect effect to be between -1 $\mathrm{Wm}^{-2}$ and -2 $\mathrm{Wm}^{-2}$ .

# 3 Data Sets

All the data used in this thesis are part of the observations and models gathered within the AEROCOM project. This project is an open international initiative of scientists interested in the advancement of the understanding of the global aerosol and its impact on climate. A large number of observations (including MODIS, POLDER, MISR, AVHHR, SEAWIFS, TOMS, AERONET, etc) and results from more than 14 global models have been gathered and assembled to document and compare state of the art modeling of the global aerosol (Aerocom, website).

## 3.1 Introduction to Caliop

### 3.1.1 General Description

The Cloud-Aerosol Lidar and Infrared Pathfinder Satellite Observations, (CALIPSO) was launched on April 2006 with three instruments on board: the Cloud-Aerosol Lidar with Orthogonal Polarisation (Caliop), the Wide Field Camera (WFC) and the Imaging Infrared Radiometer (IIR). Part of the satellite constellation called 'A-train' composed of the satellites Aura, Parasol, Cloudsat and Aqua (see Fig. 3.1.1), at an altitude of about 705 km, it has a sun-synchronous polar orbit with an inclination of 98.2° which allows a large coverage from 82°S to 82°N with a 16-day cycle.

### 3.1.2 Characteristics of Caliop

Caliop is the first lidar optimized for aerosols and cloud measurements and also the first polarized lidar in space. Its Nd:YAG laser operates at two wavelengths, $\lambda = 532$ nm and $\lambda = 1064$ nm and measures the detailed vertical distribution of aerosols and clouds based on their microphysical and optical properties. It performs measurements every 30 minutes, near-simultaneously with the observations of the instruments MODIS, AIRS and CERES in the 'A-train', with a vertical resolution of 70 m and a horizontal resolution of 333 m.

More precisely, Caliop measures the backscattered radiation coming from the earth/atmosphere system. The extinction coefficients, $b_{ext}(\lambda, z)$, and therefore the optical depth, $\tau(\lambda)$, measured by Caliop, take into account absorption and scattering in all directions. Retrieving optical depths and extinction profiles from the Caliop measurements requires an estimate of the extinction-to-backscatter ratio, called lidar ratio. These estimates are based on a-priori information depending on the type and subtype of the layer analyzed for both

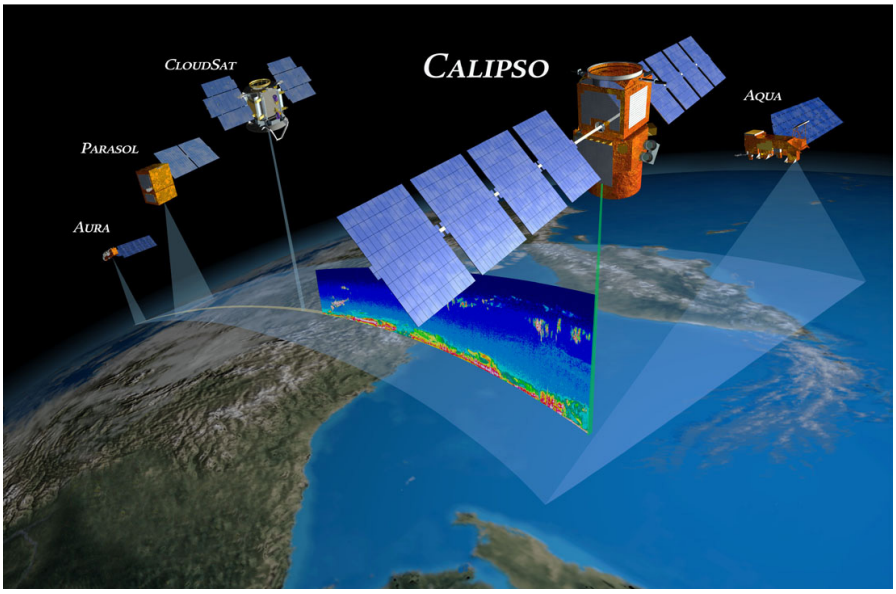


Figure 3.1.1: *The satellite CALIPSO part of the constellation 'A-train'*

wavelengths considered (see Table 3.1.1). Moreover the Caliop extinction retrieval algorithm includes some error-correcting mechanisms that adjust the initial estimate of the lidar ratio to a more suitable value (NASA, website). However, even if the Caliop instrument performs precise backscatter coefficient measurements, the optical depth retrievals are subjected to inherent uncertainties due to these estimates of the lidar ratio which makes the Caliop optical depth data set of lower reliability compared to 'direct' measurements of the extinction coefficients as performed by ground-based platforms like the Aerosol Robotic Network for instance.

| **Type** | **Subtype** |
|---|---|
| Cloud | Water |
| | Ice |
| Aerosol | Marine |
| | Desert Dust |
| | Polluted Continental |
| | Clean Continental |
| | Polluted Dust |
| | Biomass Burning |
| Stratospheric | All |

Table 3.1.1: Type and subtype of the layers on which the estimates of the lidar ratio at $\lambda = 532$ nm and $\lambda = 1064$ nm are based on.

### 3.1.3 The Caliop dataset

The Calipso product is based on the location of layers within the atmosphere, the discrimination of aerosol layers from clouds and an estimation of the optical depth of each layer detected (Schuster et al. 2012).

The quality of the Caliop data is a function of the Cloud/Aerosol Discrimination score (CAD score) which provides a numerical confidence level for the discrimination of layers by the Caliop cloud-aerosol discrimination algorithm.

The standard CAD score ranges between -100 and 100. The sign of the CAD score indicates the feature type: positive values signify clouds, whereas negative values signify aerosols. The absolute value of the CAD score provides a confidence level for the classification. The larger the magnitude of the CAD score, the higher the confidence that the classification is correct, so that:

- High confidence = $|\text{CAD score}| \geq 70$
- Medium confidence = $50 \leq |\text{CAD score}| < 70$
- Low confidence = $20 \leq |\text{CAD score}| < 50$
- No confidence = $|\text{CAD score}| < 20$

And an absolute value of 100 therefore indicates complete confidence (NASA, website).

The Caliop data treated by AEROCOM are differenciated into two categories: clear sky and all sky. The clear-sky conditions are identified as the total absence of cloud layers, that is to say a CAD score equals to 100 while the all-sky conditions are identified as measurements performend with a CAD score higher than 50 (Koffi et al. 2012).

Therefore given the range of confidence listed previously, only clear-sky data have been used in this study. The Caliop data are available from June 2006 to August 2011, however in order to allow the comparison with the other datasets, only the data from 2006 to 2010 have been considered in this study.

## 3.2 Introduction to AERONET

### 3.2.1 Description

The AErosol RObotic NETwork (AERONET) program is a federation of ground-based remote sensing aerosol networks initially established by the NASA and PHOTONS (Univ. of Lille 1, CNES, and CNRS-INSU) but

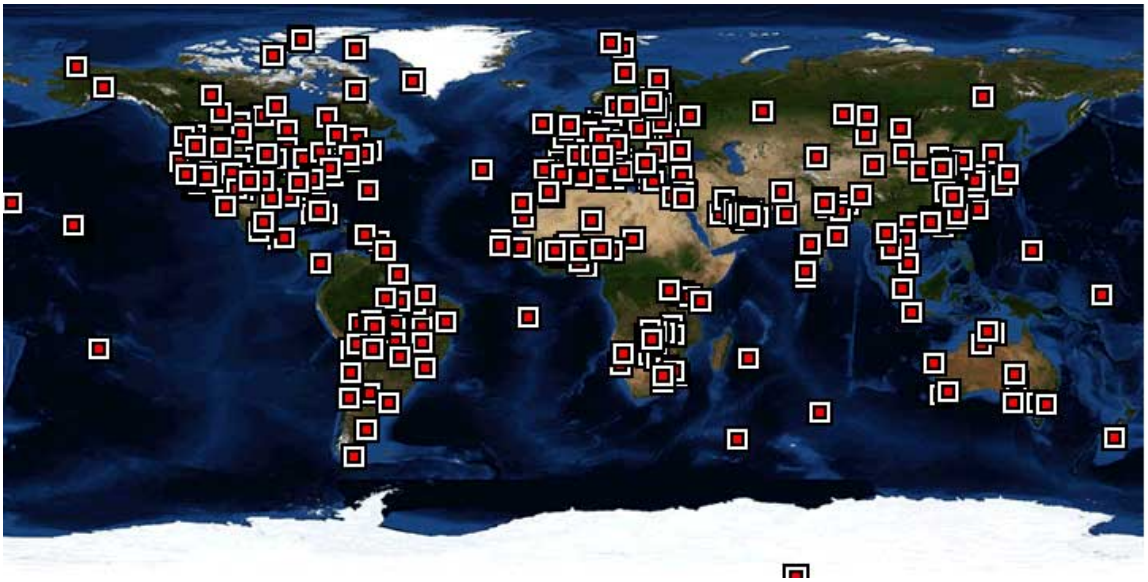

Figure 3.2.1: *Aeronet sunphotometers around the world. (Aeronet, website)*

expanded by collaborators from national agencies, institutes, universities, individual scientists, and partners. The program provides a long-term, continuous and readily accessible public domain database of aerosol optical, microphysical and radiative properties for aerosol research and characterization, validation of satellite retrievals, and synergism with other databases. The network imposes standardization of instruments, calibration, processing and distribution.

### 3.2.2 Characteristics of AERONET

The Aerosol Robotic Network is composed of 400 sunphotometers spread around the world (see Fig.3.2.1) measuring the extinction of the direct beam spectral solar radiance at eight different wavelengths, $\lambda = [340, 380, 440, 500, 670, 870, 940$ and $1020]$ nm. The aerosol optical depth, $\tau(\lambda)$, is then retrieved with the Beer-Lambert law (3.2.1) considering the estimated attenuation due to Rayleigh scatter, ozone absorption and gaseous pollutants. Aerosol optical depth measurements are obtained every 5-25 minutes depending on the solar zenith angle. The uncertainty of the optical depth measurements is estimated to be between 0.01 and 0.02 (Aeronet, website).

$$\frac{I}{I_0} = e^{-\tau(\lambda)} \tag{3.2.1}$$

### 3.2.3 The Aeronet Data set

The Aeronet data are available on the NASA wesite of Aeronet: http://aeronet.gsfc.nasa.gov/.

Globally distributed observations of spectral aerosol optical depth (AOD), inversion products, and precipitable water in diverse aerosol regimes can be downloaded there. More precisely, the aerosol optical depth data are computed for three different quality levels: Level 1.0 (unscreened), Level 1.5 (cloud-screened), and Level 2.0 (cloud-screened and quality-assured). The data retrieved from the sunphotometers might have a wide time coverage ranging from 1993 to 2012 according to the sunphotometer considered. However, in order to allow the comparison with the other datasets, only the data Level 2.0 for the years 2006 to 2010 have been considered in this study.

## 3.3 Introduction to MODIS

### 3.3.1 General Description

The MODerate resolution Imaging Spectrometer (MODIS) is a key instrument located on the Earth Observation System's Terra (EOS AM) and Aqua (EOS PM) satellites, respectively launched in 1999 and 2002. Both satellites have a polar orbit, descending (southward) for Terra and ascending (northward) for Aqua crossing the equator respectively at 10:30 and 13:30 local sun time. At an altitude of about 705 km with a view scan of $\pm 55°$, both instruments view the Earth with a swath of about 2330 km, covering therefore the entire globe on a daily basis, on a 16-day orbit cycle (MODIS, website).

### 3.3.2 Characteristics of MODIS

The fundamental aerosol products from MODIS are the total spectral aerosol optical depth (AOD or $\tau$) and the Fine aerosol Weighting (FW or $\eta$) that is to say the fractional contribution of fine aerosols to the total optical depth.

Terra and Aqua MODIS acquire data in 36 spectral bands from the solar to thermal infrared spectrum region ranging from 0.41 to 14.235 $\mu$m. The aerosol retrievals make use of seven of them ([0.620-0.670]$\mu$m, [0.841-0.876]$\mu$m, [0.459-0.479]$\mu$m, [0.545-0.565]$\mu$m, [1.230-1.250]$\mu$m, [1.628-1.652]$\mu$m, [2.105-2.155]$\mu$m) and a number of other bands to help with cloud discrimination and other screening procedures. Only data from MODIS performed during the daytime are considered for retrieval.

The MODIS aerosol retrievals are made of two independent algorithms, one for deriving aerosols over land and the second for aerosols over ocean with respective uncertainties. Input parameters are required by both algorithms: calibrated and geolocated reflectances, pre-assumptions on the general structure of the size distribution and the volume-size distribution.

To ensure good quality data, a 'Quality Assurance' (QA) factor of the retrieved products is assigned based on the behavior of the algorithms. Whether ocean or land aerosol retrievals are performed, the products are assigned a QA confidence (QAC) flag that indicates how the retrievals should be considered. The QAC value ranges from 3 to 0, where 3 means good quality and 0 means bad quality. This QAC flags are used in the retrievals as weights: The retrievals with $QAC = 3$ are assigned higher weights than those with $QAC = 2$ or $QAC = 1$ while retrievals with $QAC = 0$ are not included.

The expected uncertainty of the optical depth, $\tau$, was found to be (Levy et al. 2009, 2010):

- $\Delta\tau = \pm 0.03 \pm 0.05\tau$ over ocean
- $\Delta\tau = \pm 0.05 \pm 0.15\tau$ over land

The expected errors were designated for the 0.55 $\mu$m channel, but were found to apply in other channels as well. If in general the MODIS retrievals match the expected accuracy, under certain conditions they did not. For instance the MODIS algorithm over ocean was found to have two major sources of error over coastal regions. One is due to cloud contamination that leads to an overestimation of AOD, and the other one is due to wrong assumption about the surface wind speed that leads to an underestimation of the aerosol optical depth (Anderson et al. 2012).

### 3.3.3 The MODIS dataset

The MODIS dataset used in this study has been provided by the Swedish Meteorological and Hydrological Institute (SMHI). They cover the years 2006 to 2010 and fulfills the criterion described above.

## 3.4 Introduction to the Emep model

### 3.4.1 General Description

The *European Monitoring and Evaluation Programme* (Emep) is a scientifically based and policy driven programme under the *Convention on Long range Transboundary Air Pollution* for internationnal co-operation to solve transboundary air pollution problems. The main objective of this programme is to provide scientific

information to governments to support the development and evaluation of the international protocols on emission reductions negociated within the Convention (EMEP, website).

The Emep programme relies on three main elements:

- Collection of emission data
- Measurements of air and precipitation quality
- Modelling of atmospheric transport and deposition of air pollutions

The Emep/MSC-W model, considered in this thesis, is the merge of the previous different modelling tools developped by Emep.

### 3.4.2 Characteristics of the Emep model

The model uses a $1° \times 1°$ resolution, representing a $110 \times 110$ km grid-size at the Equator and it is made of 20 vertical layers (see Fig.3.4.1) defined with the so-called $\sigma$ coordinates such as:

$$\sigma = \frac{P - P_t}{P_s - P_t} \tag{3.4.1}$$

where $P$ is the pressure at $\sigma$-level, $P_t$ is the pressure at the top of the model domain, and $P_s$ is the pressure at the surface.

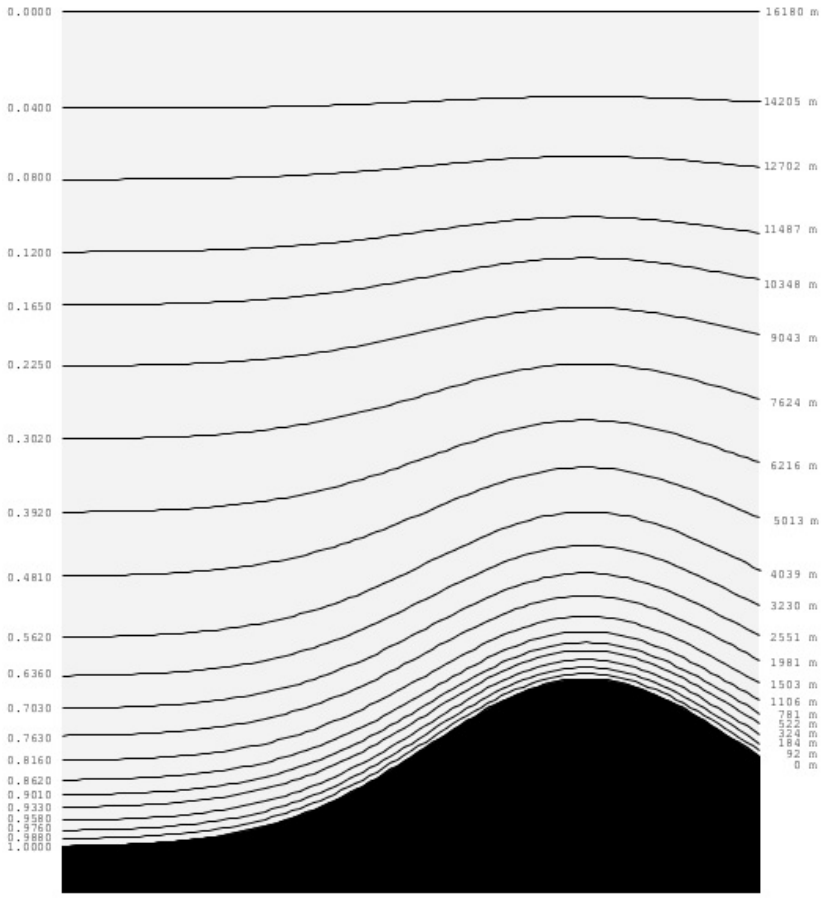


Figure 3.4.1: *Vertical structure of the Emep/MSC-W model. The troposphere is represented in the model by 20$\sigma$ layers. Sigma values for the boundaries of each level are shown on the left hand side of the figure. The corresponding height above the ground, computed for a standard atmosphere, is given on the right-hand side.*

The Emep model includes emissions, chemical transformation, dynamics, transport, as well as dry and wet deposition of atmospheric aerosol (Simpson et al. 2012).

More precisely, 8 chemical aerosol components are considered in the fine and the coarse mode (see section 2.1.1): sulphate ($SO_4$), nitrate ($NO_3$), ammonium ($NH_4$), organic carbon (OC), elemental carbon (EC) mineral dust (DU) and sea salt (SS). The model includes a so-called volatility basis set (VBS) approach to account for the secondary organic aerosol (SOA) formation (see Donahue et al. (2009)).

As inputs, the Emep model requires meteorological, emissions and land use datasets as well as initial boundary conditions (Simpson et al. 2012).

Meteorological data are required with a 3-hour resolution and consist of 12 parameters used for the calculation of dry deposition, advection, chemical reactions...(see Table 3.4.1). Some other parameters are also derived from them, such as air density.

| **Parameter** | **Unit** | **Main Purpose** |
|---|---|---|
| 3-D fields - for the 20 $\sigma$ levels: | | |
| Wind velocity components | $ms^{-1}$ | Advection |
| Specific humidity | $kgkg^{-1}$ | Chemical reactions, dry deposition |
| Vertical wind in $\sigma$ coordinates | $s^{-1}$ | Vertical Advection |
| Potential Temperature | K | Chemical reactions, eddy diffusion |
| Cloud cover | % | Wet removal, photolysis |
| Precipitation | mm | Wet and dry deposition |
| Convective updraft flux | kg $m^{-2}s^{-1}$ | Vertical transport, wet removal |
| Convective downdraft flux | kg $m^{-2}s^{-1}$ | Vertical transport, wet removal |
| 2-D fields - for surface: | | |
| Surface Pressure | hPa | Surface air density |
| Temperature at 2 m height | K | Dry deposition, Stability |
| Surface flux of sensible heat | $Wm^{-2}$ | Dry deposition, Stability |
| Surface stress | $Mm^{-2}$ | Dry deposition, Stability |
| Surface flux of latent heat | $Wm^{-2}$ | Dry deposition |
| Sea surface temperature | K | Sea-Salt |
| Snow depth | m | Dry deposition |
| Fraction of ice | % | Dry deposition |

Table 3.4.1: Meteorological data used in the Emep model.

Landuse data give for each square resolution the fractional coverage of different vegetation types for dry deposition modelling and estimation of biogenic emissions. In total, 16 different types of vegetation are identified: Temperate/boreal coniferous forests, Temperate/boreal ciduous forests, Mediterranean needle-leaf forests, Mediterranean broadleaf forests, Temperate crops, Mediterranean crops, Root crops, Seminatural/Moorland, Grassland, Mediterranean scrub, Wetlands, Tundra, Desert, water, Ice and Urban.

Both anthropogenic and biogenic emissions are considered in the Emep model.

The anthropogenic emission input consists of gridded annual national emissions of sulphur dioxide ($SO_2$), nitrogen oxides ($NO_x$ = NO+$NO_2$), ammonia ($NH_3$), non-methane volatile organic compounds (NMVOC), carbon monoxide (CO), and particulates ($PM_{2.5}$ , $PM_{10}$ ). These emissions are provided for 10 anthropogenic source-sectors (see Table 3.4.2) and are vertically disributed according to a standard distribution (see Supplementary material : The Emep MSC-W chemical transport model - technical description (Simpson et al. 2012) for more information).

The biogenic emissions of isoprenes, pool-dependent and light-dependent monoterpenes are derived from the landuse dataset. Emission rates for the Emep aggregated land-cover classes ($\Lambda_c$) are developed from maps of the different land-cover types ($\lambda_c$) with (Simpson et al. 2012):

$$E^*_{\Lambda_{c,i}} = \frac{\sum_{\lambda_c} \epsilon^*_{\lambda_c,i} A_{\lambda_c} D_{\lambda_c} \delta(\lambda_c \in \Lambda_c)}{\sum_{\lambda_c} A_{\lambda_c}} \tag{3.4.2}$$

where $E^*_{\Lambda_{c,i}}$ is the area-specific reference emission rate ($\mu gm^{-2}h^{-1}$) for a land-cover class at standard environmental conditions, $\epsilon^*_{\lambda_c,i}$ is the mass-specific emission rate ($\mu gm^{-2}$ (dry weight) $h^{-1}$) for the biogenic VOC compound $i$ and a particular land-cover class $\lambda_c$ at these standard conditions, $A_{\lambda_c}$ is the area and $D_{\lambda_c}$ the foliar

| No. | Sources |
|---|---|
| 1 | Combustion in energy and transformation industries |
| 2 | Non-industrial combustion plants |
| 3 | Combustion in manufacturing industry |
| 4 | Production processes |
| 5 | Extraction and distribution of fossil fuels and geothermal energy |
| 6 | Solvents and other product use |
| 7 | Road Transport |
| 8 | Other mobile sources and machinery |
| 9 | Waste treatement and disposal |
| 10 | Agriculture |

Table 3.4.2: Sectors contributing to the anthropogenic emissions included in the Emep model.

biomass density of that species. The biogenic VOC have a high season dependency with emissions peaking during the months of June, July and August. The figure (3.4.2) shows indeed an increase of the biogenic isoprene and monoterpene emissions during the summer in Poland, Ukraine and Spain for the year 2006 while the non-methane VOC (NMVOC) emissions are constant along the year.

Emissions from volcanoes and emissions of $NO_x$ from lightning are also included.

(See The Emep/MSC-W Model - User's Guide for further details about the input and output files of the Emep model.)

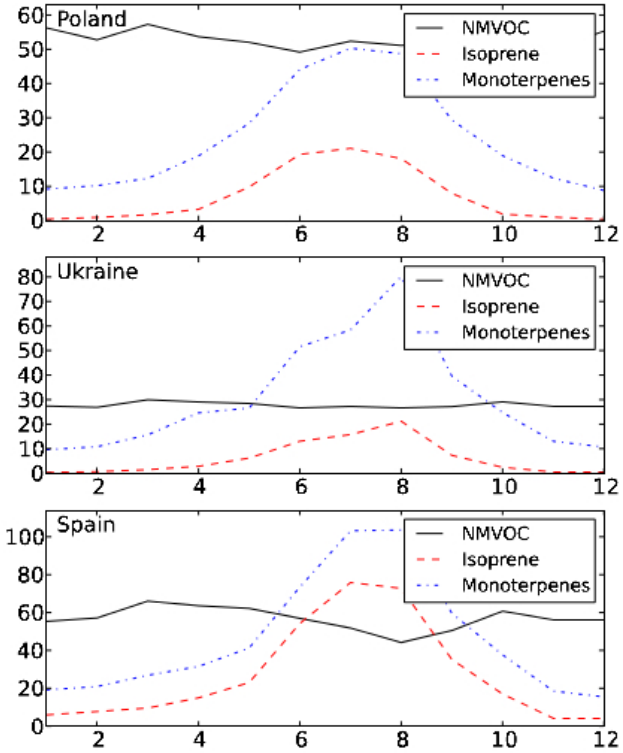


Figure 3.4.2: *Monthly emissions of anthropogenic non-methane VOC, biogenic isoprene and monoterpene in Poland, Ukraine and Spain for the year 2006. Units are Gg month$^{-1}$. (Simpson et al. 2012)*

### 3.4.3 Aerosol Optical Depth and Aerosol Extinction Coefficient computations in the Emep model (A. Valdebenito and Schulz 2012)

The Emep calculation scheme of the aerosol extinction in the different layers of the troposphere of the Emep model is based on the works of Chin et al. (2002) and Hess et al. (1998), so that the optical depth in the Emep model is computed as:

$$\tau = \sum_{k=1}^{k_{top}} \sum_{i} (M_{dry,i,k} E_{ext,i}) \Delta z_k \tag{3.4.3}$$

where $M_{dry,i,k}$ [g/m$^3$] is the mass concentration of dry aerosol component $i$ in the model layer $k$, $E_{ext,i}$ [m$^2$/g] is the specific cross-section for the aerosol component $i$ and $z_k$ is the depth of model vertical layer and $k = 1$ and $k = k_{top}$ are the bottom and the top layer of the model domain. The product $M_{dry,i,k} \times E_{ext,i}$ corresponds therefore to the aerosol extinction coefficient.

The specific cross-section for the aerosol $i$ is calculated such as:

$$E_{ext} = \frac{3 Q_i M_i}{4 \rho_i r_{e,i} M_{dry,i}} \tag{3.4.4}$$

where $Q_i$ is the extinction efficiency for wet aerosol, calculated based on the Mie-scattering; $M_{dry,i}$ and $M_i$ are the aerosol dry mass and wet mass, that is to say the dry mass plus the mass of uptaken water, $\rho_i$ and $r_{e,i}$ are the density and effective radius of the wet aerosol.

The extinction efficiencies $Q_i$ and the radius of the wet aerosol $r_{e,i}$ are calculated for a series of relative humidity values and then interpolated to derive $Q_i$ and $r_{e,i}$ for actual conditions.

The mass concentration of dry aerosol component $i$ in the model layer $k$, $M_{dry,i,k}$ [g/m$^3$], is derived from the continuity, convective and advection equations considering emissions, chemical transformations as well as dry and wet deposition of the aerosols: $SO_4$, $NO_3$, $NH_4$, OC, EC, DU and SS (see Simpson et al. (2012) for further information).

### 3.4.4 The Emep data set

The output files are available as netCDF files (extension *.nc*) with four different time basis: Base_hour.nc, Base_day.nc, Base_month.nc and Base_year.nc. From the ouput files, for each unit area, defined by the spatial resolution of the Emep model, it can be especially looked at:

- The temporal evolution of the total optical depth along the day, the month or the year according to the time basis considered.
- The temporal evolution of the optical depth due to one specific aerosol defined in the Emep model along the day, the month or the year.
- The vertical distribution of the total extinction along the 20 vertical layers averaged over the day, the month or the year according to the time basis considered.
- The vertical distribution of the extinction due to one specific aerosol defined in the Emep model averaged over the day, the month or the year.

The Emep simulations on a global scale only deal with the year 2009 for this study. However, the Emep data set is of high relevance for this study since it is the only source of information used giving direct information about organic aerosols.

# 4 Preliminary Study: Optical Depth and Extinction Coefficient

Since the Caliop data does not provide any specific information about organic aerosols, it was essential to compare first the Caliop data with the simulations of the Emep model in terms of optical depth and extinction coefficients, so that information could be derived on organic aerosol in case of a good matching. Moreover to ensure the relevancy of such a comparison, the quality of the Caliop data needed to be certified with another source of observations.

To process, the evolution of the optical depth along the year was looked at with the aim of identifying seasonal patterns.

Thus the seasonal comparison of the different datasets would emphasize the relevancy of the Caliop observations. And sensitivity tests of the Emep model were also performed in order to improve the matching between the Caliop data and the model simulations as regarding the extinction vertical distribution.

## 4.1 Delimitations of the study

Three datasets were available for comparison: Aeronet, Caliop and Modis. However, Aeronet performs ground-based measurements, that is to say local measurements in very specific areas, while Caliop and Modis, on-board satellites, perform global measurements. Therefore the data needed to be processed in such a way that the comparison was relevant. For this reason, the data have been compared on a monthly basis, averaged within $5° \times 5°$ areas for ten specific areas chosen to be representative of different aerosol contributions.

Given the observation properties of the satellite CALIPSO, it has been chosen to compare the data on a monthly basis in order to identify seasonal patterns. Its 16-day cycle around the Earth does indeed not provide daily measurements, and does not even guarantee quality-assured measurements on a monthly basis in case of 'bad' measurements due to the presence of clouds for instance. However month-averaged data is the best time basis to reveal seasonal trends in the annual optical depth evolution.

Given that the sunphotometers of the Aerosol Robotic Network perform local measurements at the sites where they are located, it has been decided to look at the satellite data only in defined areas around the sunphotometers. Therefore the satellite data have been averaged in these areas, around the position of one - or several if available - sunphotometer(s). Moreover, in order to ensure a sufficient number of observations within these defined areas, they should not be smaller than $5° \times 5°$ ($\sim$ 550 km $\times$ 550 km at the Equator). The coordinates of the areas have been set so that the Aeronet station(s) match(es) at best with the center of the areas.

Eventually, to restrict the study, a limited number of areas have been selected with different aerosol contributions to the optical depth according to the Emep model (see figures 4.1.2 and 4.1.3). In total, ten areas have been selected representating four different aerosol contributions (see Map 4.1.1). The details of the areas selected are presented in the table 4.3.1.

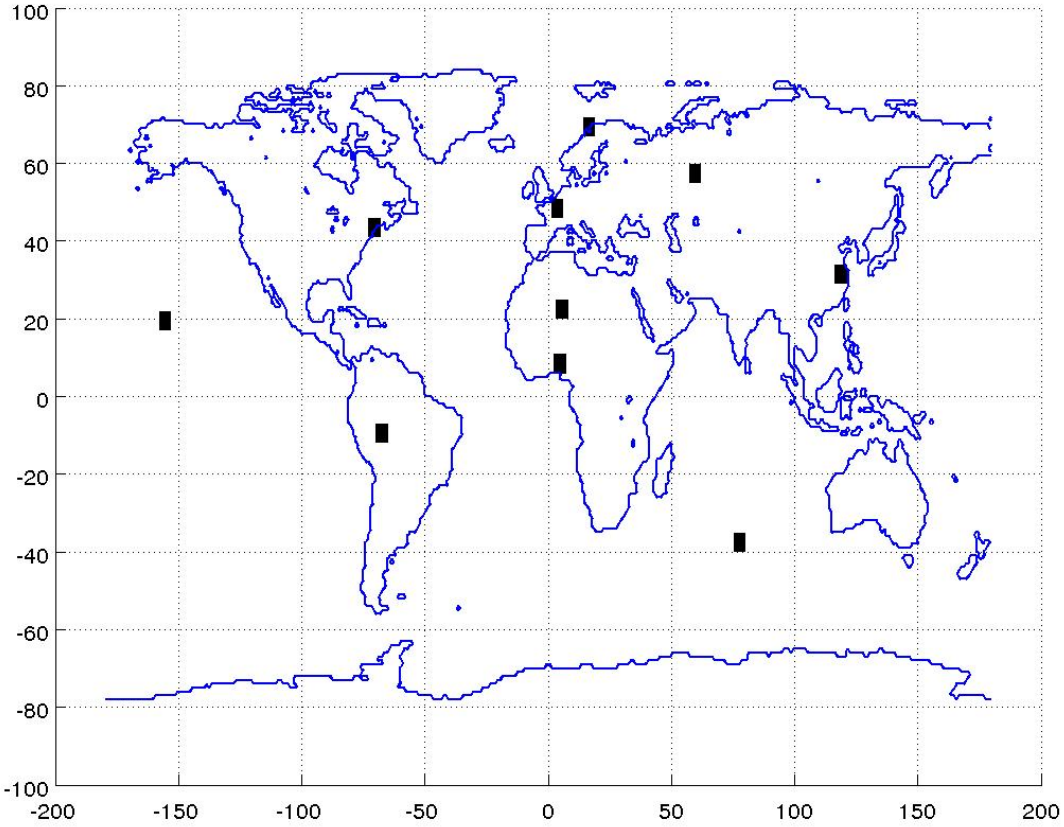


Figure 4.1.1: $5° \times 5°$ *areas selected to represent five different aerosol contributions for optical depth comparison.*

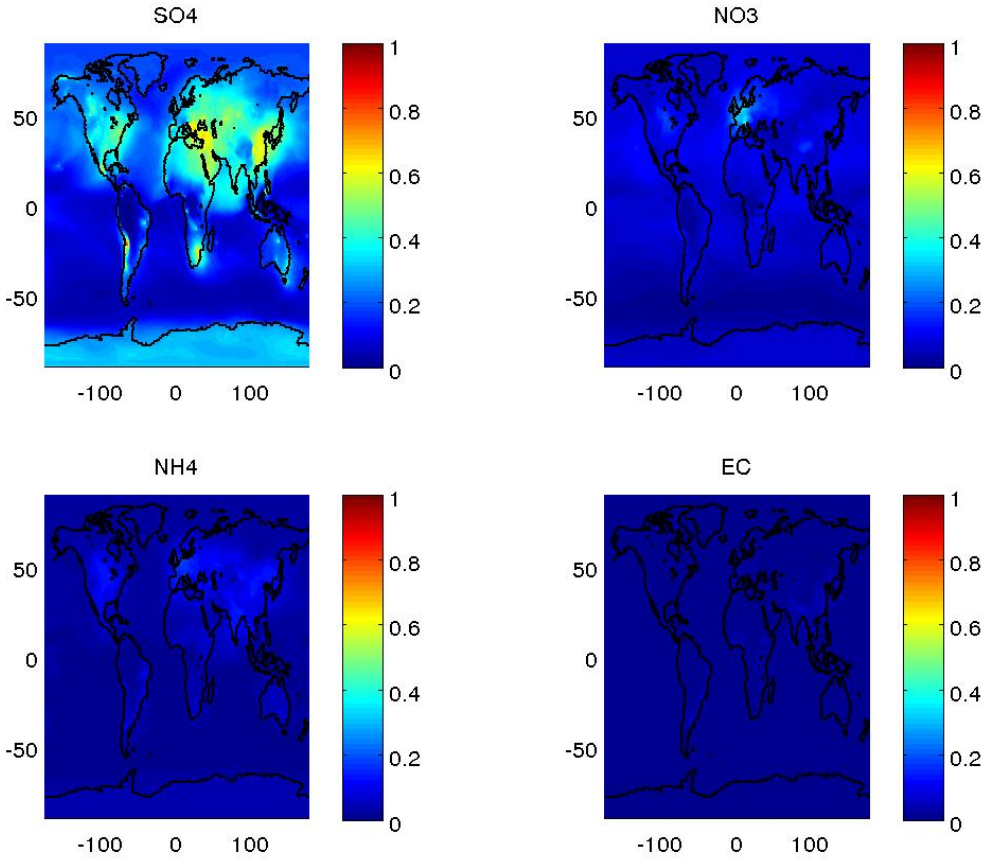


Figure 4.1.2: *Contribution of $SO_4$, $NO_3$, $NH_4$ and Elemental Carbon (EC) to the total optical depth (%).*

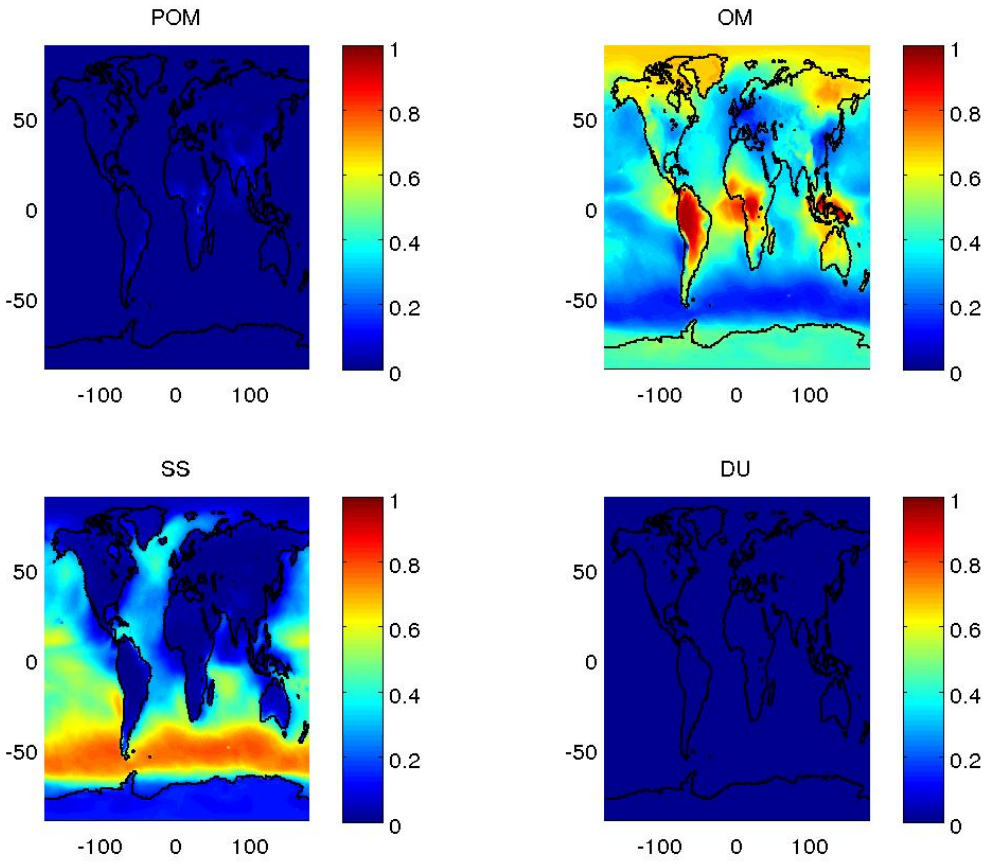


Figure 4.1.3: *Contribution of Primary Organic Matter (POM), Organic Matter (OM), Sea salts (SS) and Dust (DU) to the optical depth (%).*

| **No.** | **Aeronet** | | **Satellite Areas** | | **Aerosol Contribution** |
|---|---|---|---|---|---|
| | Name of the station | Coordinates | Name of the area* | Coordinates | |
| 1 | Tamanrasset | N 22°47'24", E 05°31'48" | Sahara | [20-25]°N × [03-08]°E | $SO_4/OM$ |
| 2 | Amsterdam Island | S 37°48'36", E 77°34'22" | Indian Ocean | [35-40]°S × [75-80]°E | Sea Salt |
| 3 | Mauna Loa | N 19°32'20", W 155°34'40" | Pacific Ocean | [17-22]°N × [153-158]°W | Sea Salt |
| 4 | Ilorin | N 08°19'12", E 04°20'24" | Central Africa | [06-11]°N × [02-07]°E | OM |
| 5 | Rio Branco | S 09°57'25", W 67°52'08" | Amazonia | [07-12]°S × [65-70]°W | OM |
| 6 | Yekaterinburg | N 57°02'16", E 59°32'42" | Central Russia | [55-60]°N × [57-62]°E | $SO_4/OM$ |
| 7 | Andenes | N 69°16'40", E 16°00'32" | North Scandinavia | [67-72]°N × [14-19]°E | $SO_4/OM$ |
| 8 | Taihu | N 31°25'15", E 120°12'54" | China | [29-34]°N × [116-121]°E | $SO_4$ |
| 9 | Creteil<br>Palaiseau<br>Paris | N 48°47'16", E 02°26'34"<br>N 48°42'00", E 02°12'28"<br>N 48°52'01", E 02°19'58" | Paris | [46-51]°N × [00-05]°E | $SO_4/NO_3$ |
| 10 | Billerica<br>Cartel<br>Harvard Forest<br>Appledore Island<br>Thompson Farm<br>Howland | N 42°31'40", W 71°16'08"<br>N 45°22'44", W 71°55'51"<br>N 42°31'55", W 72°11'16"<br>N 42°59'13", W 70°36'53"<br>N 43°06'32", W 70°56'52"<br>N 45°12'00", W 68°43'58" | North America | [41-46]°N × [68-73]°W | $SO_4/OM$ |

** These names are the ones used afterwards to refer to these areas.*

Table 4.1.1: Details of the ten areas selected to represent the contribution of five different aerosols.

## 4.2 Data processing

Identifying seasonal patterns in the optical depth along the year assumes a certain repetitiveness from one year to another. Since in total five years of data were available, it was therefore possible to look at the average trend over these five years for the different sets of data in the selected areas.

However occasional and isolated phenomenon can occur in specific areas and therefore disrupt the average trend. For instance, several hundred wildfires broke out in West Russia during JJA 2010 which released enormous amounts of organic matter in the atmosphere. And as it can be seen on the figure 4.2.1, the Aeronet sunphotometer measured an abnormal optical depth for the month of August 2010.

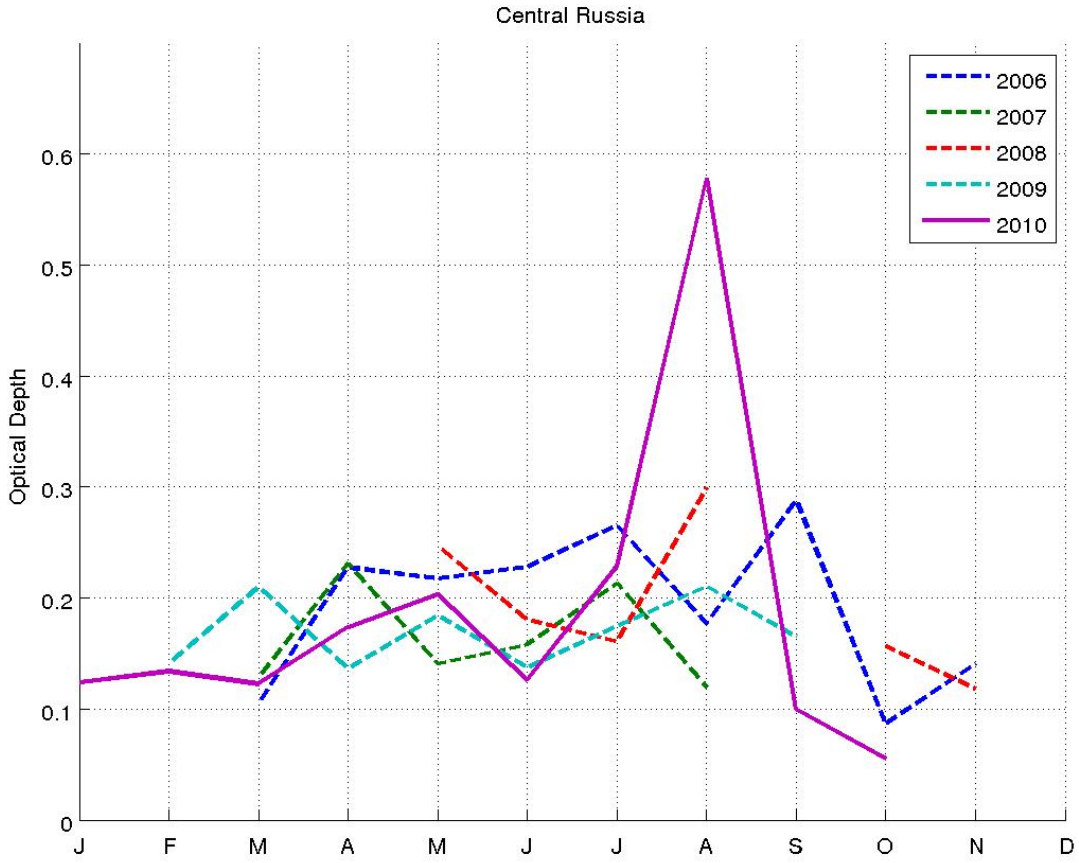


Figure 4.2.1: *Month-averaged optical depth measurements observed by Aeronet from 2006 to 2010. The optical depth for the month of August 2010 is abnormally high, correlating with the organic matter released by the wildfires.*

Therefore all the data have been processed with a specific algorithm described below to get rid of this unusual events.

The basic idea of this algorithm is based on a recursive calculation of the average optical depth over the years for each month excluding the values whose absolute value is P % different than the average value. P has been set at 25 % which allows a reasonable number of data for the calculation of the average and excludes the very different values.

More precisely, the algorithm is described on the sketch 4.2.2 and the corresponding MatLab code, part of the file *SeasonalTrend.m* performing the data comparison, is available in the Appendix C.2. The algorithm can be described in four different steps:

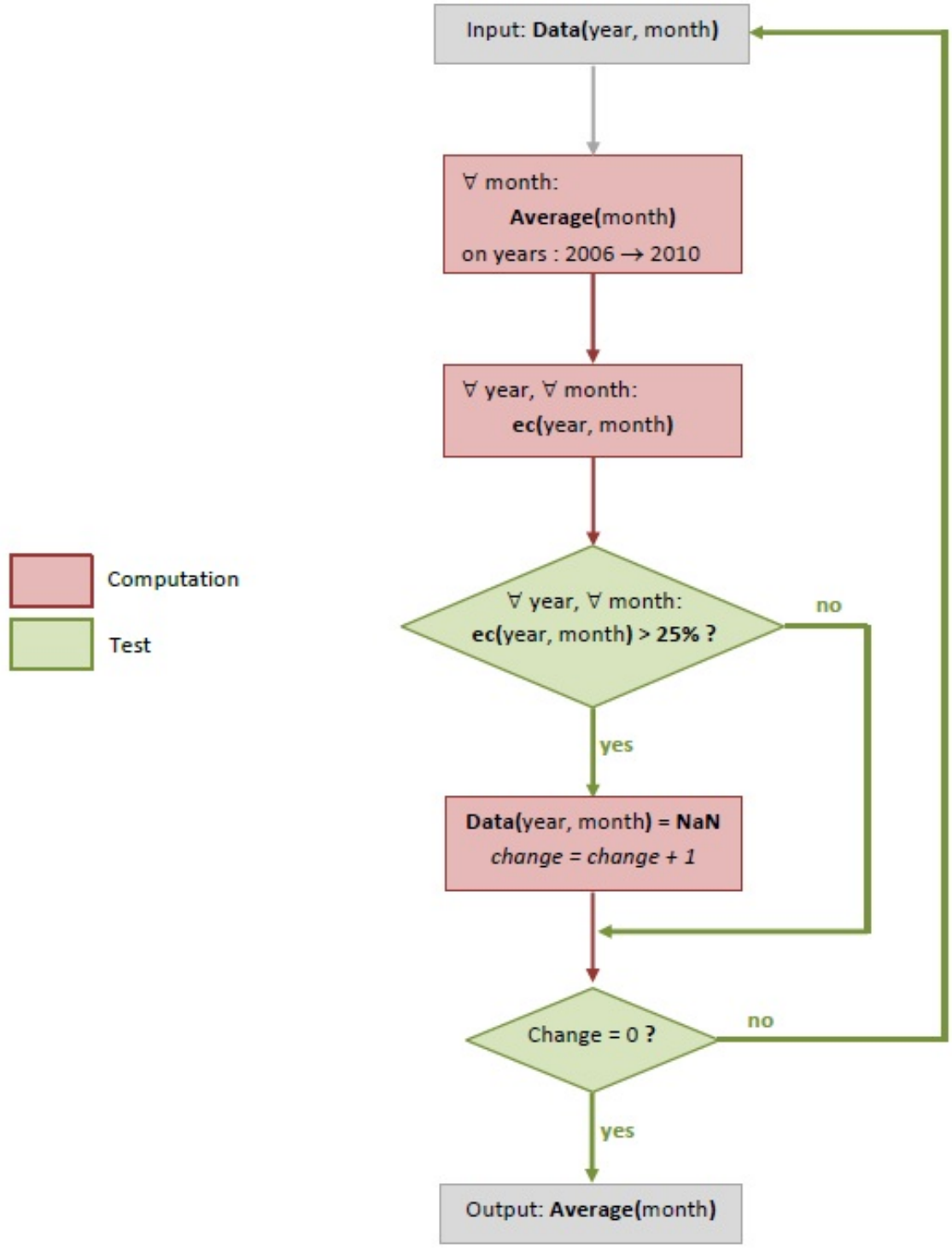


Figure 4.2.2: *Description of the algorithm used to remove the optical depth values corresponding to abnormal events. (ec(.,.) stands for relative error, see text)*

- *Previous to applying the algorithm, all the data are processed to have the same format, that is to say a two-dimension matrix: the first dimension refers to the year and the second one refers to the month, so that Data = Data(year, month).*
- The average over the years 2006 to 2010 is calculated for each month, and the values are stored in a vector *average(month).*

- Relative deviations *ec(year, month)* between the initial *data(year, month)* and the *average(month)* vector are calculated such as:

$$ec(year, month) = |\frac{data(year, month) - average(month)}{average(month)}| \tag{4.2.1}$$

- *data(year = y, month = m)* is replaced by a NaN (Not a Number) when the corresponding *ec(year = y , month = m)* is greater than $P$ (%).

- As long as values of the vector *data* are replaced by NaNs, the algorithm is repeated.

The result of applying this algorithm can be seen on the figure 4.2.3 showing the average trend for Central Russia from Aeronet: The peak observed in August 2010 is not included in the calculation of the month-averaged optical depth.

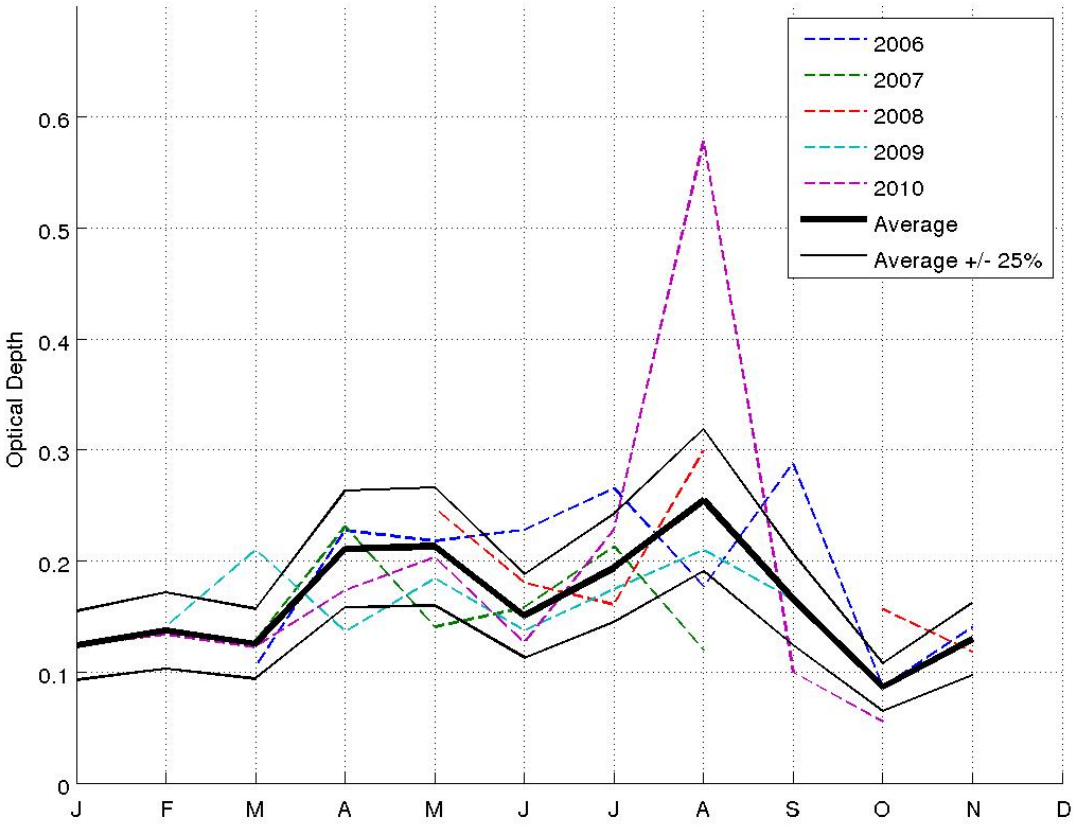


Figure 4.2.3: *Average optical depth over the years 2006 to 2010 computed with the algorithm previously described: The abnormal event of August 2010 is excluded in the processed average.*

## 4.3 Data Comparison

### 4.3.1 Optical Depth Comparison

#### Optical Depth Patterns

The comparison between the Caliop data, the Modis data, the Aeronet data and the Emep model for the ten areas selected are shown on the figures (4.3.1), (4.3.2) and (4.3.3) below and in Appendix B.1.

It can clearly be seen that the areas selected are characterized by various patterns and different optical depth intensities. Deviations of the different datasets from the expected pattern, that is to say the Emep predictions, are described below.

The main contribution to the optical depth in the Saharan area is $SO_4$ and organic matter according to the figures 4.1.2 and 4.1.3, and not dust contrary to what could be expected. More precisely, it can be seen discrepancies between the different datasets - Modis data excluded since measurements are only available for 4 months. First of all, it can be seen that the Emep model predicts an increase of the optical depth during the months of June, July and especially August. But the intensity of the optical depth is clearly underestimated compared to the Caliop and Aeronet measurements by a factor 2 at least. Nevertheless, the Aeronet and Caliop measurements also reveal an increase of the optical depth during the "summer". According to the Aeronet dataset, the optical depth peaks around 0.7 both in June and September while the Caliop dataset shows a "bell shape" with only one maximum in June. The rest of the year, the two datasets seems to agree providing the same intensity for the optical depth. Different reasons might be raised to explain this inconsistency for the peak observed in September. These are explored further in the text (see section 4.3.1).

The Indian and Pacific ocean areas likely dominated by sea-salts and organic aerosols (see Fig. 4.1.3) present similar flat patterns over the year. A peak is nevertheless measured by the three instruments around September in the Indian Ocean. But it does not appear to be related to any well-known atmospheric phenomenon: The area considered is too far south and the peak is too late to make any link with the asian monsoons that usually occur from beginning of June to late August. In the Pacific ocean, the pattern is more regular, however there is a huge gap between the intensities provided by Caliop/Modis and Aeronet (see below for further details and see Table 4.3.1).

The equatorial forest areas show interesting results. Patterns can cleary be identified from the observations. In Amazonia, the three instruments agree both on the shape of the pattern and the intensity of the optical depth. The optical depth is characterized by a sudden peak occuring in September but with a slight discrepancy in intensity ranging from 0.6 for Caliop to almost 1.0 for Aeronet while it is relatively low the rest of the year, around 0.1. As regarding the Emep model, the same pattern can be identified, but the peak occurs in August and is clearly underestimated. The pattern in Central Africa seems to follow the exact opposite pattern with a high optical depth, around 1.0, during DJF and a low one, around 0.5, during JJA. However the shape is more diffuse, closer to a "bell shape" centered on the month of January/February. Central Africa is usually subjected to massive biomass burnings during the dry season (December, January, February) which agrees with the observations: tremendous amounts of organic matter is released from December to March, increasing dramatically the optical depth. The same trend seems to be computed by the Emep model, but the optical depth is clearly underestimated of a factor of about 4.

No clear patterns emerge from the areas representative of both $SO_4$ and $NO_3$, that is to say China and Paris (see Fig. 4.1.2). A wide "bell shape" seems nevertheless to emerge in China with a small maximum in June but it is not confirmed by the Caliop data. However, it can be said that the year-average optical depth for this area is remarkably high, around 0.75, probably kept up by a strong pollution. The year-average optical depth for the area of Paris is much lower, around 0.15, but the three instruments do not provide agreeing observations. The trend seems nevertheless to follow a slight increase during the first half of the year and a slight decrease for the rest of the year. As for the Emep optical depth, it is in the right order of magnitude.

No conclusion can be raised for North Scandinavia and Russia due to missing data. The latitude of these areas is indeed such that they are not covered all the year long by the instruments on-board satellites Caliop and Modis, decreasing dramatically the number of measurements. North America seems to present the expected pattern due to an increase of organic aerosols during JJA, despite some missing Caliop data. Furthermore all the instruments agree well on the optical depth intensity with average relative errors ranging from 25.8 % to 38.1 % (see Table 4.3.1 and read below). The peak in the optical depth occurs however in June/July contrary to the expected one, computed in August by the Emep model.

From a data perspective, the observations provided by Caliop, Modis and Aeronet seems to agree and to

follow an acceptable trend in five of the areas considered: Sahara, Indian Ocean, Central Africa, Amazonia and North America. The Emep model seems however to have difficulties to reproduce these trends, most of the time underestimating the optical depth and sometimes overestimating it.

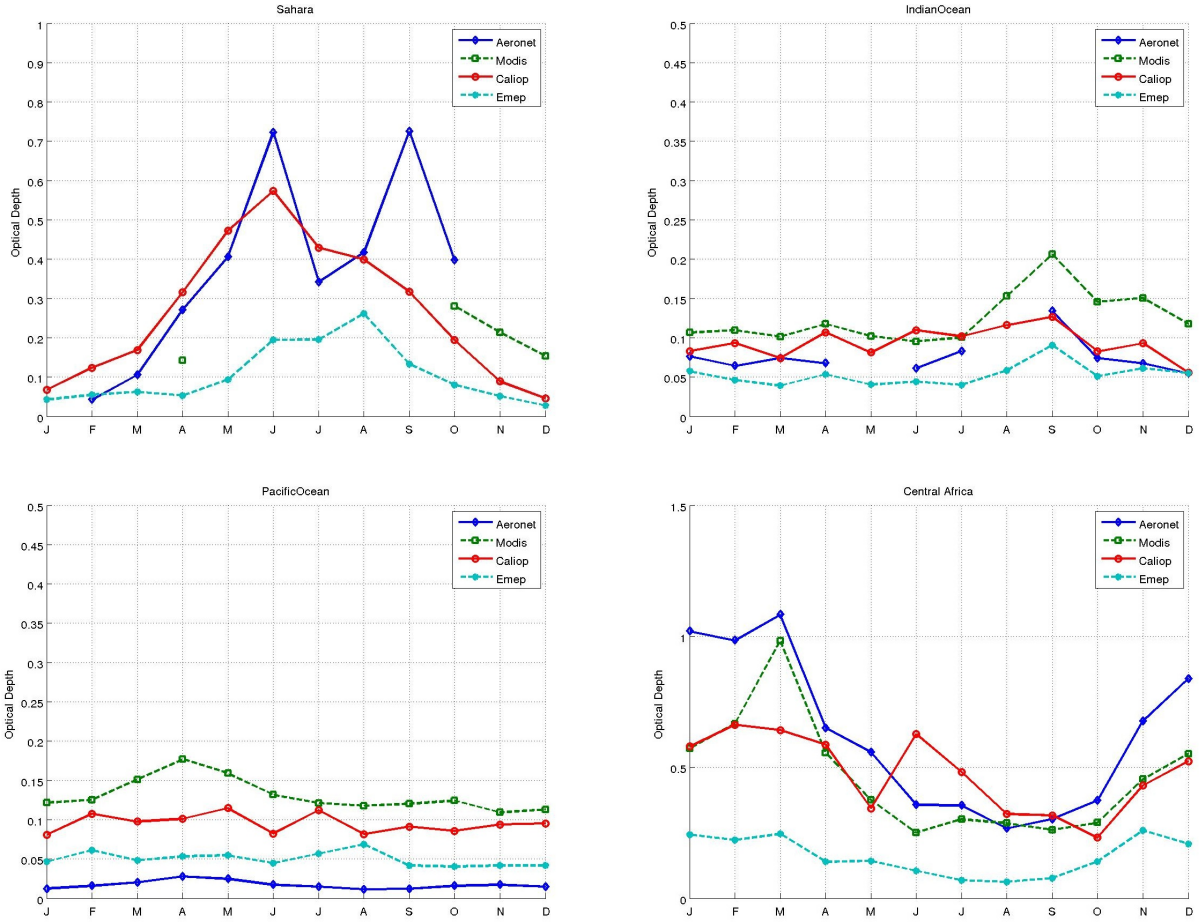


Figure 4.3.1: *Comparison of the Optical Depth measured by Caliop, Modis and Aeronet and predicted by the Emep model for the areas of Sahara, Indian Ocean, Pacific Ocean and Central Africa and averaged over the years 2006 to 2010.*

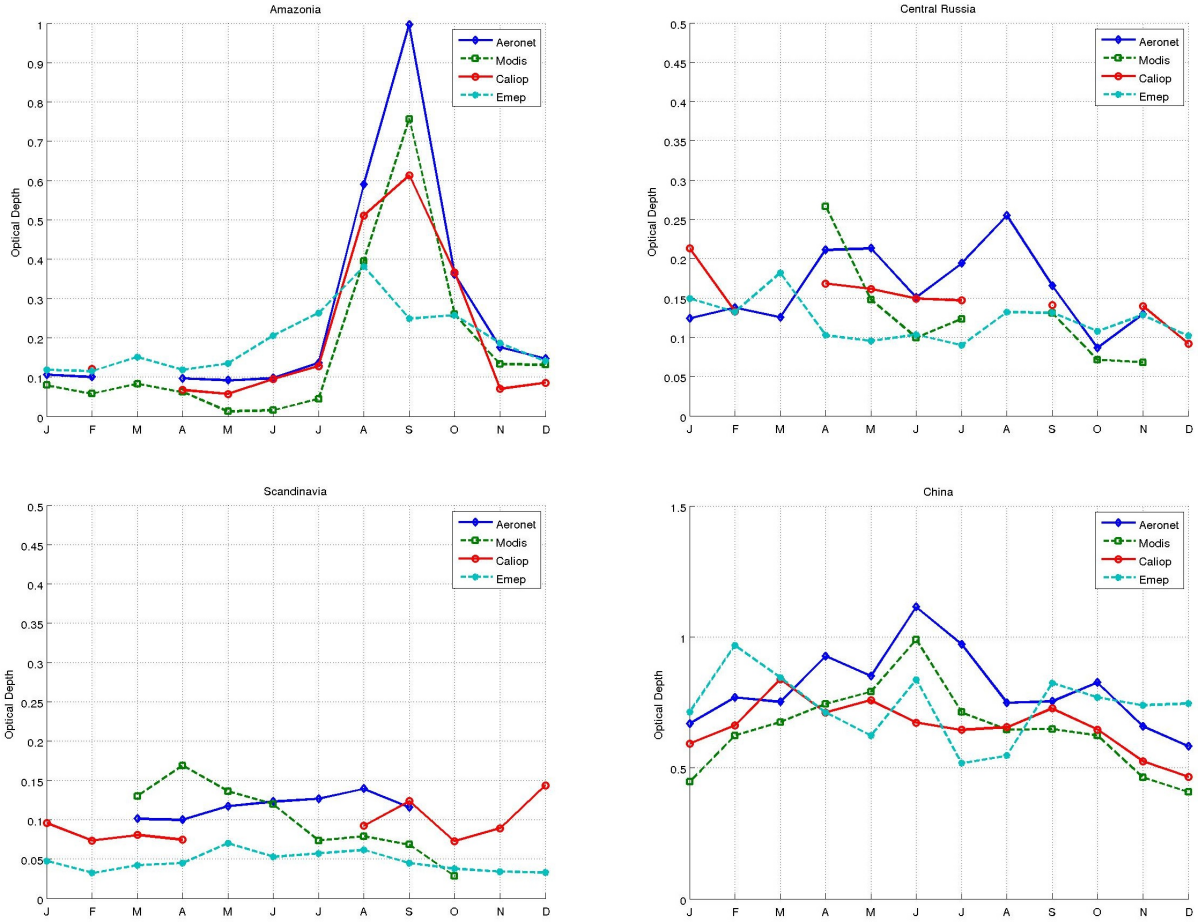


Figure 4.3.2: *Comparison of the Optical Depth measured by Caliop, Modis and Aeronet and predicted by the Emep model for the areas of Amazonia, Central Russia, Scnadinavia and China and averaged over the years 2006 to 2010.*

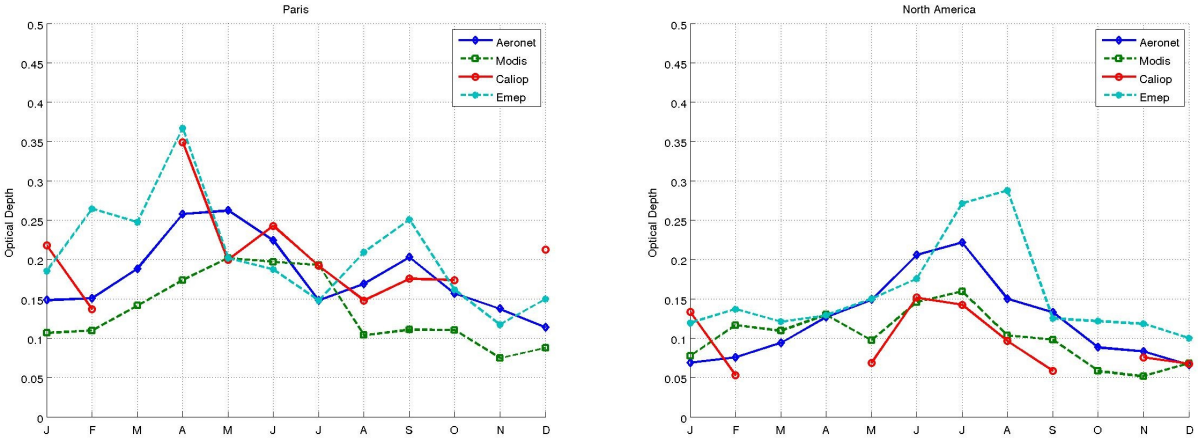


Figure 4.3.3: *Comparison of the Optical Depth measured by Caliop, Modis and Aeronet and predicted by the Emep model for the areas of Paris and North America and averaged over the years 2006 to 2010.*

### Statistical comparison of the Caliop, Modis and Aeronet datasets

To make relevant the comparison with the Emep model, a visual comparison is not enough. That is why in this section, a statistical approach is adopted.

Thus, the relative deviations between the Caliop, Modis and Aeronet datasets are summarized in the table 4.3.1 for each month and for each region. It can be seen, excepted in the Pacific Ocean area, that the relative difference of the Caliop dataset compared to the Aeronet dataset ranges between 15 and 50 % while the relative difference of the Modis dataset compared to the Aeronet dataset ranges between 15 and 70 %. The range of the relative difference of the Caliop dataset compared to the Modis is wider, going from 10 % to 140 %. Averaged over the year and over these nine areas, the relative difference of Caliop compared to Modis reaches 49 % while the relative difference of the Caliop dataset compared to the Aeronet dataset is only 27 % and the relative difference of the Modis dataset compared to Aeronet 31 %. However these last two numbers dramatically increase if all areas are considered reaching respectively 76 % and 101 %. The Pacific area excluded, the relative bias between Caliop and Aeronet is in the same order of magnitude as the one emphasized by Schuster et al. (2012), who compared Caliop data over 147 Aeronet sites and found a relative bias of 13 % and a rejection of the null hypothesis at 97 % confidence level, indicating a statistically significant difference between the datasets as the previous figures suggest it.

### Discrepancies between the datasets

Several reasons can be raised to explain such discrepancies.

First, one has to remember that the quality of the aerosol optical depth measurement is based on the design of the instruments, the calibration of the instruments and the correct identification of clear sky conditions. And as regarding the Caliop retrievals, it also depends on the layer detection sensitivity and the accurate layer classification.

As emphasized by Schuster et al. (2012), on one hand Aeronet uses a ground-based platform and its fields of view is a pencil beam from the solar disc to the instrument contrary to Caliop (and Modis) which is on-board a satellite and provides average data on the vertical resolution and horizontal resolution along near vertical columns above the satellite track. Thus the Aeronet instruments are more affected by local pollution events. Moreover Aeronet operates only during the daytime, that is to say when it is the most challenging time for Caliop retrievals because of the solar radiation scattered into the lidar telescope. In other words, the daytime Caliop measurements are not as reliable as the ones performed during the nighttime. As for Modis, it mainly performs measurements during the daytime but NASA also receives Modis-data during the nighttime (MODIS, FAQ). Therefore, these three instruments rarely sample the same part of the atmosphere which obviously leads to differences between the optical depth measurements.

Furthermore, all these instruments do not operate at the same wavelength, and yet the optical depth is a function of the wavelength, $\tau = \tau(\lambda)$, which can lead to small differences. And even if a second order variation of the Angström relation (4.3.1) is used to interpolate all the wavelengths for the Aeronet data, it is still another potential source of error.

$$ln(\tau(\lambda)) = a_0 + a_1 ln\lambda + a_2 (ln\lambda)^2 \tag{4.3.1}$$

The estimates of the lidar ratio for the Caliop retrievals, as mentioned before, is also a source of error. Schuster et al. (2012) clearly showed that more research and analysis in this area is desirable, indicating the poor reliability of the lidar-ratio algorithm used in Caliop retrievals.

Differences can also appear with the presence of clouds. Since the measurements are not synchronised, one instrument can detect clouds and not the others. As mentioned before, the quality of the optical depth measurements depends on the correct identification of clear sky conditions. However, Huang et al. (2011) and Chew et al. (2011) have shown that the Aeronet cloud screening procedure often misses thin cirrus in SouthEast Asia which implies that it could also miss other clouds somewhere else. Redemann et al. (2012) also pointed out that Caliop performs measurements only when an aerosol layer is detected. In regions where aerosol layers are more tenuous, that is to say spread over greater geometric depth, Caliop likely fails to detect such aerosol layers, contributing to the errors emphasized in the table 4.3.1.

| Area | Comparison * | J | F | M | A | M | J | J | A | S | O | N | D | Average ** |
|---|---|---|---|---|---|---|---|---|---|---|---|---|---|---|
| Sahara | Caliop-Aeronet | NaN | 191 | 60 | 17 | 16 | -21 | 26 | -4 | -56 | -51 | NaN | NaN | **49** |
| | Modis-Aeronet | NaN | NaN | NaN | -47 | NaN | NaN | NaN | NaN | NaN | -29 | NaN | NaN | **38** |
| | Caliop-Modis | NaN | NaN | NaN | 121 | NaN | NaN | NaN | NaN | NaN | -31 | -58 | -70 | **70** |
| Indian Ocean | Caliop-Aeronet | 9 | 45 | 0 | 58 | NaN | 80 | 23 | NaN | -5 | 11 | 39 | 2 | **30** |
| | Modis-Aeronet | 40 | 71 | 37 | 74 | NaN | 56 | 21 | NaN | 54 | 96 | 124 | 116 | **69** |
| | Caliop-Modis | -22 | -15 | -27 | -9 | -20 | 15 | 1 | -24 | -38 | -43 | -38 | -53 | **25** |
| Pacific Ocean | Caliop-Aeronet | 560 | 582 | 383 | 261 | 365 | 382 | 660 | 608 | 647 | 440 | 450 | 548 | **490** |
| | Modis-Aeronet | 891 | 694 | 648 | 532 | 545 | 671 | 721 | 923 | 887 | 682 | 539 | 669 | **700** |
| | Caliop-Modis | -33 | -14 | -35 | -43 | -28 | -38 | -7 | -31 | -24 | -31 | -14 | -16 | **26** |
| Central Africa | Caliop-Aeronet | -43 | -33 | -41 | -10 | -38 | 76 | 36 | 20 | 5 | -38 | -36 | -38 | **34** |
| | Modis-Aeronet | -44 | -32 | -9 | -15 | -33 | -30 | -15 | 8 | -14 | -23 | -33 | -34 | **24** |
| | Caliop-Modis | 1 | -1 | -35 | 6 | -8 | 151 | 60 | 12 | 22 | -20 | -5 | -5 | **27** |
| Amazonia | Caliop-Aeronet | NaN | 20 | NaN | -31 | -38 | -2 | -6 | -13 | -38 | 2 | -60 | -42 | **25** |
| | Modis-Aeronet | -25 | -42 | NaN | -36 | -86 | -84 | -67 | -33 | -24 | -28 | -24 | -11 | **41** |
| | Caliop-Modis | NaN | 108 | NaN | 8 | 348 | 525 | 186 | 29 | -19 | 41 | -47 | -35 | **135** |
| Central Russia | Caliop-Aeronet | 72 | -4 | NaN | -20 | -24 | -1 | -24 | NaN | -15 | NaN | 8 | NaN | **21** |
| | Modis-Aeronet | NaN | NaN | NaN | 26 | -31 | -34 | -37 | NaN | -21 | -17 | -47 | NaN | **30** |
| | Caliop-Modis | NaN | NaN | NaN | -37 | 9 | 50 | 19 | NaN | 8 | NaN | 105 | NaN | **38** |
| North Scandinavia | Caliop-Aeronet | NaN | NaN | -20 | -25 | NaN | NaN | NaN | -34 | 7 | NaN | NaN | NaN | **21** |
| | Modis-Aeronet | NaN | NaN | 29 | 69 | 16 | -3 | -42 | -43 | -41 | NaN | NaN | NaN | **35** |
| | Caliop-Modis | NaN | NaN | -38 | -56 | NaN | NaN | NaN | 17 | 81 | 158 | NaN | NaN | **70** |
| China | Caliop-Aeronet | -11 | -14 | 12 | -23 | -11 | -40 | -34 | -12 | -4 | -22 | -20 | -20 | **19** |
| | Modis-Aeronet | -33 | -19 | -10 | -20 | -7 | -11 | -27 | -14 | -14 | -24 | -29 | -30 | **20** |
| | Caliop-Modis | 33 | 6 | 24 | -4 | -4 | -32 | -9 | 1 | 12 | 4 | 13 | 14 | **13** |
| Paris | Caliop-Aeronet | 25 | -26 | 32 | 45 | -24 | 3 | 40 | -17 | -7 | 10 | NaN | 82 | **28** |
| | Modis-Aeronet | -28 | -27 | -25 | -33 | -23 | -12 | 30 | -39 | -45 | -29 | -46 | -23 | **30** |
| | Caliop-Modis | 74 | 2 | 75 | 115 | -1 | 17 | 8 | 36 | 70 | 55 | NaN | 137 | **54** |
| North America | Caliop-Aeronet | 94 | -30 | NaN | NaN | -54 | -26 | -36 | -36 | -56 | NaN | -9 | 2 | **38** |
| | Modis-Aeronet | 12 | 55 | 17 | 2 | -35 | -29 | -28 | -31 | -26 | -34 | -38 | 3 | **26** |
| | Caliop-Modis | 73 | -55 | NaN | NaN | -30 | 4 | -11 | -7 | -41 | NaN | 47 | -1 | **30** |

** Calculated as the relative error of the first term compared to the second term (in %). Therefore Caliop-Aeronet stands for* $\frac{Caliop-Aeronet}{Aeronet}$ *. ** Calculated with the absolute values of the relative errors.*

Table 4.3.1: Statistical comparison* of the Modis, Caliop and Aeronet dataset for the 10 areas considered

.

**Aeronet dataset rejection**

Given all the reasons mentioned previously, the relative errors between the different datasets might appear reasonable. However, one major difference has been emphasized: ground-based measurements do not provide the same kind of measurement as instruments on-board satellites. This can explain the surprisingly high relative differences of Caliop and Modis compared to Aeronet for the Pacific ocean: on average over the year, the relative difference for Caliop is 490 % while the one for Modis reaches 700 %!

To not introduce such discrepancies in the study, the Aeronet dataset has not been taken into account for the rest of the optical depth comparison. This decision has also been supported by a more precise study performed in Aerocom as regarding the Caliop and the Aeronet data. On the AeroCom Interface - Caliop3 vs. Aeronet, it can indeed be seen a systematic bias between the two datasets but overall the correlation coefficients remain relatively high over the years (see also Fig 4.3.4). And it has been suggested by Schuster et al. (2012) that this relatively high correlation coefficient compared with the relative bias between the two datasets indicates the possibility that the assumed lidar ratio for the Caliop retrievals is too low.

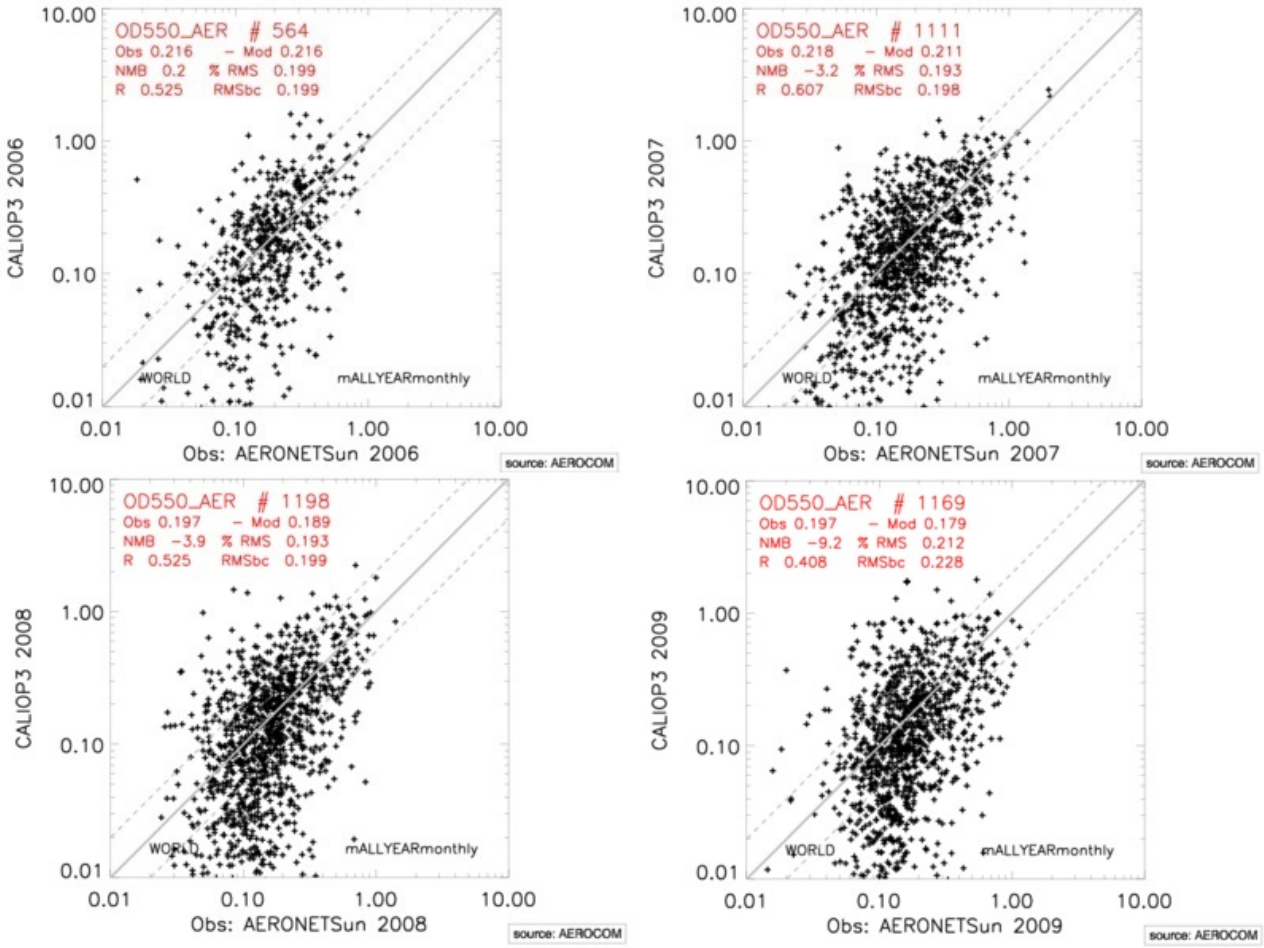


Figure 4.3.4: *Comparison of the optical depth observations performed by Aeronet around the world and Caliop for the years 2006 to 2009. Top left: 2006. Top right: 2007. Bottom left: 2008. Bottom right: 2009. (AeroCom Interface - Caliop3 vs. Aeronet)*

Therefore the only datasets considered in the rest of the study are the two satellite-based instruments: Caliop and Modis.

### 4.3.2 Extinction vertical distribution

Contrary to Modis and Aeronet, the satellite Caliop also performs extinction coefficient measurements. It is therefore possible to look at the vertical distribution of the seasonal patterns identified previously (see Optical Depth Patterns) and to compare them with the Emep model predictions.

As before, the Caliop data have been averaged over the years 2006 to 2010 and the extinction vertical distributions have been studied on a seasonal basis, considering four seasons: December/ January/ February (DJF), March/ April/ May (MAM), June/ July/ August (JJA) and September/ October/ November (SON). The MatLab code plotting these vertical distributions, is part of the file *SeasonalTrend.m* available in the Appendix C.2.

The extinction vertical distribution measured by Caliop and predicted by the Emep model for the five areas for which a seasonal pattern has been identified, are given below.

Given that the data are averaged over 3 months, the seasonal patterns identified previously are therefore emphasized here. It should be noticed the sudden decrease of the Caliop extinction coefficient near the surface that appear in most cases. This is likely due to the low signal-to-noise ratio in the lower part of the atmosphere that can distort the observations. That is why they have never been considered in the analysis below.

More precisely, in Amazonia, the seasonal vertical profiles agree with what was said before as regarding the optical depth: the extinction increases during JJA, but more especially during SON. For these two seasons, the extinction decreases rapidly with the altitude. Within three kilometers, the extinction goes from its maximum to zero at around 4.5 km of altitude. During DJF and MAM, the extinction is lower, and decreases at a slower rate with altitude. However whatever the season, the Emep model fails to reproduce the observations. It can especially be observed during JJA and SON a big difference between the altitude at which the extinction should drop, according to the Emep model, and the one at which the extinction actually drops, according to the Caliop observations. This discrepancy suggests that the mixing height set in the Emep model should be higher.

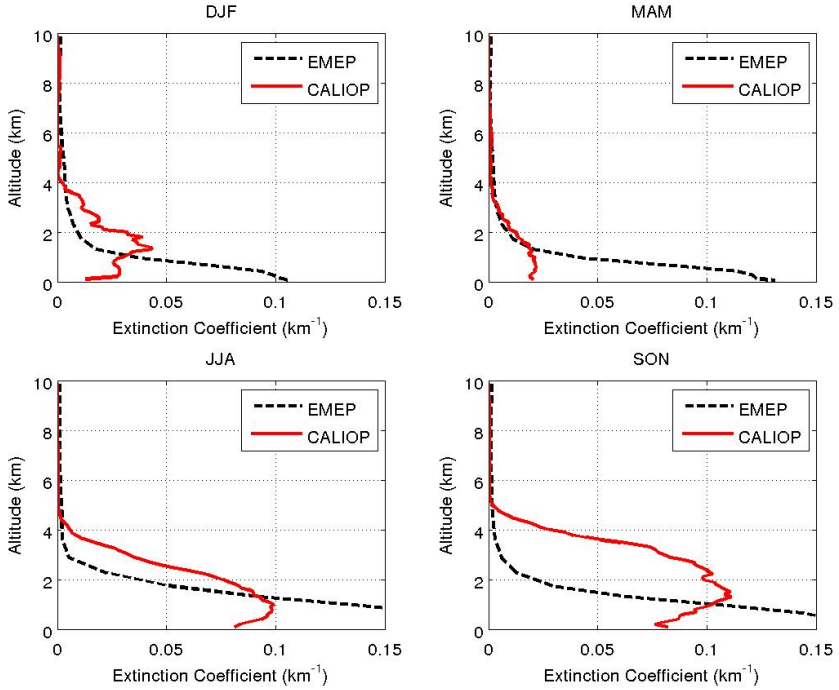


Figure 4.3.5: *Seasonal extinction vertical distributions measured by Caliop (averaged over the years 2006 to 2010) and the ones predicted by the Emep model for the region of Amazonia.*

A seasonaly opposite pattern can be observed in Central Africa, as already mentioned previously. Some differences can however be raised. During JJA, the extinction decreases in two steps: a quick decrease from $0.2\text{km}^{-1}$ to about $0.1\text{km}^{-1}$ in the two first kilometers followed by an almost constant extinction until 4 km of altitude, and then a quick decrease again to reach zero around 5.5 km. A maximum of extinction occurs during

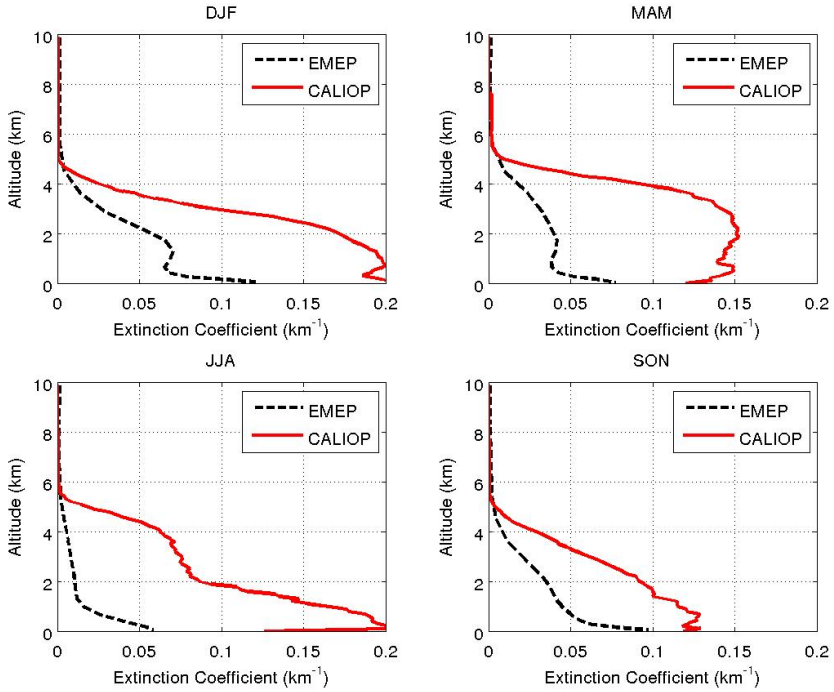


Figure 4.3.6: *Seasonal extinction vertical distributions measured by Caliop (averaged over the years 2006 to 2010) and the ones predicted by the Emep model for the region of Central Africa.*

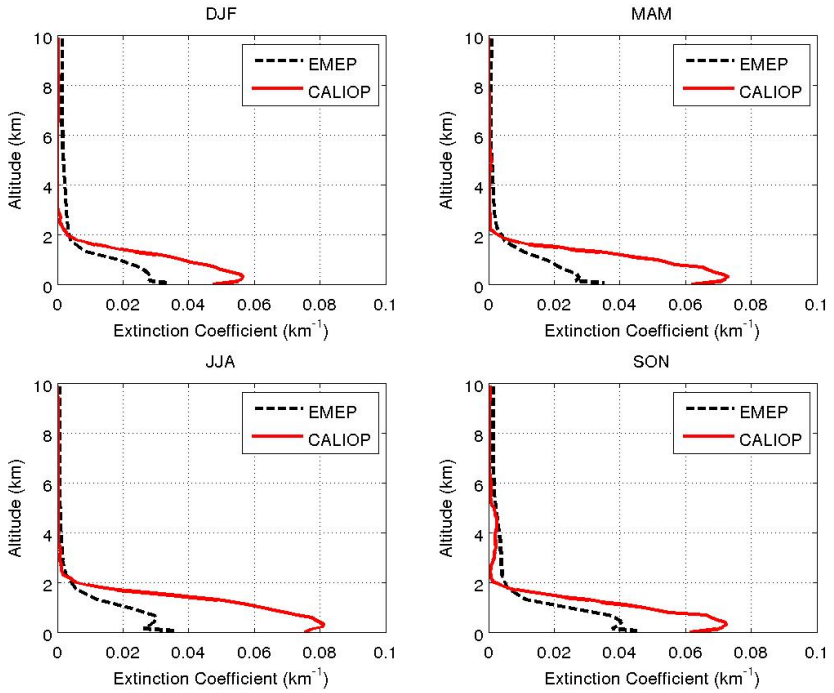


Figure 4.3.7: *Seasonal extinction vertical distributions measured by Caliop (averaged over the years 2006 to 2010) and the ones predicted by the Emep model for the region of Indian ocean.*

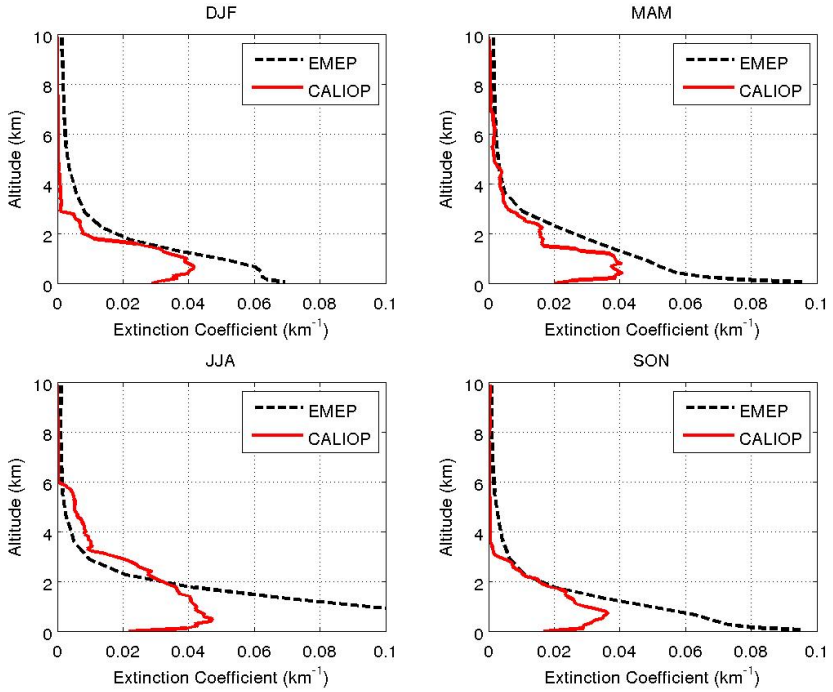


Figure 4.3.8: *Seasonal extinction vertical distributions measured by Caliop (averaged over the years 2006 to 2010) and the ones predicted by the Emep model for the region of North America.*

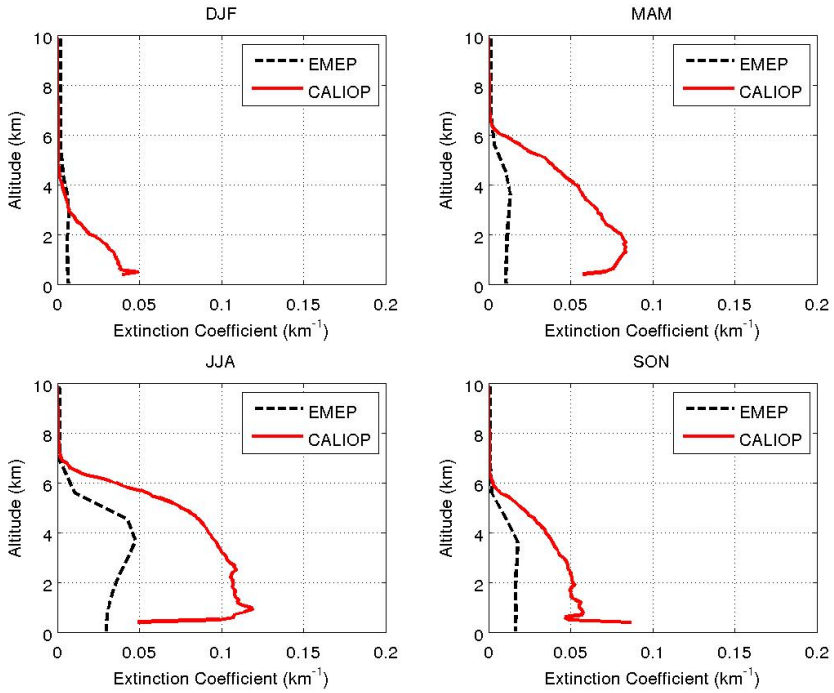


Figure 4.3.9: *Seasonal extinction vertical distributions measured by Caliop (averaged over the years 2006 to 2010) and the ones predicted by the Emep model for the region of Sahara.*

DJF near the surface, to finally decrease rapidly to reach zero around 5 km of altitude. During MAM, the extinction seems constant along the first three kilometers of altitude but then suddenly drops to reach zero around 5km of altitude. SON is the only season during which the extinction decreases regurlarly with altitude. Like in Amazonia, the Emep model fails to reproduce the observations. And like in Amazonia, the plots suggest a greater the mixing height in the Emep model.

In the Indian ocean, the vertical distribution is similar all the year long. The bulk of the extinction occurs below 2 km. But there is nevertheless a small increase during JJA, with a maximal extinction peaking around 0.08 $km^{-1}$. The Emep model computes the same shape as well as the same mixing altitude after which the extinction is almost zero. However in the two first kilometers, it is clearly underestimated of a factor 2.

In north America, the extinction seems to be staggered, decreasing steeply two times suggesting the contribution of two different aerosols with different physical and chemical properties. The altitudes at which the extinction drops vary a little bit with the seasons, reaching respectively about 3 km and 6 km during JJA when the extinction is stronger and decreasing respectively below 2km and around 3 km during DJF and MAM when the extinction is smaller. During SON, this two-step process cannot really be identified. The Emep model does not manage to reproduce this two-step decrease: the extinction decreases continuously with altitude, and is overestimated all the year long.

The Sahara is characterized by a clear seasonal pattern with low extinction during DJF, increasing during MAM, peaking during JJA and finally decreasing during SON. JJA peak is marked by high extinction coefficients until 5 km. Overall, DJF excepted, the extinction is still significant at 5 km of altitude; it is only around 6 km that it tends to zero. The Emep model clearly underestimates the extinction and shows higher extinction at 4 km than at the ground level whatever the season which does not match at all with the Caliop observations.

## 4.4 Sensitivity of the Emep model

It has been seen that most of the time the Emep vertical distributions for the five areas considered do not match with the Caliop observations. The extinction is either overestimated or underestimated. Moreover the Emep model usually fails to reproduce the same "shape" of distribution.

However the Emep model includes parameters whose values are subjected to many uncertainties. It was therefore possible to look at the sensitivity of the results while varying these parameters with the aim of adjusting these parameters to get a better matching between the model and the data. However the scope of the work has been restricted, so that only two parameters have been considered. Obviously the results would only be suggestions of adjustements for the Emep model and would require a deeper analysis.

The two parameters considered for the sensitivity tests are:

- The Organic Carbon background, that is to say the natural organic carbon in the atmosphere due to volcanoe activities, ocean adsorption... This value was initially set at 0.05 $\mu$ g(C)/$m^3$.

- The scale height $H_{OC}$, characterizing the exponential decrease of the organic carbon background with the altitude, such as:

$$OC^{\text{background}}(z) = OC^{\text{background}}_{z=0} * \exp(-\frac{z}{H_{OC}}) \tag{4.4.1}$$

  Its initial value set in Aerocom was 4.0 km. A logical comparison with the barometric formula (4.4.2) estimating the atmospheric pressure as a function of the altitude suggests that the scale height $H_{OC}$ should be in the same order of magnitude as the one in the barometric formula **if the organic carbon is assumed to have a constant mixing ratio at all altitudes.**

$$P(z) = P_0 * exp(\frac{-z}{H_0}) \tag{4.4.2}$$

  **where $H_0 = \frac{RT}{Mg} \simeq$ 8.4 km for the troposphere.**

However there are many other sources of organic carbon, with a large number of uncertainties. And looking at theses sources may lead to similar, better or worse, results than the ones described further.

### 4.4.1 Optical Depth

#### Organic Carbon Background Sensitivity

As regarding the Organic Carbon background, it clearly appears a linear relationship between the Organic Carbon background and the optical depth computed as shown on the figure 4.4.1 where the optical depth has been averaged on a global scale. Moreover, the same linear relationships are found if the $5° \times 5°$ areas previously selected are considered individually (see Appendix B.2.1).

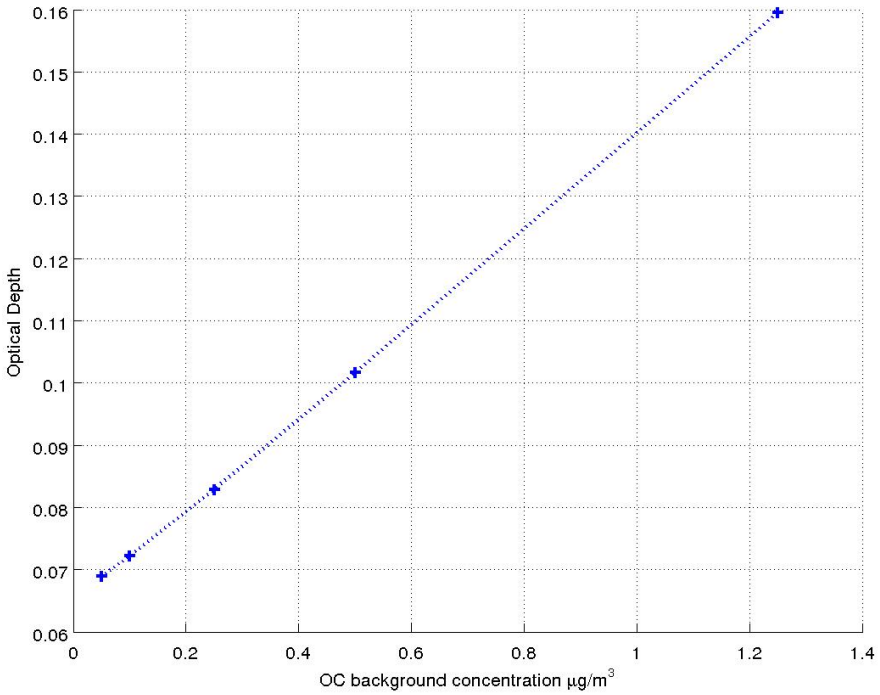


Figure 4.4.1: *Relationship between the Organic Carbon background on the world-average optical depth for the year 2009 according to the Emep model.*

| No. | Geographical Area | Constant ($m^3/\mu g(C)$) |
|---|---|---|
| 1* | Sahara | **0.0386** |
| 2* | Indian Ocean | 0.0768 |
| 3 | Pacific Ocean | 0.0713 |
| 4* | Central Africa | 0.0875 |
| 5* | Amazonia | 0.0984 |
| 6 | Russia | 0.0758 |
| 7 | Scandinavia | 0.0775 |
| 8 | China | 0.0723 |
| 9 | Paris | 0.0735 |
| 10* | North America | 0.0747 |
| | World-Average | 0.0754 |

** areas for which a seasonal pattern has been identified*

Table 4.4.1: Proportionality coefficient between the Organic Carbon background and the optical depth in the ten areas considered.

Considering the optical depth averaged on a world scale leads to the following equation:

$$\tau = C_{OC} * OC_{background} \tag{4.4.3}$$

with $C_{OC} = 0.0754$ m$^3/\mu$g(C).

However this constant is not uniform throughout the world. The table 4.4.1 shows indeed that nine of the ten areas have a constant close to the world-average constant while the one for the Sahara is divided by a factor two, explainable with the low relative humidity in this area decreasing the extinction coefficient and therefore the optical depth (Bian et al. 2009).

#### Scale Height Sensitivity

As for the scale height, the relationship appears to be more complicated, and not exponential contrary to what one could think according to the formula 4.4.1. The figure 4.4.2 shows indeed the world-average optical depth as a non-linear function of the inverse of the logarithm of the scale height. Once more, the same results are found if the $5° \times 5°$ areas are considered individually (see Appendix B.3.1).

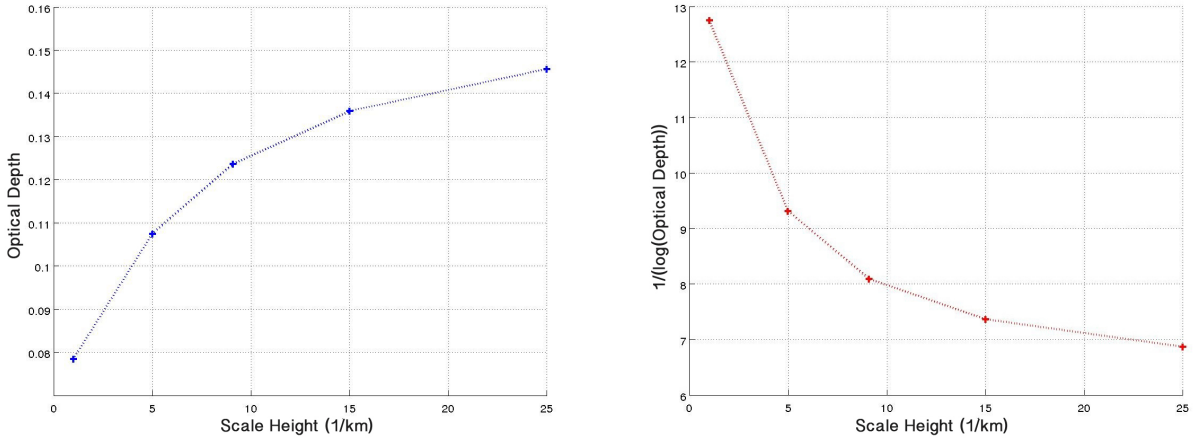


Figure 4.4.2: *Relationship between the scale height on the world-average optical depth for the year 2009 according to the Emep model. Left: $\tau$ is plotted as a function of the scale height. Right: the inverse of the logarithm of $\tau$ is plotted as a function of the scale height.*

### 4.4.2 Vertical Distribution

#### Organic Carbon Background Sensitivity

Five different Organic Carbon background have been implemented in the Emep model, all other parameters remaining equal. The Emep model predictions resulting have been compared with the world extinction vertical profile measured by Caliop and averaged over the years 2006 to 2010.

A change in the Organic Carbon background seems to only influence the intensity of the extinction and does not affect the shape of the vertical distribution, at least for the altitudes below 4km as shown on the figure 4.4.3. A linear relationship can actually be found such as:

$$\frac{b_{ext}(z, OC)}{b_{ext}(z, OC_{ref.})} - 1 = C(z) * \frac{OC}{OC_{ref.}} \tag{4.4.4}$$

where OC refers to the Organic Carbon background, $OC_{\text{ref}}$ to the initial Organic Carbon background (0.05 $\mu$gm$^{-3}$).

According to the previous results concerning the optical depth, it seemed reasonable that such a linear relationship was found. Nevertheless this relationship is a function of the altitude: *C(z)* increases with the altitude from $C(z = 0) = 0.04$ km$^{-1}$m$^3\mu$g$^{-1}$.

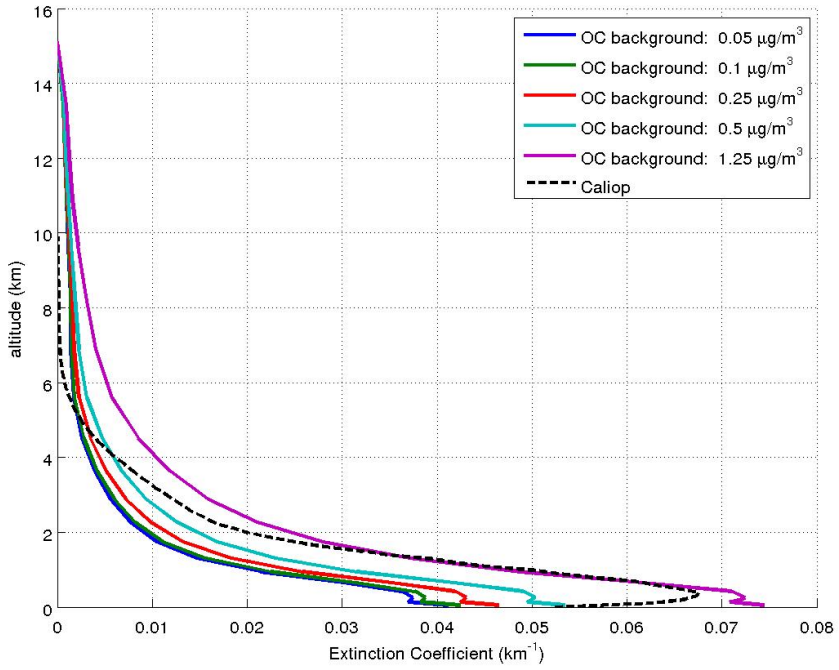


Figure 4.4.3: *Year-average vertical extinction coefficient profiles computed for five different Organic Carbon background and compared with the Caliop observations on a global scale.*

Considering that there should not be any reason for the sudden decrease of $b_{\text{ext}}^{\text{Caliop}}$ near the ground, the Emep model computed with an Organic Carbon background of 1.25 $\mu\text{gm}^{-3}$ is the one that matches the most with the Caliop data until the altitude of 2 km. In the higher altitudes, $b_{\text{ext}}^{\text{Caliop}}$ is decreasing faster than any of the Emep predictions.

On a regional scale, the same tendency is of course observed: the higher the organic carbon background, the higher the extinction. However, looking at the year-average extinction profiles as well as the seasonal profiles lead to contradictory conclusions as regarding the optimal Organic Carbon background. Moreover, one should keep in mind that increasing the organic carbon from other sources may give a more consistent matching between the model and the data.

The figures (4.4.4) and (4.4.5), representing the year-average extinction profiles for the Indian Ocean and North America, show indeed opposite trends. In the Indian Ocean, the Emep model computed with an Organic Carbon background of 1.25 $\mu\text{gm}^{-3}$ fits the best the observations, contrary to North America where it is the one with an Organic Carbon background of 0.05 $\mu\text{gm}^{-3}$.

As regarding the seasonal time basis, the vertical distributions are so irregular that none of the Emep model computed can be said to fit or not the observations. However, exceptions exist when the extinction vertical distribution is constant over the seasons. It is especially the case for the Indian Ocean, as it can be seen on the figure (4.4.6) where the Emep model with an Organic Carbon background of 1.25 $\mu\text{gm}^{-3}$ matches the most with the observations. However, the same discrepancies as described before can be observed: the decrease of the extinction computed is smoother than the one observed.

All the year-average and seasonal extinction profiles computed with different Organic Carbon backgrounds and compared with the Caliop observations for the areas of Sahara, Indian Ocean, Central Africa, Amazonia and North America are available in the Appendix (B.2.2).

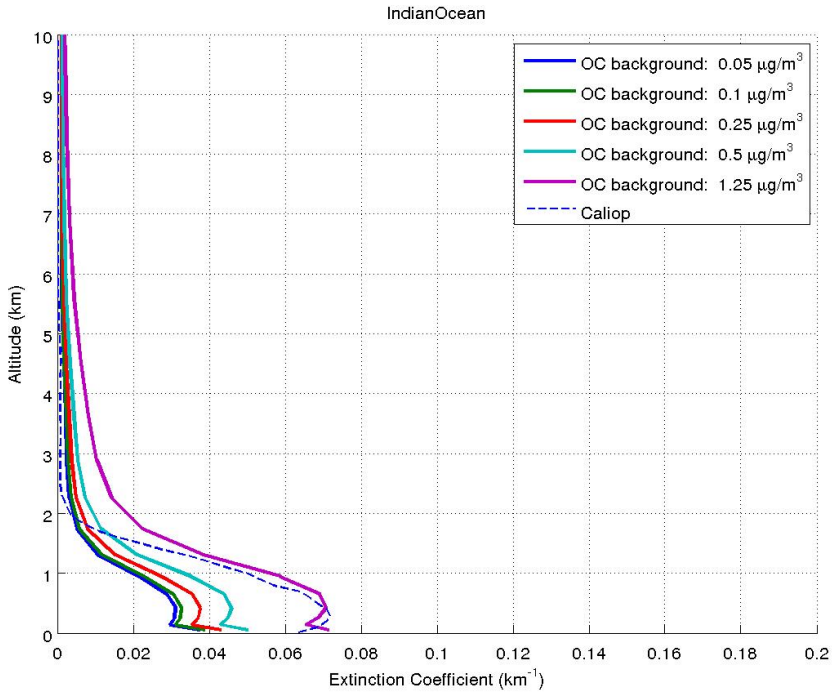


Figure 4.4.4: *Vertical extinction profiles computed for five different Organic Carbon background and compared with the Caliop observations on a year basis in the Indian Ocean.*

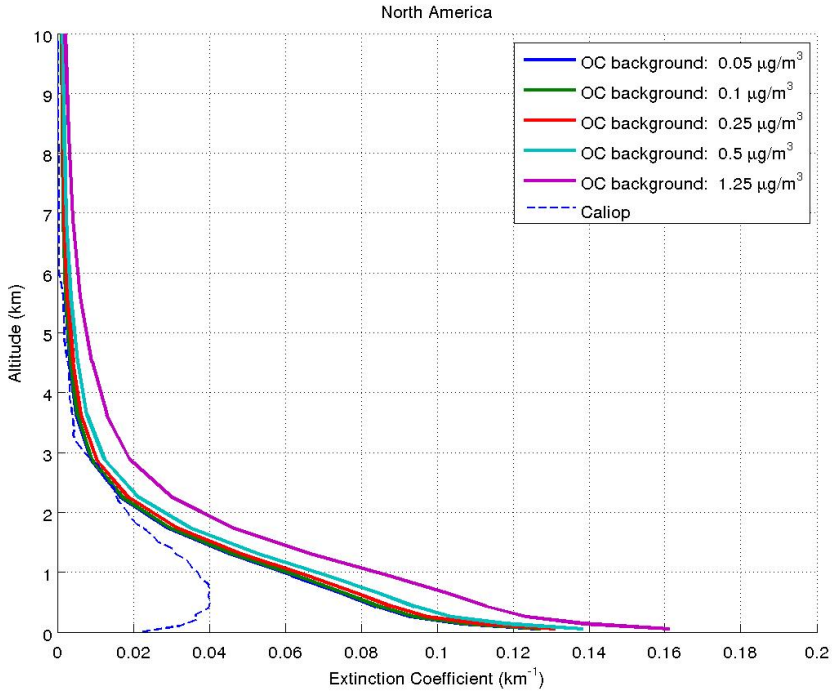


Figure 4.4.5: *Vertical extinction coefficient profiles computed for five different Organic Carbon background and compared with the Caliop observation on a year basis in North America.*

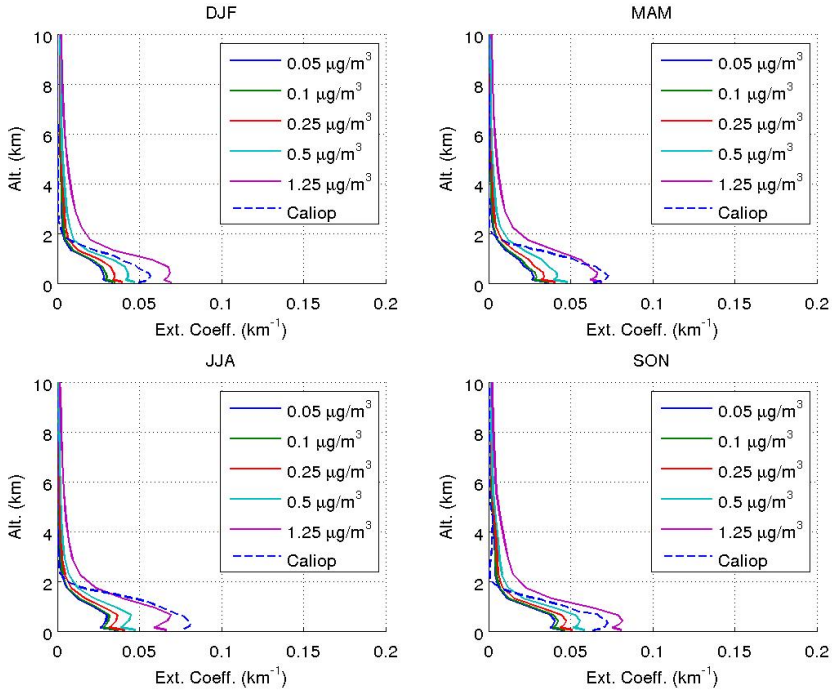


Figure 4.4.6: *Vertical extinction coefficient profiles computed for five different Organic Carbon background and compared with the Caliop observation on a seasonal basis in the Indian Ocean.*

### Scale Height Sensitivity

Five different scale heights, $H_{OC}$ have also been computed, with an Organic Carbon background set at 0.5 $\mu$gm$^{-3}$, all parameters remaining equal.

A change in the scale height affects the intensity of the decrease of the extinction with the altitude as shown on the figure 4.4.7. On a global scale, the vertical profiles are mainly differentiated above 1.5 km of altitude, that is to say when the extinction actually becomes lower than 0.02. The greater the scale height, the slower $b_{\text{ext}}$ is decreasing with altitude. And it can clearly be seen that the shape of the vertical profile measured by Caliop tends to the one computed with the lowest scale height, that is to say far from one could have expected when comparing with the barometric formula (4.4.2).

On a regional scale, the same conclusion can be drawn. Both the year-average and seasonal extinction distributions clearly show that the Emep model computed with the lowest scale height, that is to say 1 km$^{-1}$, fits the most with the observations. This is especially evident in the Indian Ocean as shown on the figure (4.4.8).

As regarding the seasonal time basis (see Appendix (B.3.2)), as already said before the vertical distributions are very irregular, making any conclusion difficult. However, it can be still observed that the smaller the scale height, the better the matching between the observations and the Emep model.

All the year-average and seasonal extinction profiles computed with different scale heights and compared with the Caliop observations for the areas of Sahara, Indian Ocean, Central Africa, Amazonia and North America are available in the Appendix (B.3.2).

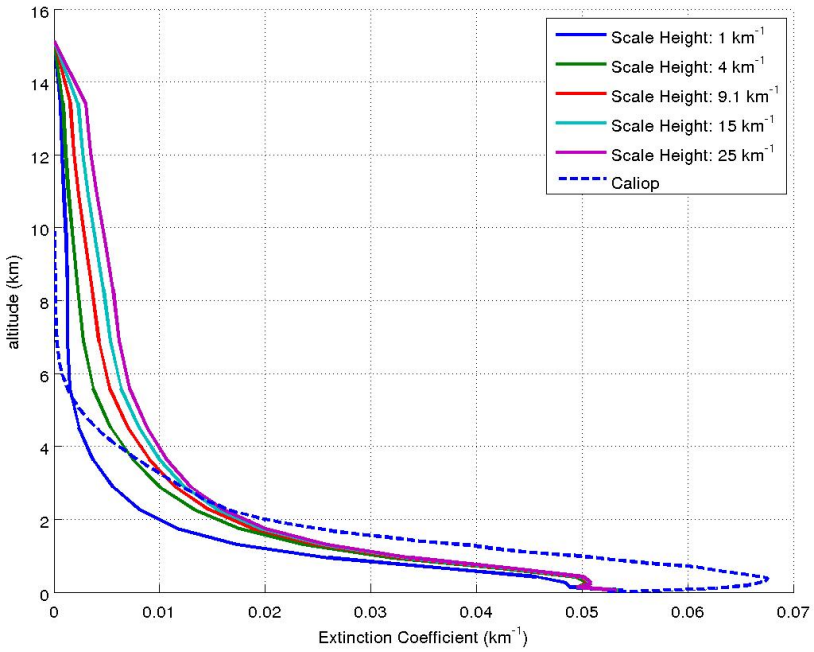


Figure 4.4.7: *Year-average vertical extinction coefficient profiles computed for five different scale heights and compared with the Caliop observation on a global scale.*

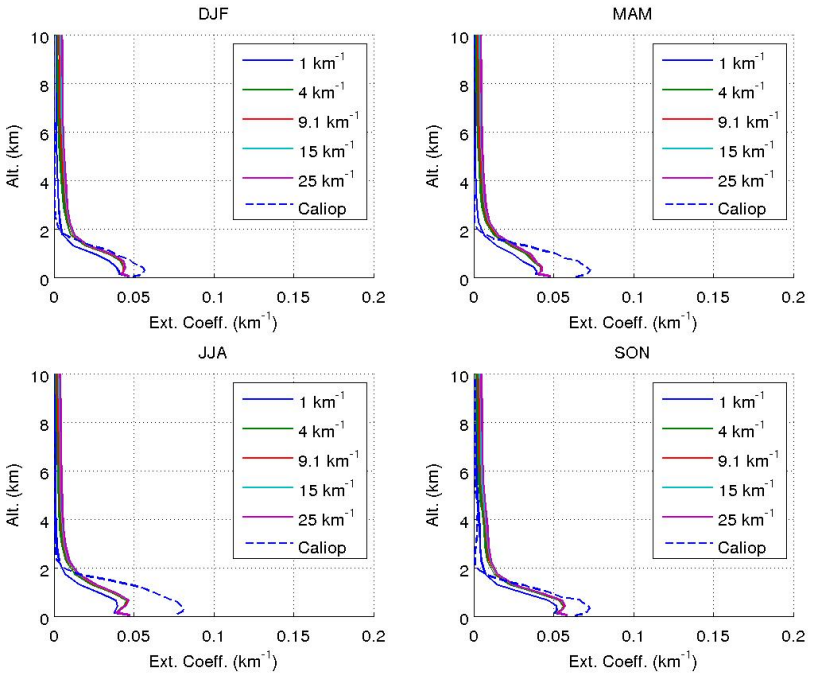


Figure 4.4.8: *Vertical extinction coefficient profiles computed for five different scale heights and compared with the Caliop observation on a seasonal basis in the Indian Ocean.*

### 4.4.3 Adjustement of the Organic Carbon Background and the Scale Height

On a global scale, according to what was previously said, it seems possible to find an (unique) adjustement of these two parameters to improve the matching between the Caliop observations and the Emep model predictions.

A low scale height and a high Organic Carbon background lead indeed to a better fit. The figure 4.4.9 shows the vertical extinction coefficient profile computed with an Organic Carbon background of 1.25 $\mu$gm$^{-3}$ and a scale height of 1 km$^{-1}$. A more precise analysis could determine a better fit, adjusting at best these two parameters.

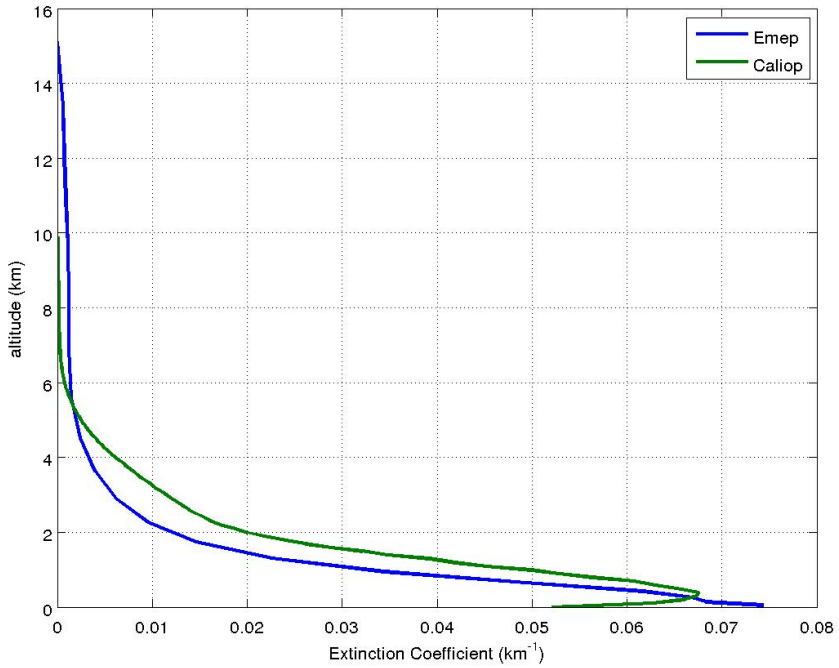


Figure 4.4.9: *Caliop observation compared with the Emep model computed with an Organic Carbon background of 1.25 $\mu gm^{-3}$ and a scale height of 1 $km^{-1}$.*

The regional analysis clearly showed that the Emep model computed with a small scale height gave the best fit with the Caliop observations. However the value found, $H_{OC} = 1$ km$^{-1}$, is four times smaller than the one initially set by Aerocom and eight times smaller than $H_0$, the scale height of the barometric formula (4.4.2). This result may also be suggesting that another source of organic carbon near the ground level should be considered. It is however hard to distinguish, especially due to the many uncertainties related to the organic carbon sources.

As regarding the Organic Carbon background, uncertainties remain. Moreover many other parameters, that have not been explored here, could affect the extinction vertical distribution. There is therefore still room for improvement of the Emep model.

# 5 Organic Aerosol Study

The first part of this thesis found relevant sources of comparison to ensure the quality of the Caliop data and suggested improvements for the Emep model to get a better fit between the observations and the predictions. It is therefore now possible to combine the information computed by the Emep model with the satellite observations in order to make estimations of the organic aerosol contribution around the world.

## 5.1 Procedure

In section 4.3 the Modis data were identified as a relevant source of comparison for the Caliop data. However, it has clearly been seen that observations do not always match between each other as well as the aerosol Emep predictions do not always match with the observations. Correlation criteria were defined to compute information about organic aerosol only when the observations and the model matched and a procedure, detailled below, has been developed, inspired by the algorithm developed in the previous chapter.

The figure 5.1.1 shows a sketch of the corresponding algorithm and the correponding MatLab code, part of the file *OrganicAerosolStudy.m* is available in Appendix C.3.

- Previous to applying the algorithm, the world map is divided into $5° \times 5°$ areas, representing in total 2592 areas.
- For each area, the year-trend optical depth measured by Caliop and Modis has been calculated with the previous algoritm : $Caliop_{average}(month)$ and $Modis_{average}(month)$. The year-trend optical depth is also calculated for the Emep model, $Emep_{average}(month)$.
- Since observations are not always available, the number of months, $s$, for which both Modis and Caliop data are available is calculated.
- If $s$ is greater than 5, then the correlation coefficient [1], $Rmc$, between the two data series, $Caliop_{average}(month)$ and $Modis_{average}(month)$, is calculated.
- If $Rmc$ is greater than 0.5, then the average of the data series is calculated: $satellite_{average}(month)$.
- The correlation coefficient, $Res$, between the satellite average data serie, $satellite_{average}(month)$, and the Emep data, $Emep_{average}(month)$, is computed.
- If $Res$ is greater than 0.5, then the contribution of organic aerosol [2] to the optical depth computed by the Emep model is assumed to be "right". And the optical depth corresponding to the only effect of the organic aerosol, $\tau_{OM}$, is calculated such as:

$$\tau_{OM} = \frac{\tau_{tot}^{Obs.}}{\tau_{tot}^{Emep}} * \tau_{OM}^{Emep} \tag{5.1.1}$$

The threshold values for the parameteres $s$, $Rmc$ and $Res$ have been set, respectively at 5, 0.5 and 0.5, so that the calculations are made for a reasonnable number of areas. Initially set at more stringent values, respectively 5, 0.75 and 0.75, correlation between the Caliop data, the Modis data and the Emep model was found for only 5.2 % of the 2592 areas. The current set of values allows computation for 18.5 % of the areas, which corresponds to 25 to 30 % of the coverage of the satellites given that they do not perform measurements in the very high and very low latitudes.

## 5.2 Computation of the Optical Depth due to Organic Aerosols

The different results computed by the algorithm previously described are shown below (Figures 5.2.1, 5.2.2, 5.2.3).

[1] The correlation coefficient used here is the "Pearson product-moment correlation coefficient" between two variables.
[2] The organic aerosol considered encompass primary organic matter (POM) and secondary organic aerosol (SOA).

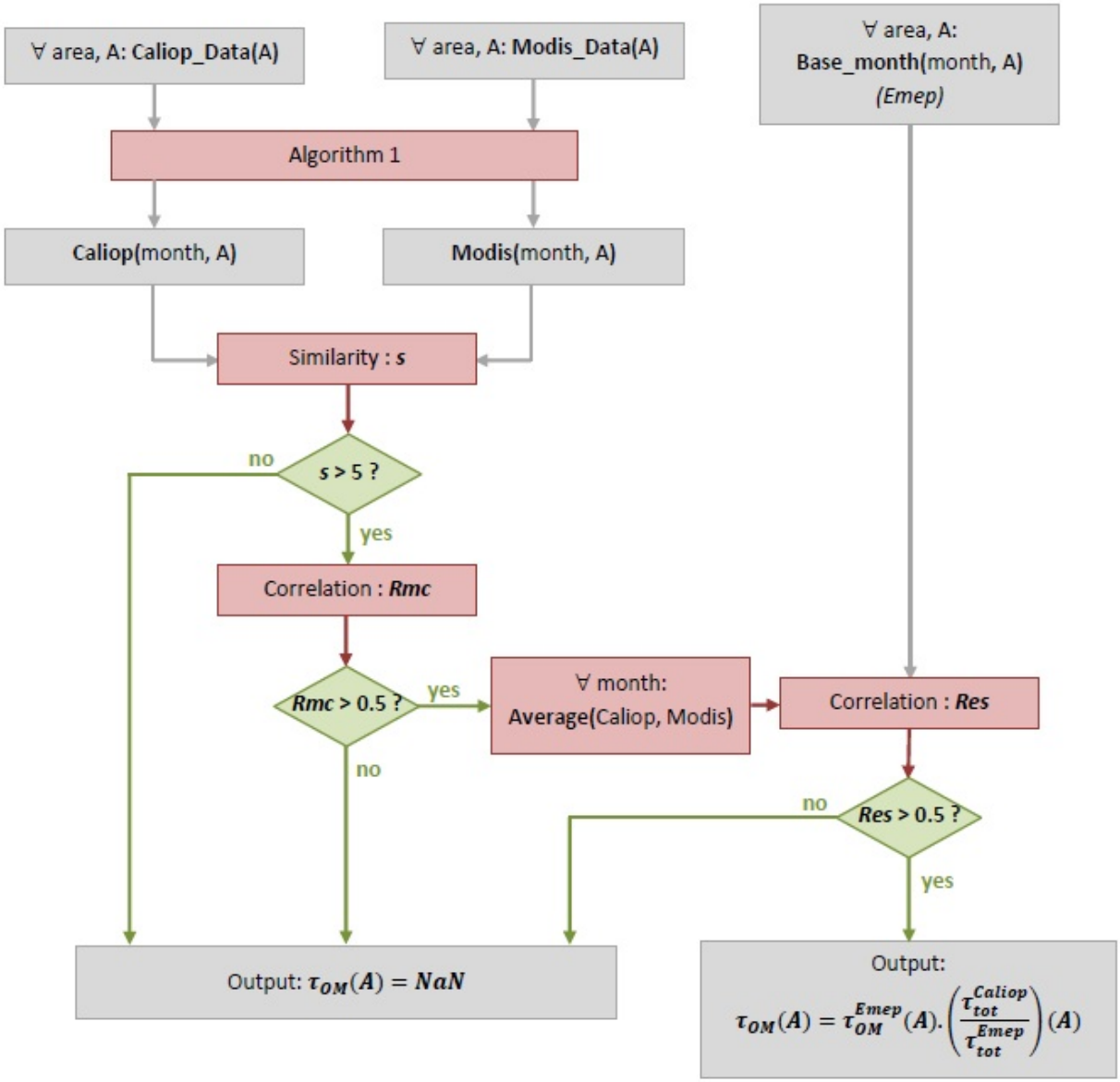


Figure 5.1.1: *Description of the algorithm used to calculate the contribution of organic aerosol to the total optical depth.*

Thus, the figure 5.2.1 shows the year-average contribution of organic aerosol as a fraction of the total optical depth around the world. Correlation between the Caliop data, the Modis data and the Emep model was mainly found in areas between 20°S and 40°N. About 60% of the 720 5°x5° areas in this region are represented on the figure 5.2.1. Almost no correlation was found at latitudes higher than 50°N and lower than 50°S providing very few information for North America, Europe and Russia/North Asia.

Different interesting characteristics can nevertheless be observed:

- In Equatorial Forest areas such as Central Africa and Amazonia, organic aerosols contribute to the bulk of the total optical depth, usually more than 70 %.
- In the Atlantic, Indian and Pacific oceans, the contribution of organic aerosols seems to be uniform, accounting for about 40 % of the total optical depth. Nevertheless, this number drops to 20 % in the Austral ocean.
- Despite few areas where a correlation was found, Europe seems to be characterized by a low contribution

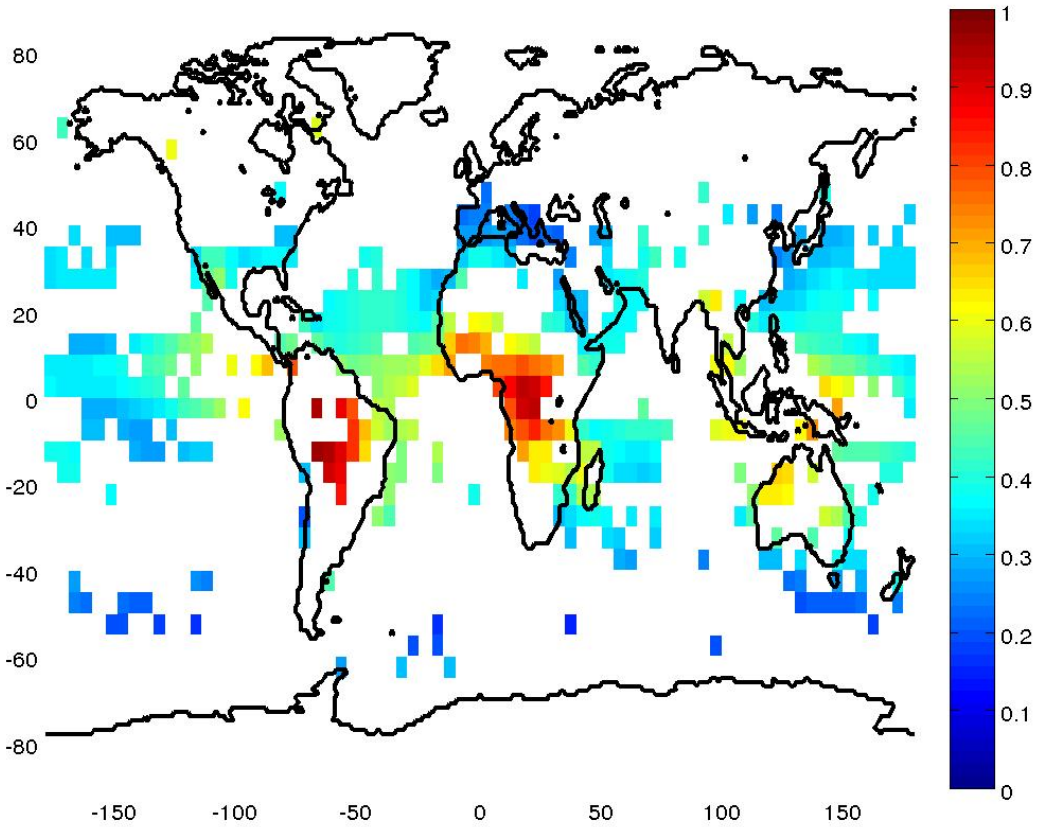


Figure 5.2.1: *Year-average contribution of organic aerosol as a fraction of the optical depth around the world when a correlation between the Caliop data, the Modis data and the Emep model has been found.*

of organic aerosols to the total optical depth. It is indeed likely that pollutants, $SO_4$ and $NO_3$, play a greater role.

The figure 5.2.2 shows the year-average organic aerosol optical depth in absolute numbers that is to say the optical depth corresponding to the only effect of organic aerosols. And it can be seen that organic aerosols have a significant influence in a wide area in Central Africa with an average optical depth greater than 0.2 and a peak at about 0.38 just below the Equator. Amazonia and South-Est Asia seem also concerned by the influence of organic aerosols, some areas in these two regions are indeed characterized by an optical depth greater than 0.2. However the algorithm gives too few 5°x5° results to draw any serious conclusion.

It can be surprising that Amazonia has a much lower optical depth due to aerosols than Central Africa. However according to the figure 5.2.1 the organic aerosols are clearly dominant in this region, which still makes the results logical. This suggests that Amazonia experiences less biomass burning than Central Africa.

It seems also surprising that the contribution of organic aerosols to the total optical depth is quite important in the Atlantic ocean where sea salts should be dominant. The figure 5.2.3 shows indeed that the contribution of sea salts as a fraction of the total optical depth is relatively important in the Pacific ocean, the Indian ocean and the Southern ocean but not in the Atlantic ocean. However, the westerly winds are likely responsible for aerosol particles transportation from Africa above the Atlantic ocean towards America, explaining why the sea salt contribution is minor in this area.

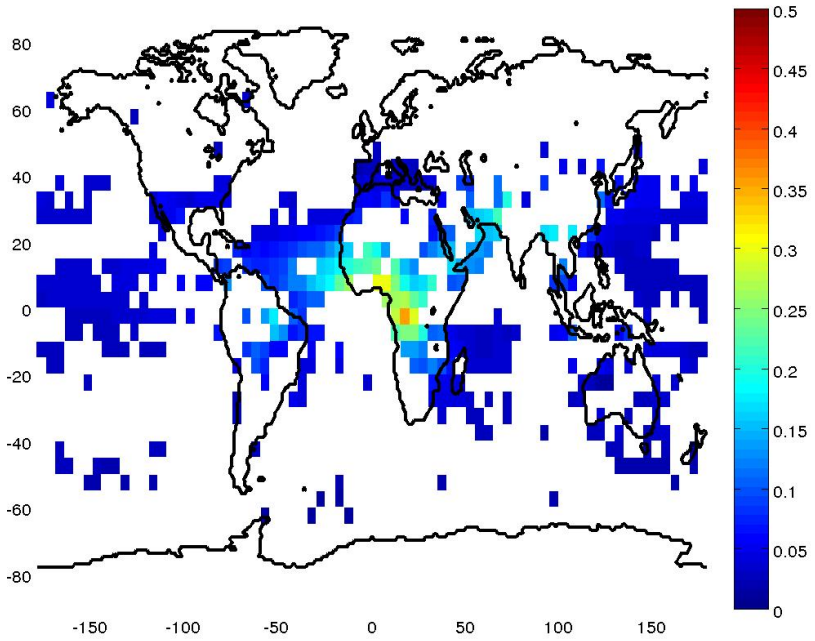


Figure 5.2.2: *Optical depth attributable to organic aerosols (in absolute numbers) around the world for the areas where a correlation between the Caliop data, the Modis data and the Emep model has been found.*

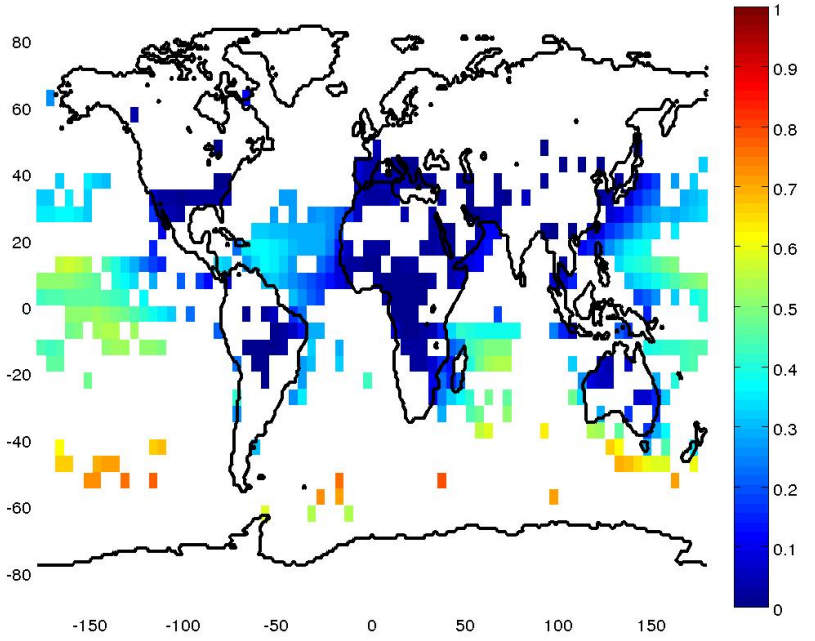


Figure 5.2.3: *Contribution of sea salts as a fraction of the total optical depth around the world for the areas where a correlation between the Caliop data, the Modis data and the Emep model has been found.*

## 5.3 Extinction Vertical Profiles

Proceeding the same way as described before, it is also possible to look at the vertical distribution of organic aerosols in areas where a correlation between the Caliop data, the Modis data and the Emep model has been found.

Therefore new areas have been selected to look at the extinction vertical distribution due to organic aerosols. These areas have been chosen such as a correlation was found in the surrounding areas. The five areas selected are shown on the figure 5.3.1 and the coordinates are defined in the table 5.3.1.

| No. | Name* | Coordinates | Aerosol Contribution |
|---|---|---|---|
| 1 | Equatorial Africa II | [0-5]°S x [15-20]°E | OA |
| 2 | Amazonia II | [10-15]°S x [55-60]°W | OA |
| 3 | Pacific Ocean II | [25-30]°N x [140-145]°E | Sea Salt |
| 4 | Indian Ocean II | [10-15]°S x [60-65]°E | Sea Salt |
| 5 | SouthWest Europe | [35-39]°N x [0-5]°E | $SO_4$ & $NO_3$ |

** These names are the ones used afterwards to refer to these areas.*

Table 5.3.1: Details of the new 5 areas selected.

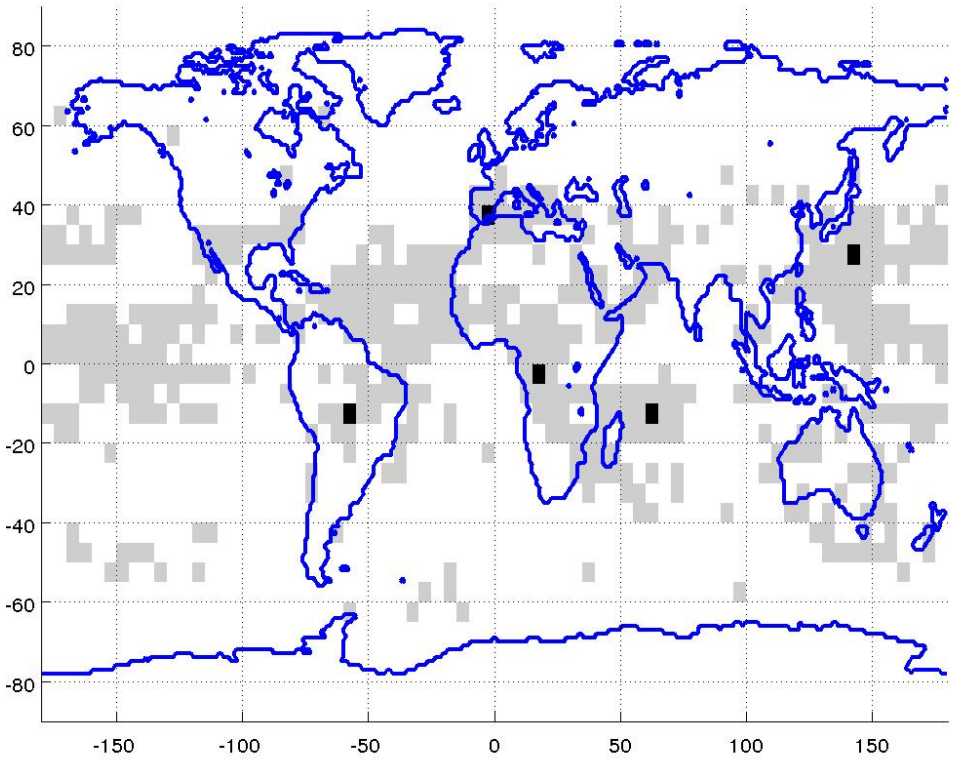


Figure 5.3.1: *The five areas selected (in black) have been chosen such as to be surrounded by areas where a correlation between the Caliop and the Modis data has been found (in grey).*

Using the Caliop extinction coefficient measurements and the Emep computations, the organic aerosol

vertical distribution has been estimated such as, for each area $a$, for each altitude $k$:

$$\gamma^{OA}(a,k) = \gamma^{OA}_{Emep}(a,k) * \frac{\gamma_{Caliop}(a,k)}{\gamma_{Emep}(a,k)} \tag{5.3.1}$$

Given that the altitudes at which Caliop performs measurements do not match with the ones computed in the Emep model, a specific transformation of the data needed to be applied in order to compute the equation 5.3.1. Caliop measurements have indeed one hundred altitude levels ranging between 0 and 10 km of altitude while the Emep model considers only twenty altitude levels ranging between 0 and 15 km of altitude. Therefore the Caliop data have been approximated so to fit with the altitudes of the Emep model. The Matlab code *ExtinctionCoefficient.m* performing these approximations and computing the organic aerosol vertical distributions for the five areas considered above is available in the Appendix C.4.

The seasonal extinction measured by Caliop - and averaged over the years 2006 to 2010 - and the estimated extinction due to organic aerosols computed with the Emep model predictions and the Caliop observations according to the equation 5.3.1 are shown below for the five areas previously selected.

As already noticed, there is a-priori no "atmospherical reason" of the sudden decrease of the extinction coefficient that appears in most cases near the surface, but distortion occurs near the surface because of a low signal-to-noise ratio. Therefore the following analysis does not take into account the extinction in the lowest part of the atmosphere.

More precisely Central Africa II is logically characterized by an important contribution of organic aerosol to the total extinction all the year long as shown on the figure 5.3.2. The same characteristics, in terms of seasonal pattern and vertical distribution, are found as in the previous chapter where a different region of Central Africa was considered. The same shape of vertical distribution is however found throughout the seasons: the bulk of the extinction occurs until 4 km of altitude and then the extinction decreases until zero at about 6 km.

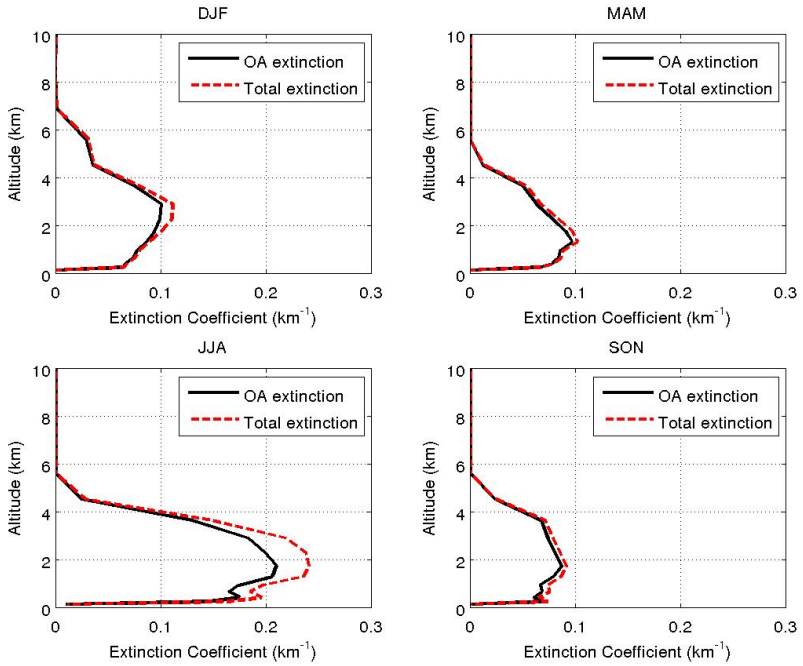


Figure 5.3.2: *Seasonal extinction measured by Caliop (averaged over the years 2006 to 2010) and the estimated extinction due to organic aerosols computed with the Emep model predictions and the Caliop observations according to the equation 5.3.1 in Central Africa II.*

Amazonia II presents the same seasonal extinction profiles as in Amazonia. The figure (5.3.3) shows indeed that the bulk of extinction occurs during the fall, and the summer to a lesser extent. The organic aerosols account for almost all the extinction, especially during the winter and the spring. Other species in the first three kilometers play a minor role in the extinction during the summer and the fall.

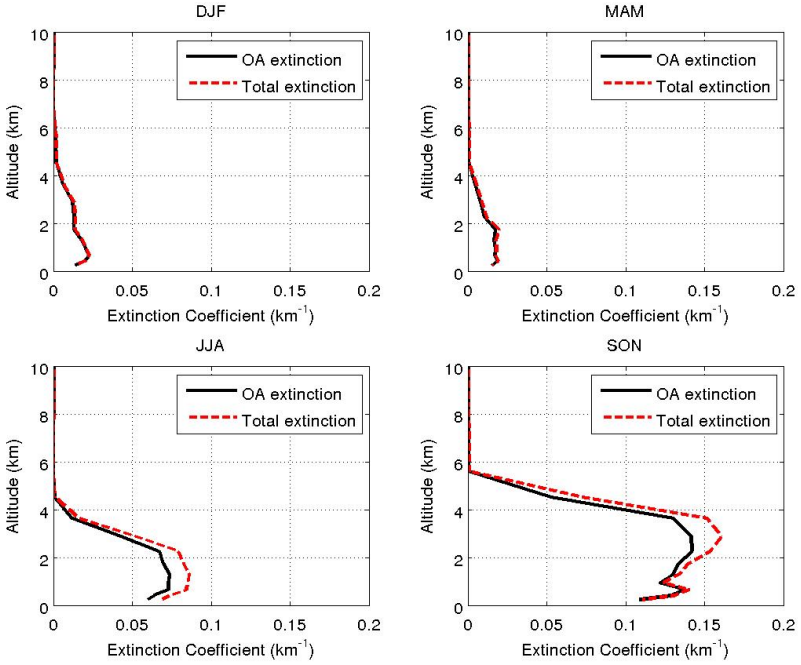


Figure 5.3.3: *Seasonal extinction measured by Caliop (averaged over the years 2006 to 2010) and the estimated extinction due to organic aerosols computed with the Emep model predictions and the Caliop observations according to the equation 5.3.1 in the area Amazonia II.*

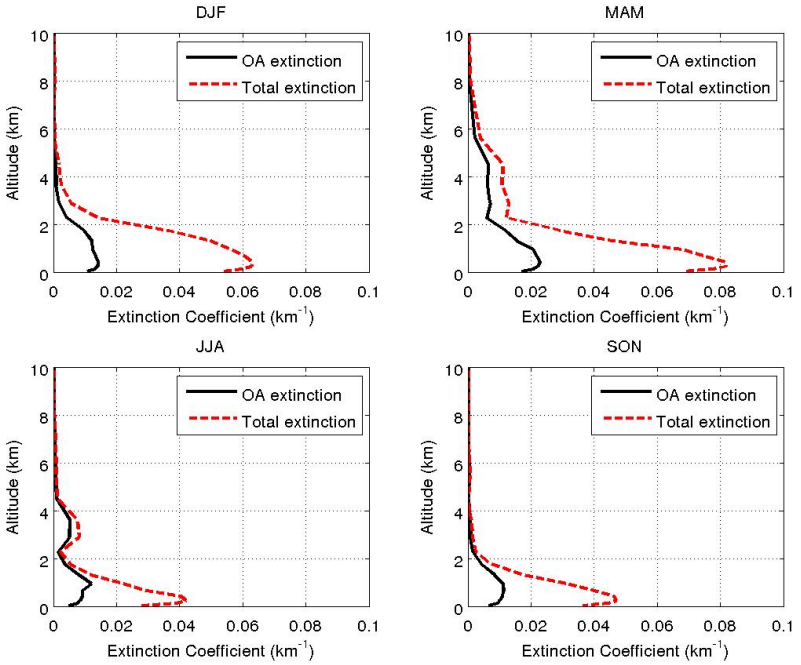


Figure 5.3.4: *Seasonal extinction measured by Caliop (averaged over the years 2006 to 2010) and the estimated extinction due to organic aerosols computed with the Emep model predictions and the Caliop observations according to the equation 5.3.1 in the area Pacific Ocean II.*

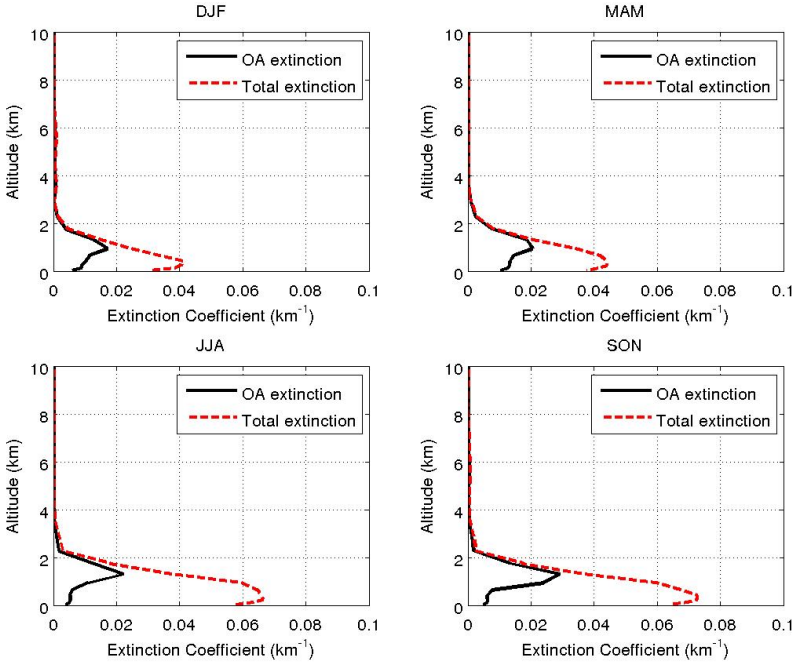


Figure 5.3.5: *Seasonal extinction measured by Caliop (averaged over the years 2006 to 2010) and the estimated extinction due to organic aerosols computed with the Emep model predictions and the Caliop observations according to the equation 5.3.1 in the area Indian Ocean II.*

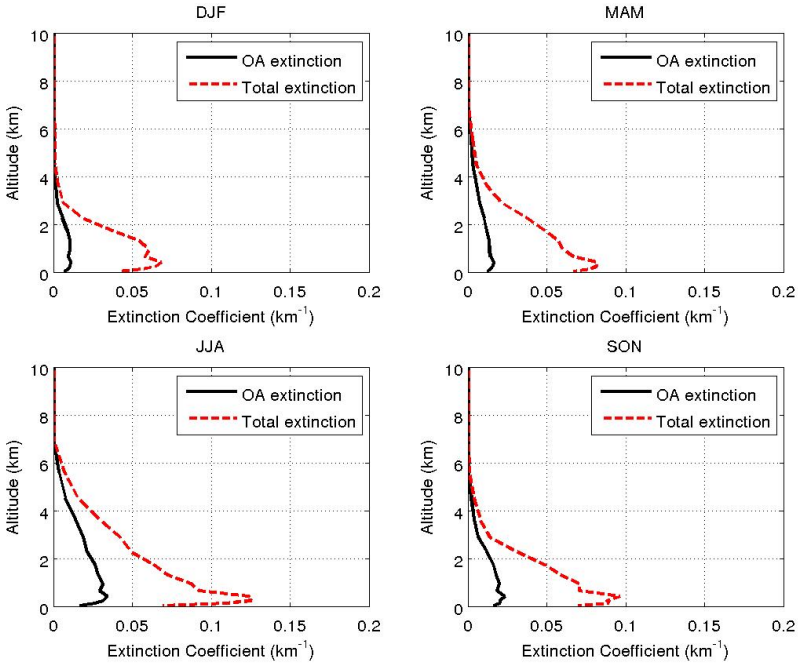


Figure 5.3.6: *Seasonal extinction measured by Caliop (averaged over the years 2006 to 2010) and the estimated extinction due to organic aerosols computed with the Emep model predictions and the Caliop observations according to the equation 5.3.1 in the area SouthWest Europe.*

The Indian Ocean II presents the same characteristics in terms of extinction profiles as the area considered in the previous chapter. As already noticed before, if the sea salts remain the main contributors to extinction, the organic aerosols still contribute for a large share. It can be observed that their contribution is small near the surface, and then increases until about 1.5 km of altitude where it accounts for almost all the extinction. This distribution actually reflects that the extinction due to sea salts only occurs near the surface, mainly because sea salts originate from a surface source.

This conclusion seems to extend to the Pacific Ocean II. However, contrary to the Indian Ocean II, at high altitudes the organic aerosols do not always contribute to the bulk of extinction.

SouthWest Europe is characterized by a similar seasonal vertical profile along the year as shown on the figure 5.3.6. A very slight increase of the extinction can nevertheless be observed during the summer. The total extinction decreases regurlarly from the ground level to reach zero between 4 and 6km according to the season. The extinction due to organic aerosols seems to be constant with altitude, and accounts for a minor contribution to the extinction. As South-West Europe encompasses the Straits of Gibraltar, this area is logically affected by pollution from shipping, so that $SO_4$ and $NO_3$ are the main contributors to the total extinction.

# 6 Conclusion

This work showed that comparing different optical depth observations is not obvious and not always relevant, for different reasons. Firstly, the measurements performed by the instruments, Caliop, Modis and Aeronet, do not lead to retrievals of the same physical product. Secondly, the quality of the data retrieved can be uneven, affecting the global relevancy of the comparison. Despite these differences between the datasets, seasonal patterns were identified corresponding to what one could expect from one area to another one, with nevertheless differences in terms of intensity of the optical depth. As for the extinction vertical distribution, big differences appeared between the Caliop observations and the Emep model predictions in the five different areas considered. Despite a similar order of magnitude, the shape of the profiles are perceptibly distinct beyond the fact that the Emep aerosol model usually computes smooth profiles while the Caliop observations are as expected more irregular.

The algorithm developed to compute the contribution of organic aerosols to the total optical depth according to the matching between the observations and the Emep model predictions leads to the most interesting conclusions. Organic aerosols appeared indeed to contribute to the bulk of the extinction in Equatorial areas. Nevertheless discrepancies in terms of intensity of the corresponding optical depth exist between Amazonia and Central Africa: this latter is indeed characterized by an optical depth due to organic aerosols approximately two times greater than in Amazonia. The computation also revealed the relatively high contribution of organic aerosols over the Pacific and Indian oceans, near 40 %, while sea salts account for the rest of the extinction. Unfortunately, most of the results computed are in a limited range of latitudes, providing very few information for Asia, Europe and North America.

Eventually, organic aerosol vertical distribution derived from the combination of the Emep predicitions and the Caliop observations provided interesting conclusions. It has been indeed seen that both Indian and Pacific oceans are characterized by an increasing contribution of organic aerosols with altitude, so that the contribution of sea salts to extinction mainly occur near the surface. In the equatorial forest areas, organic aerosols clearly contribute to all the extinction during the winter and the summer while some other species can appear and play a minor role during the summer and the fall. However too few areas were studied to generalize these conclusions.

And as the sensitivity tests showed, there is also room for improvement of the Emep model. A small scale height and a high Organic Carbon background greatly improved the matching between the Caliop observations and the Emep predictions on a global scale. And a small scale, that is to say considering the $5° \times 5°$ areas, contrary conclusions came up as regarding the optimal Organic Carbon background. But it has clearly been seen that the smaller the scale height, the better the matching between the Caliop observations and the Emep model, confirming what had already been seen on a large scale. Moreover more than two of the parameters of the Emep model can be adjusted to get a better matching with the Caliop observations. This also raises the suggestion that the Emep model might be more accurate on a global scale than on small scales.

The Caliop observations could also be used in a different way: anthropogenic emissions are missing -or highly uncertain- in many areas and could therefore be estimated from the observations, in order to be finally included in the Emep model.

Further investigastions can therefore be done, so that the Emep model would provide the most accurate information available on organic aerosols accross the globe. More work is needed, including comparison with other observations, like aircraft aerosol measurements (see Appendix A), to draw more precise conclusions.

# References


A. Valdebenito, S. T. and Schulz, M.: The EMEP data assimilation system: Further development and integrity test results, Norwegian Meteorological Institute, p. 27, 2012.

AeroCom Interface - Caliop3 vs. Aeronet: AeroCom phase II Interface - Model versus data, model maps and scores, `http://aerocom.met.no/cgi-bin/aerocom/`, 2012.

Aerocom, website: `www.aerocom.met.no`.

Aeronet, website: Aerosol Robotic Network, Goddard Space Flight Center, `http://aeronet.gsfc.nasa.gov/`, 2012.

Anderson, J. C., J. Wang, J. Z., M. Petrenko, G. G. L., and Ichoku, C.: Accuracy Assessment of Aqua-MODIS aerosol optical depth over coastal regions: importance of quality flag and sea surface wind speed, Atmospheric Measurement Techniques Discussions, 2012.

Bian, H., Chin, M., Rodriguez, J. M., Yu, H., Penner, J. E., and Strahan, S.: Sensitivity of aerosol optical thickness and aerosol direct radiative effect to relative humidity, ATMOSPHERIC CHEMISTRY AND PHYSICS, 9, 2375–2386, 2009.

Charlson, R., Schwartz, S., Hales, J., Cess, R., Coakley, J., Hansen, J., and Hofmann, D.: CLIMATE FORCING BY ANTHROPOGENIC AEROSOLS, SCIENCE, 255, 423–430, 1992.

Chew, B. N., Campbell, J. R., Reid, J. S., Giles, D. M., Welton, E. J., Salinas, S. V., and Liew, S. C.: Tropical cirrus cloud contamination in sun photometer data, ATMOSPHERIC ENVIRONMENT, 45, 6724–6731, 2011.

Chin, M., Ginoux, P., Kinne, S., Torres, O., Holben, B., Duncan, B., Martin, R., Logan, J., Higurashi, A., and Nakajima, T.: Tropospheric aerosol optical thickness from the GOCART model and comparisons with satellite and Sun photometer measurements, JOURNAL OF THE ATMOSPHERIC SCIENCES, 59, 461–483, 2002.

Chylek, P. and Wong, J.: EFFECT OF ABSORBING AEROSOLS ON GLOBAL RADIATION BUDGET, GEOPHYSICAL RESEARCH LETTERS, 22, 929–931, 1995.

Climate Change 2007: Synthesis Report: .

Donahue, N. M., Robinson, A. L., and Pandis, S. N.: Atmospheric organic particulate matter: From smoke to secondary organic aerosol, ATMOSPHERIC ENVIRONMENT, 43, 94–106, 2009.

D.Simpson, A. Benedictow, H. B., Bergström R., F. H., Gauss M., H. G., Jenkin M.W., J. J., Nyiri A., S. V., Tsyro S., T. J., A., V., and P., W.: The EMEP/MSC-W Model - User s Guide, 2011.

Dubovik, O. and King, M.: A flexible inversion algorithm for retrieval of aerosol optical properties from Sun and sky radiance measurements, JOURNAL OF GEOPHYSICAL RESEARCH-ATMOSPHERES, 105, 20 673–20 696, 2000.

Dubovik, O., Smirnov, A., Holben, B., King, M., Kaufman, Y., Eck, T., and Slutsker, I.: Accuracy assessments of aerosol optical properties retrieved from Aerosol Robotic Network (AERONET) Sun and sky radiance measurements, JOURNAL OF GEOPHYSICAL RESEARCH-ATMOSPHERES, 105, 9791–9806, 2000.

EMEP, website: `http://www.emep.int/`.

Eriksson, P.: Remote Sensing Course: Radiative transfer theory, 2012.

Heald, C., Jacob, D., Park, R., Russell, L., Huebert, B., Seinfeld, J., Liao, H., and Weber, R.: A large organic aerosol source in the free troposphere missing from current models, GEOPHYSICAL RESEARCH LETTERS, 32, 2005.

Heald, C. L., Jacob, D. J., Turquety, S., Hudman, R. C., Weber, R. J., Sullivan, A. P., Peltier, R. E., Atlas, E. L., de Gouw, J. A., Warneke, C., Holloway, J. S., Neuman, J. A., Flocke, F. M., and Seinfeld, J. H.: Concentrations and sources of organic carbon aerosols in the free troposphere over North America, JOURNAL OF GEOPHYSICAL RESEARCH-ATMOSPHERES, 111, 2006.

Hess, M., Koepke, P., and Schult, I.: Optical properties of aerosols and clouds: The software package OPAC, BULLETIN OF THE AMERICAN METEOROLOGICAL SOCIETY, 79, 831–844, 1998.

H.Seinfeld, J. and N.Pandis, S.: Atmospheric chemistry and physics - From air pollution to climate change, , 1998.

Huang, J., Hsu, N. C., Tsay, S.-C., Jeong, M.-J., Holben, B. N., Berkoff, T. A., and Welton, E. J.: Susceptibility of aerosol optical thickness retrievals to thin cirrus contamination during the BASE-ASIA campaign, JOURNAL OF GEOPHYSICAL RESEARCH-ATMOSPHERES, 116, 2011.

Koffi, B., Schulz, M., Breon, F.-M., Griesfeller, J., Winker, D., Balkanski, Y., Bauer, S., Berntsen, T., Chin, M., Collins, W. D., Dentener, F., Diehl, T., Easter, R., Ghan, S., Ginoux, P., Gong, S., Horowitz, L. W., Iversen, T., Kirkevag, A., Koch, D., Krol, M., Myhre, G., Stier, P., and Takemura, T.: Application of the CALIOP layer product to evaluate the vertical distribution of aerosols estimated by global models: AeroCom phase I results, JOURNAL OF GEOPHYSICAL RESEARCH-ATMOSPHERES, 117, 2012.

Levy, R., Remer, L., Martins, J., Kaufman, Y., Plana-Fattori, A., Redemann, J., and Wenny: Evaluation of the MODIS aerosol retrievals over ocean and land during CLAMS, JOURNAL OF THE ATMOSPHERIC SCIENCES, 62, 974–992, 2005.

Levy, R. C., Lorraine A. Remer, D. T., and S. Mattoo, Y. J. K.: Algorithm for remote sensing of tropospheric aerosol over dark targets from MODIS, 2009.

Levy, R. C., Remer, L. A., Kleidman, R. G., Mattoo, S., Ichoku, C., Kahn, R., and Eck, T. F.: Global evaluation of the Collection 5 MODIS dark-target aerosol products over land, ATMOSPHERIC CHEMISTRY AND PHYSICS, 10, 10 399–10 420, 2010.

Lin, J. E. P., S. Sillman, D. T., and Lelieveld, J.: Global modeling of SOA formation from dicarbonyls,epoxides,organic nitrates and peroxides, GEOPHYSICAL RESEARCH LETTERS, 2012.

Lohmann, U. and Feichter, J.: Global indirect aerosol effects: a review, ATMOSPHERIC CHEMISTRY AND PHYSICS, 5, 715–737, 2005.

MODIS, FAQ: MODIS Frequently Asked Questions, `http://www.sat.dundee.ac.uk/modis-faq.html/`, 2012.

MODIS, website: .

Morgan, W. T., Allan, J. D., Bower, K. N., Capes, G., Crosier, J., Williams, P. I., and Coe, H.: Vertical distribution of sub-micron aerosol chemical composition from North-Western Europe and the North-East Atlantic, ATMOSPHERIC CHEMISTRY AND PHYSICS, 9, 5389–5401, 2009.

NASA, website: CALIPSO Quality Statements: Lidar Level 2 Cloud and Aerosol Layer Products, `http://eosweb.larc.nasa.gov/`, 2012.

Poschl, U.: Atmospheric aerosols: Composition, transformation, climate and health effects, ANGEWANDTE CHEMIE-INTERNATIONAL EDITION, 44, 7520–7540, 2005.

Redemann, J., Vaughan, M. A., Zhang, Q., Shinozuka, Y., Russell, P. B., Livingston, J. M., Kacenelenbogen, M., and Remer, L. A.: The comparison of MODIS-Aqua (C5) and CALIOP (V2 & V3) aerosol optical depth, ATMOSPHERIC CHEMISTRY AND PHYSICS, 12, 3025–3043, 2012.

Remer, L. A., Kaufman, Y. J., D, T., Mattoo, S., and al, e.: The MODIS Aerosol Algorithm, Products, and Validation, Journal of the Atmospheric Sciences, 62, 947–966,969–973, `http://search.proquest.com/docview/236432579?accountid=10041`, 2005.

R.Koble and G.Seufert: Novel Maps for Forest Tree Species in Europe in: A Changing Atmosphere, 8th European Symposium on the Physico-Chemical Behaviour of Atmospheric Pollutants, Torino, Italy, 17–20 September, 2001.

Schuster, M. V., D. MacDonnell, W. S., D. Winker, O. D., and T. Lapyonok, C. T.: Comparison of CALIPSO aerosol optical depth retrievals to AERONET measurements, and a climatology for the lidar ratio of dust , Atmospheric Chemestry and Physics Discussions, 2012.

Simpson, D., Fagerli, H., Jonson, J., Tsyro, S., Wind, P., and Tuovinen, J.: Transboundary Acidification, Eutrophication and Ground Level Ozone in Europe, Part I, Unified EMEP Model Description, 2003.

Simpson, D., Benedictow, A., Berge, H., Bergström, R., Emberson, L. D., Fagerli, H., Hayman, G. D., Gauss, M., Jonson, J. E., Jenkin, M. E., Nyiri, A., Richter, C., Semeena, V. S., Tsyro, S., Tuovinen, J.-P., Valdebenito, A., and P.Wind: The EMEP MSC-W chemical transport model - technical description, Atmospheric Chemestry and Physics, 2012.

Thunman, H.: Combustion Engineering, Reproservice, Chalmers University of Technology, 2012.

Winker, M.Hunt, D., McGill, W., and Matthew, J.: Initial performance assessment of CALIOP, GEOPHYSICAL RESEARCH LETTERS, 2007.

# A Appendix: Aircraft Aerosol Measurements.

## A.1 Introduction

Direct and indirect aerosol radiative forcing strongly depend on aerosol properties as a function of height. That is why several aircraft measurement campaigns over different regions have been performed to determine vertical profiles of different aerosols, especially organic carbon (OC) aerosol.

The formation processes of organic carbon are highly uncertain but its main sources are biomass burning, fuel emission and biogenic secondary organic aerosols (SOA). The SOA come from the oxidation of volatile organic compounds (VOC) and are usually underestimated in models. Globally the OC aerosol concentrations in the free troposphere are underestimated in all the models considered which suggests larger anthropogenic sources of OC aerosol. This would lead to larger implications for intercontinental pollution transport and radiative forcing. It is therefore essential to get a better representation of aerosol formation and processes in the free troposphere.

## A.2 The ACE-Asia Campaign

The ACE-Asia campaign aimed at characterizing the radiative properties of Asian aerosols transported over the NW Pacific. This campaign launched between **2002** and **2004** measured concentrations of organic carbon (OC), elemental carbon (EC) and sulfates in the troposphere.

As emphasized by Heald et al. (2005), this campaign revealed remarkably high OC aerosol concentrations in the free troposphere, averaging 4 $\mu g.sm^{-3}$ up to 6.5 $km$ altitude. This value is 10 to 100 times higher than the predictions of the GEOS-Chem global 3D chemical transport model (CTM) as shown on the Figure A.2.1.

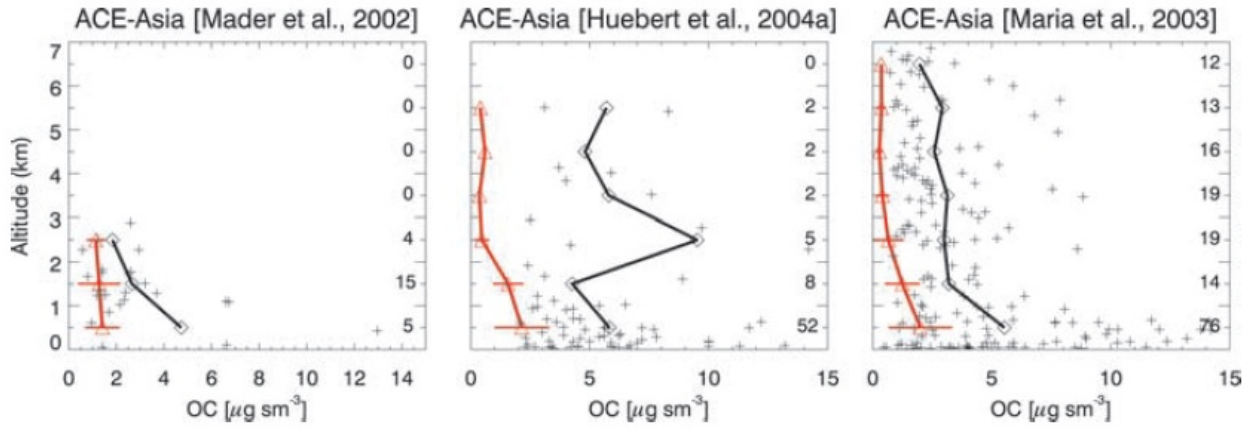


Figure A.2.1: *Mean vertical profiles of organic carbon (OC) aerosol concentrations from the ACE-Asia aircraft mission off the coast of Japan. Observations are shown in black, with individuals measurements as crosses. Results from the GEOS-Chem model are shown in red with standard deviations for each altitude interval. The number of observations in each averaging interval is shown at the right of each panel.*

More precisely, the model is 50% too low in the boundary layer which could be explained by an underestimation of the Asian emissions. However this reason cannot explained the 10 to 100 times underestimation in the free troposphere. This suggests an OC aerosol background which would range between 1 and 3 $\mu g.sm^{-3}$ and that would not be correlated with CO or sulphates emissions. The most likely explanation for the origin of this background is the sustained formation of SOA following the venting of insoluble VOC to the free troposphere. This background is however not inconsistent with independent estimates of the global organic carbon balance.

As for the sulfates, the model overestimates the concentration by about 50% which can suggest an error of the rate of $SO_2$ oxidation. while the EC concentration measurements fit well with the model predictions (Fig. A.2.2).

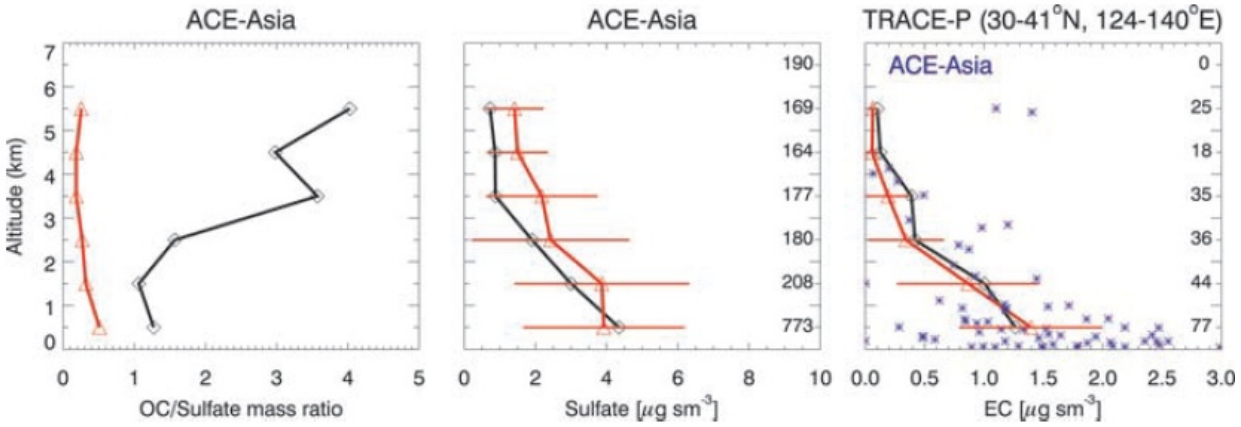


Figure A.2.2: *Mean vertical profiles of OC/sulfate mass ratio (left) and sulfate concentrations (center) from the ACE-Asia campaign, and elemental carbon (EC) aerosol concentrations from the TRACE-P campaign (right). Observations are shown in black. Results from the GEOS-Chem model are shown in red with standard deviations for each altitude interval. Individual EC observations from the ACE-Asia campaign are shown as blue symbols. The number of observations in each averaging interval is shown at the right of each panel.*

## A.3 The ITCT-2K4 campaign

The Intercontinental Transport and Chemical Transformation 2004 (ITCT-2K4) aircraft campaign was conducted during the **summer 2004** over North America together with surface observations from the Interagency Monitoring of Protected Visual Environments (IMPROVE). It looked at different aerosols in particular organic carbon (OC), water soluble organic carbon (WSOC) and sulphur oxides (Heald et al. 2006).

The summer 2004 was rich in fires in the boreal regions of Alaska and NW Canada. According to the National Interagency Coordination Center (NICC), an area as big as 8 times the 10-year average for the region has burnt. Filters have been used on the data collected during this period to get rid of these disturbances. It has been estimated that these fires accounted for 42% of the organic carbon aerosols in the free troposphere. The differences in the organic carbon aerosol in the free troposphere between the filtered data-set and the raw data can be seen on the Figures A.3.1c and A.3.1d. The figures A.3.1a and A.3.1b represent the OC aerosol concentrations in the boundary layer for the aircraft and ground-based measurements. These observations are quite consistent as the average OC aerosol concentration is estimated to be 2.1 $\mu g.C.m^{-3}$ for the IMPROVE data compared to 2.3 $\mu g.C.m^{-3}$ for the ITCT-2K4 measurement.

WSOC is thought to include secondary organic aerosol (SOA) as well as aged primary components of OC aerosol, so therefore accounts for most of OC aerosol mass in air remote from primary sources. The figure A.3.3b shows indeed that the WSOC aerosol account for the bulk of the OC aerosol in the model. And the figure A.3.3c shows the source contributions to the simulated OC aerosol.

The vertical profile of observed WSOC is shown on the figure A.3.2. On average, the filtered concentration of WSOC aerosol observed during ITCT-2K4 in the free troposphere over North America is $0.9 \pm 0.9 \mu g.C.m^{-3}$. Compared to the figure A.3.3b, the model estimates the WSOC aerosol concentration in the free troposphere (2-6 km) at $0.7 \pm 0.6 \mu g.C.m^{-3}$ that is to say 25% below the observations.

The comparison with the vertical profile of sulphur oxides (Figure A.3.3a) reveals that the $SO_x$ concentrations decrease by a factor 10 between the surface to 6 km altitude contrary to the WSOC aerosol whose concentration only decreases by a factor 2. According to Heald et al. (2006), this suggests that the WSOC aerosols observed in the free troposphere are not transported from the boundary layer.

Overall the GEOS-Chem model to which the dataset has been compared matches within 25% the mean OC aerosol concentration in the free troposphere. However, the small correlation coefficient $R = 0.21$ between the model and the data reveals that the mechanisms controlling the OC aerosol formation and losses are not described properly by the GEOS-Chem model.

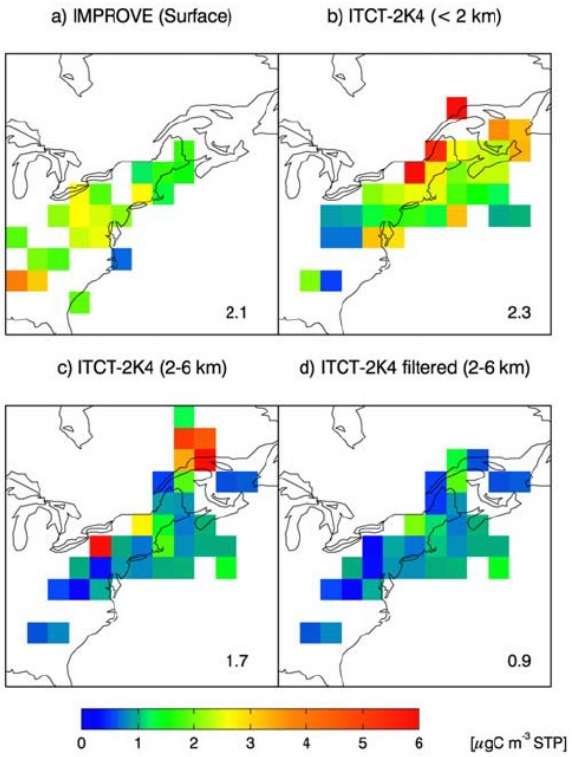


Figure A.3.1: *Mean gridded (2° x 2.5°) concentrations of organic carbon (OC) aerosol observed over northeastern North America in July-August 2004 in mixing ratio units of mg C* $m^{-3}$ *at standard conditions of temperature and pressure (STP). (a) OC aerosol measurements at IMPROVE surface sites; (b) ITCT-2K4 aircraft observations of water-soluble organic carbon (WSOC) aerosol in the boundary layer (0-2 km); (c) ITCT-2K4 aircraft observations of WSOC in the free troposphere (2-6 km); (d) ITCT-2K4 aircraft observations of WSOC in the free troposphere filtered to remove the influence of biomass-burning in the boreal regions. Mean values are shown in each panel.*

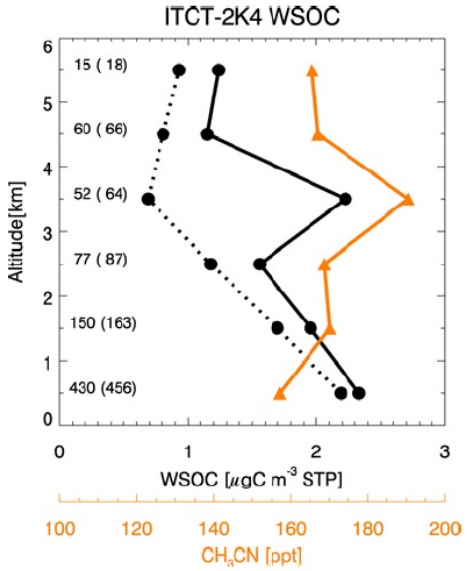


Figure A.3.2: *Mean vertical profiles of observed water-soluble organic carbon aerosol (WSOC, black circles) and acetonitrile (CH3CN, orange triangles) for all the ITCT-2K4 flights (solid line). The mean filtered WSOC profile is shown as the dotted line. Concentrations are reported at standard temperature and pressure conditions. The number of observations in each altitude bin is given on the left of the figure, with the total number of filtered observations given in parentheses.*

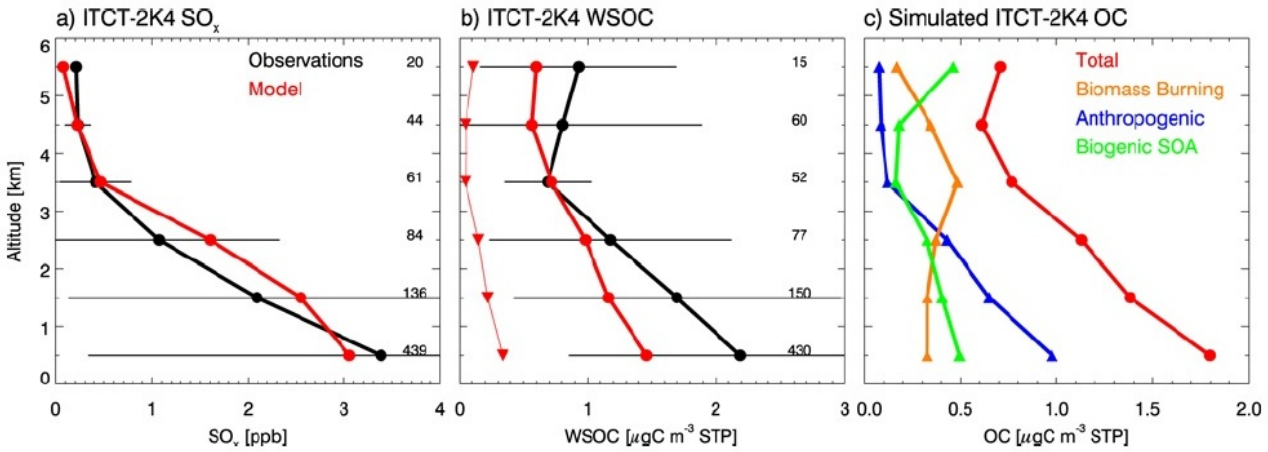


Figure A.3.3: *Mean vertical profiles of (a) sulfur oxides ($SO_x$ = $SO_2$ + sulfate) and (b) water-soluble organic carbon aerosol (WSOC) as observed (solid black) and simulated by the GEOS-Chem model (thick red line) for the filtered ITCT-2K4 data. Simulated hydrophobic OC aerosol (not included in WSOC) is also shown in Figure 8b as a thin red line (inverted triangles). (c) Contributions to total (red line) simulated OC aerosol from biomass-burning (orange line), anthropogenic (blue line), and biogenic (green line) sources. The standard deviation of the observations in each altitude bin is shown as an error bar with the number of observations in each bin given on the right of the figure.*

## A.4 The FAAM BAe-146 research campaign

The UK Facility for Airborne Atmospheric Measurements (FAAM) BAe-146 research aircraft performed aerosol measurements in the UK region between **April 2005** and **September 2006**. The UK region considered is representative of NW Europe and NE Atlantic. Vertical profile measurements of four kinds of aerosols (organics, sulphate, nitrate and ammonium) have been performed up to 10.5 km with the Aerodyne Quadrupole Aerosol Mass Spectrometer (Q-AMS).

Summary statistics of aerosol concentrations measured by the Q-AMS for the full dataset are presented in Fig. A.4.1 and A.4.2 Morgan et al. (2009)

The sulphate and organics profiles are characterized by a relatively small Inter Quartile Range (IQR, defined as the difference between the 75th and the 25th percentile); IQR ranges between 0 and 2 $\mu g.m^{-3}$ which is interpreted as background mass concentration levels, while the higher concentrations above the 75th percentile are associated with pollution plumes.

Above 4000m, data coverage is much more limited and the mass of aerosol is significantly decreased. However sulphate and nitrate mass concentrations have low variability contrary to organics and ammonium concentrations. The organics mass concentration profile presents a relatively high variability above 4000m. Furthermore above approximately 7000m the organic median mass becomes higher than in the boundary layer. This suggests potentially low statistical signifance above this level.

This complex vertical distribution enhances the requirement for an accurate representation of aerosol formation in the free troposphere.

## A.5 Lin et al. (2012)

This article goes more into delails of the atmospheric chemestry and the mechanisms involved. Different simulations have been performed for the regions of East Asia and North America. However the results are compared to the same set of measurement data set as the ones described in the previous articles.

The three simulations run, called A, B and C, are based on different properties of atmospheric chemestry. The simulation A is based on Ito et al. (2007). The chemistry mechanisms and epoxide formation from isoprene are taken from Paulot et al. (2009), without HOx recycling. It uses emissions for year 2000, and meteorology for 1997. The simulation B includes the mechanism in Simulation A with some reactions modified in accordance with the recent literature and HOx regeneration through isoprene oxidation proposed by Peeters et al.(2009). The simulation C uses the same chemistry mechanism as Simulation B, but with a reduced rate for the 1,5-H

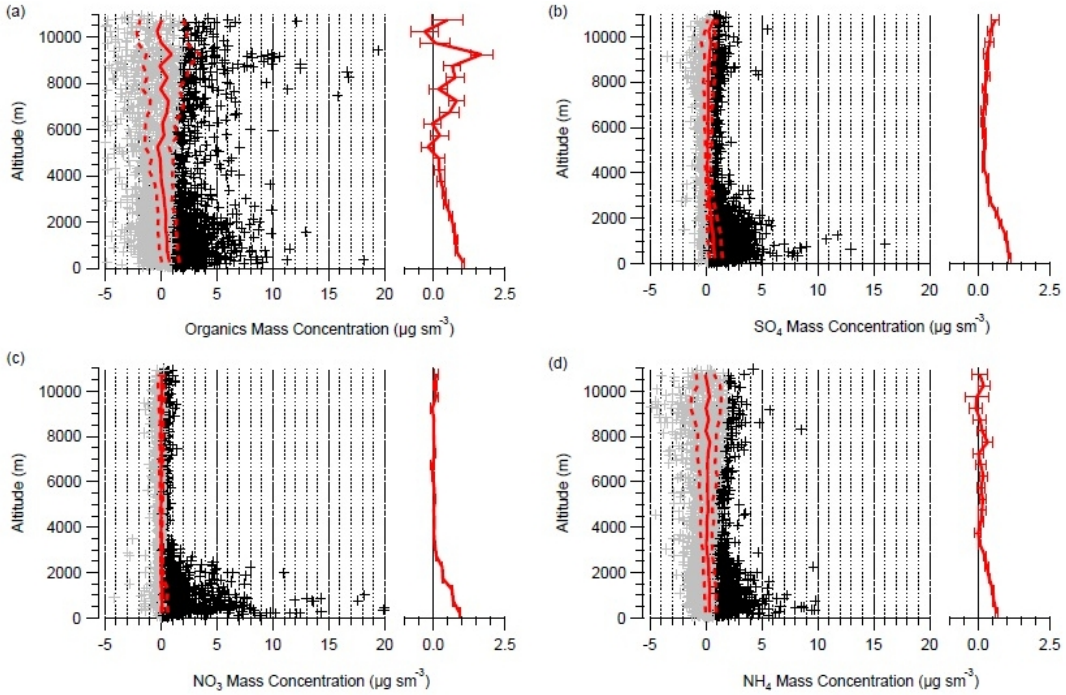


Figure A.4.1: *Vertical profiles of aerosol chemical composition from the AMS for the UK for each chemical species. Black crosses are individual data points above the 2σ profile for each species whilst grey crosses correspond to those below. Red lines are the 25th, 50th and 75th percentiles for 500 m altitude bins. On the right hand side panel for each species the red line shows the mean for each altitude bin with the horizontal bar indicating the variability about the mean value.*

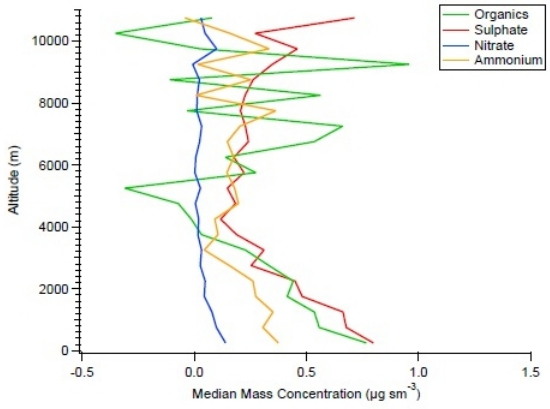


Figure A.4.2: *Sulphate, organics, nitrate and ammonium median mass concentration profiles for the full dataset.*

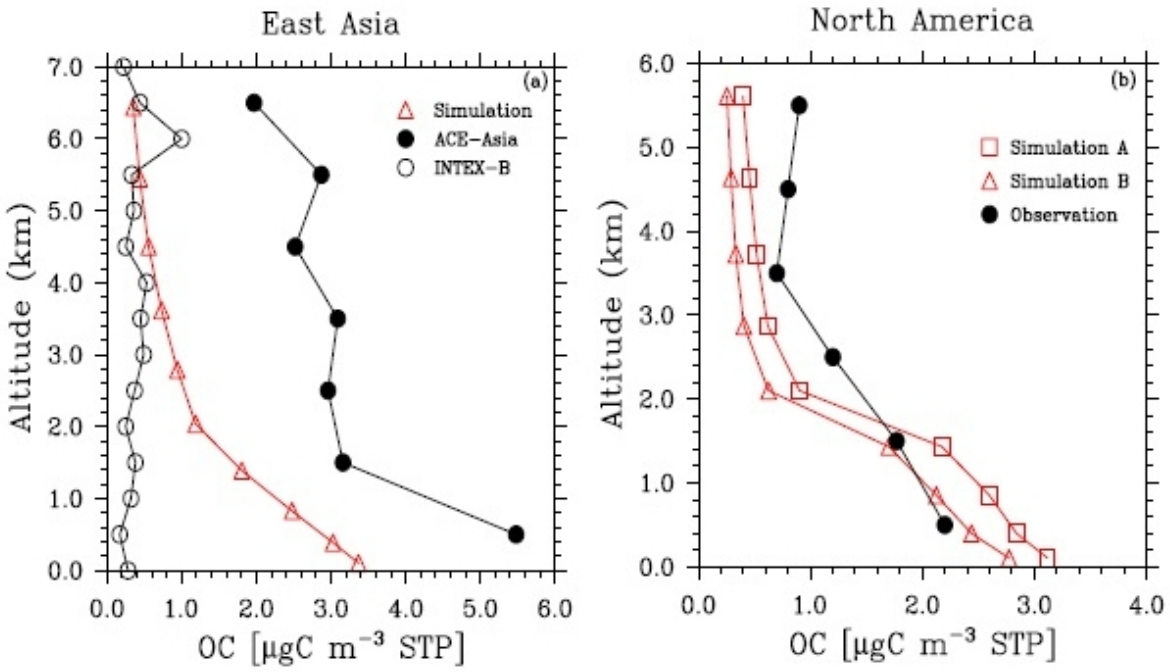


Figure A.5.1: *Mean vertical profiles of total organic carbon at standard conditions of temperature and pressure. Observed mean profiles (black solid circles) were measured during the ACE-Asia campaign (left plot) and during the ITCT-2K4 aircraft campaign over NE North America that took place in the Summer (July to August) 2004 (right plot). The black empty circles in the left plot represent average vertical profile of aerosol species for Asian pollution layers measured during the INTEX-B campaign made during April to May in 2006. The model results are the average values over the months of the campaigns. Three simulations produce very similar profiles over East Asia, thus only one simulated profile is shown in (a). The vertical profile over North America produced in Simulation C is omitted because it is almost identical to that of Simulation A.*

and 1,6-H shifts in isoprene radicals by a factor of 10.

What can be seen is that they are still large discrepancies between the simulations and the ACE-Asia campaign (Figure A.5.1*a*) but they are smaller than the ones reported by Heald et al. 2005. For North America the simulation "A" performs reasonably well in the boundary layer but still underestimates the OC aerosol concentration in the free troposphere (2-6 km). The mean model value of Simulation A was $0.574 \pm 0.172 \mu g.C.m^{-3}$ (vs. $0.9 \pm 0.9 \mu g.C.m^{-3}$ for the observations.)

# B Appendix: Figures.

## B.1 Optical Depth Patterns

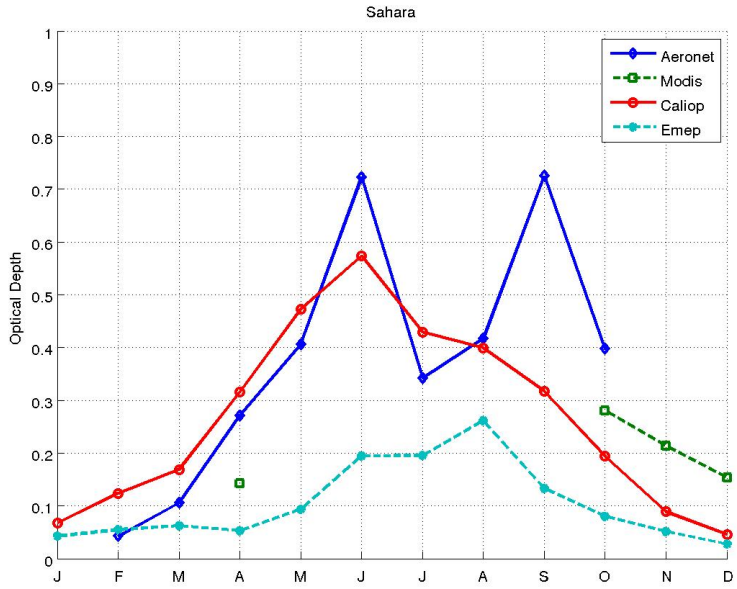


Figure B.1.1: *Comparison of the Optical Depth measured by Caliop, Modis and Aeronet and predicted by the Emep model in the Sahara and averaged over the years 2006 to 2010.*

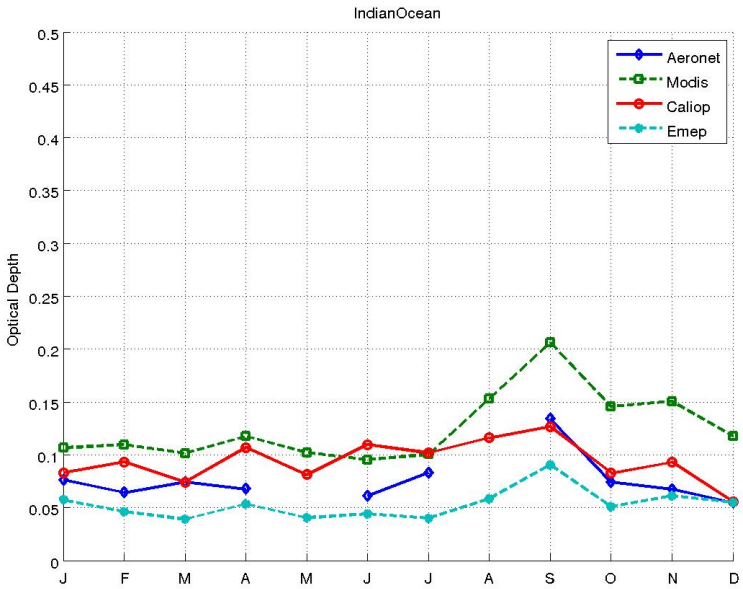


Figure B.1.2: *Comparison of the Optical Depth measured by Caliop, Modis and Aeronet and predicted by the Emep model in the Indian Ocean and averaged over the years 2006 to 2010.*

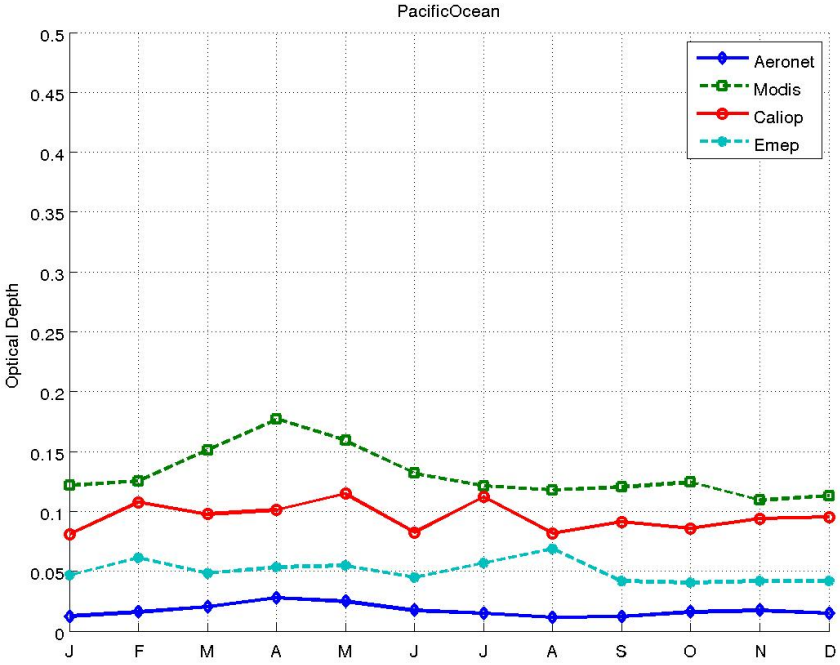


Figure B.1.3: *Comparison of the Optical Depth measured by Caliop, Modis and Aeronet and predicted by the Emep model in the Pacific Ocean and averaged over the years 2006 to 2010.*

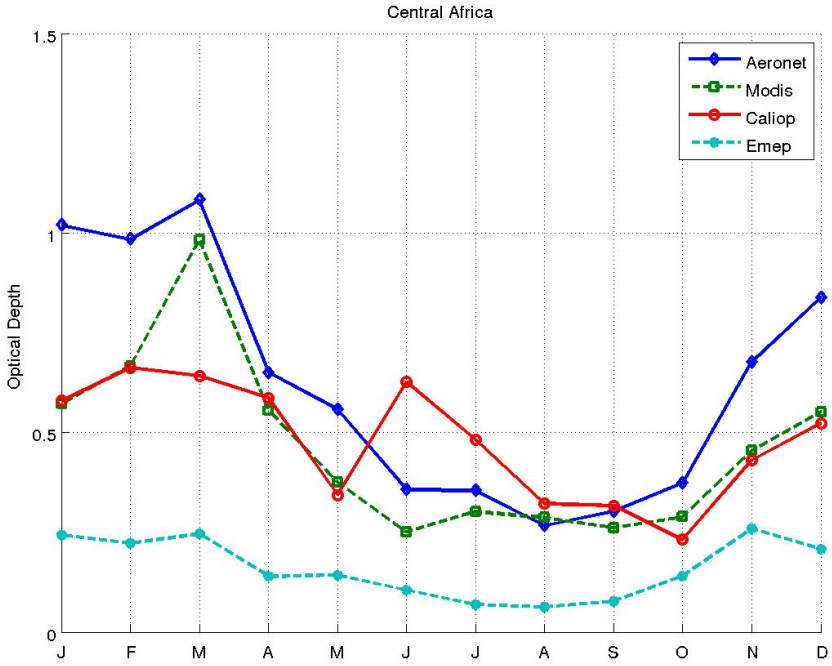


Figure B.1.4: *Comparison of the Optical Depth measured by Caliop, Modis and Aeronet and predicted by the Emep model in Central Africa and averaged over the years 2006 to 2010.*

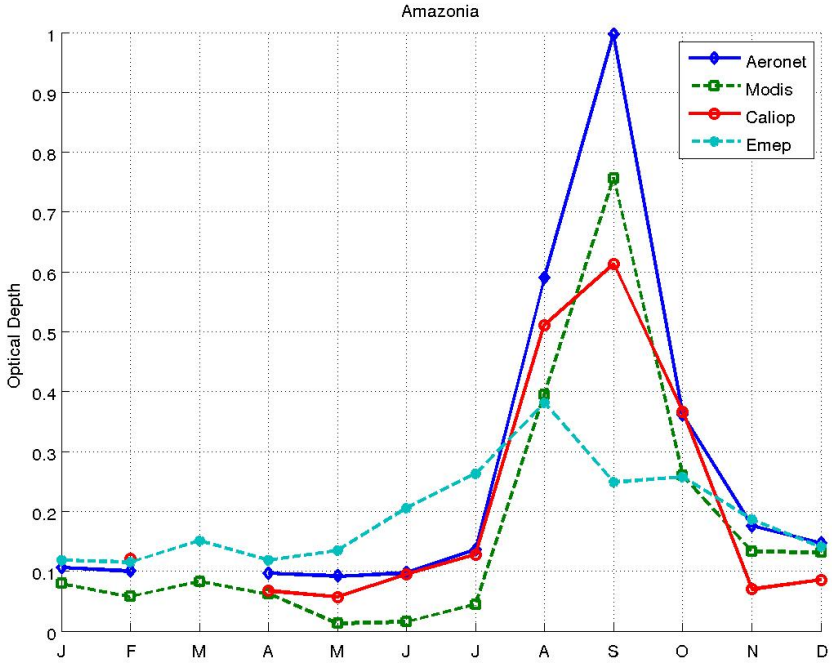


Figure B.1.5: *Comparison of the Optical Depth measured by Caliop, Modis and Aeronet and predicted by the Emep model in Amazonia and averaged over the years 2006 to 2010.*

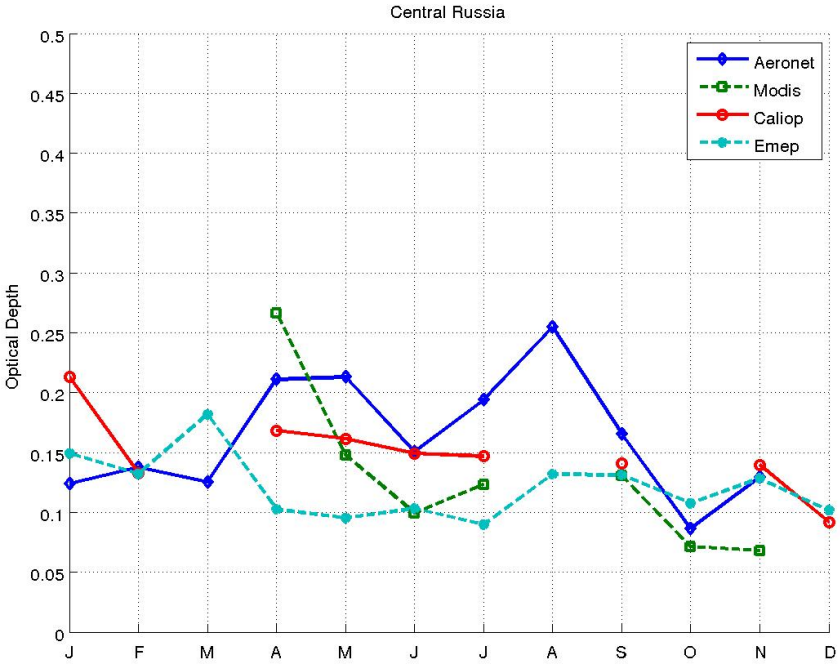


Figure B.1.6: *Comparison of the Optical Depth measured by Caliop, Modis and Aeronet and predicted by the Emep model in Central Russia and averaged over the years 2006 to 2010.*

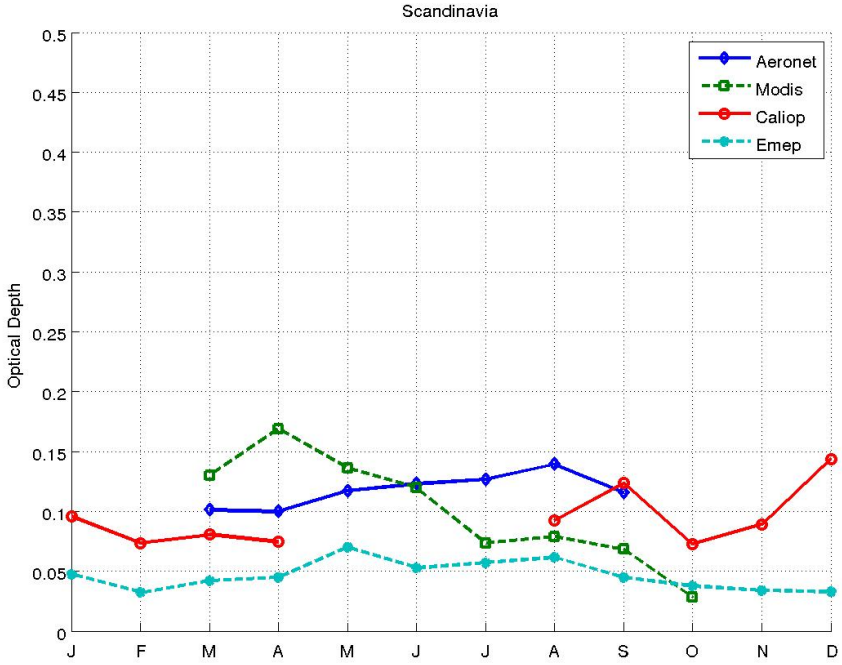


Figure B.1.7: *Comparison of the Optical Depth measured by Caliop, Modis and Aeronet and predicted by the Emep model in Scandinavia and averaged over the years 2006 to 2010.*

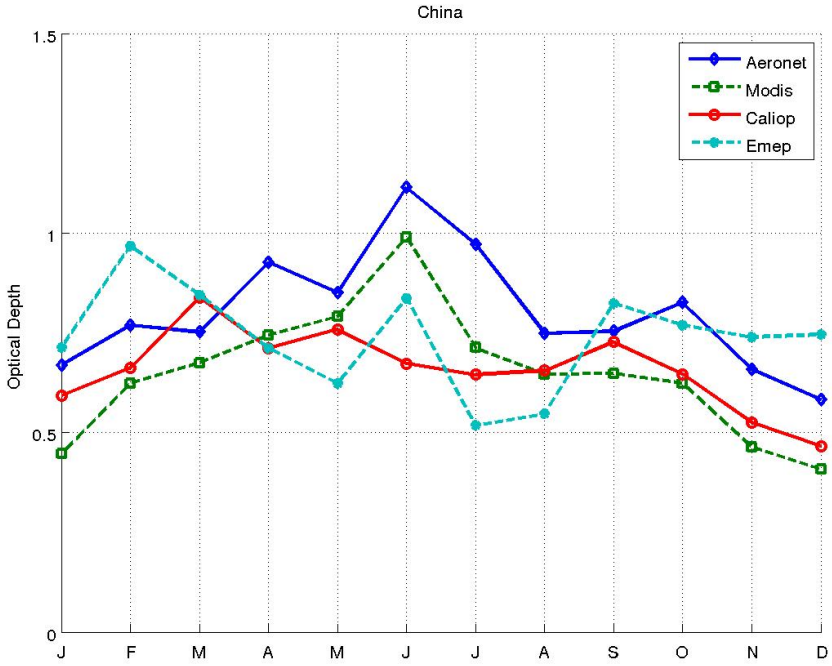


Figure B.1.8: *Comparison of the Optical Depth measured by Caliop, Modis and Aeronet and predicted by the Emep model in China and averaged over the years 2006 to 2010.*

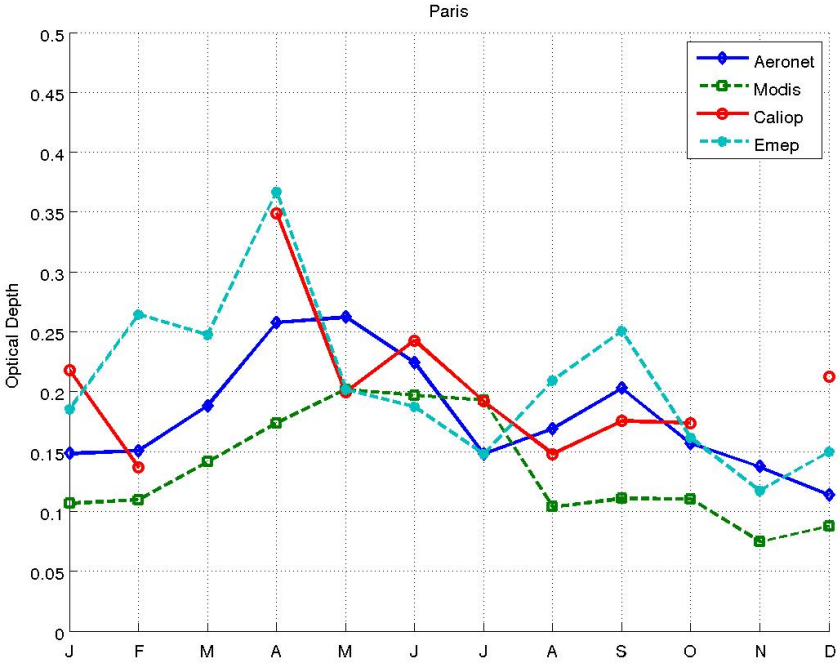


Figure B.1.9: *Comparison of the Optical Depth measured by Caliop, Modis and Aeronet and predicted by the Emep model in Paris and averaged over the years 2006 to 2010.*

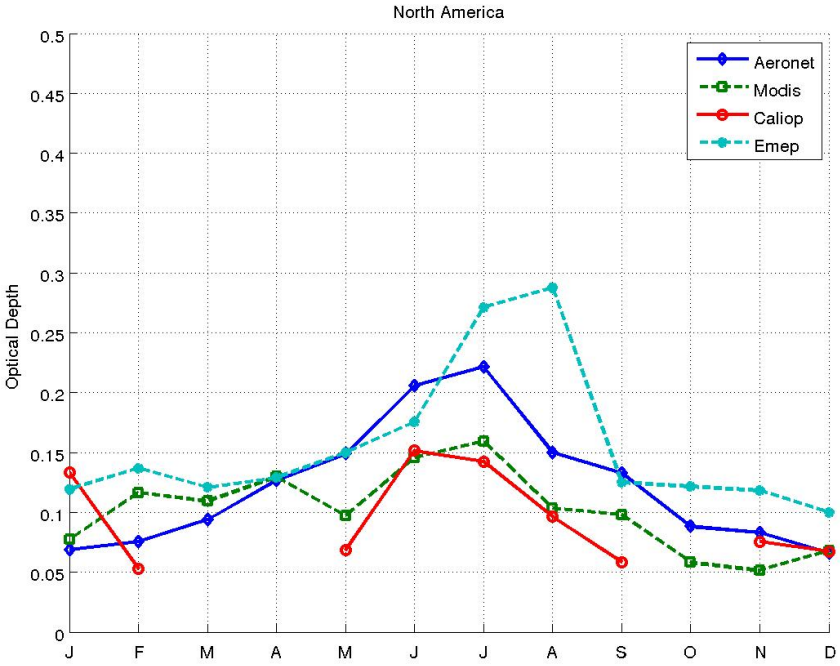


Figure B.1.10: *Comparison of the Optical Depth measured by Caliop, Modis and Aeronet and predicted by the Emep model in North America and averaged over the years 2006 to 2010.*

## B.2 EMEP model Sensitivity to the Organic Carbon Sensitivity

### B.2.1 Optical Depth

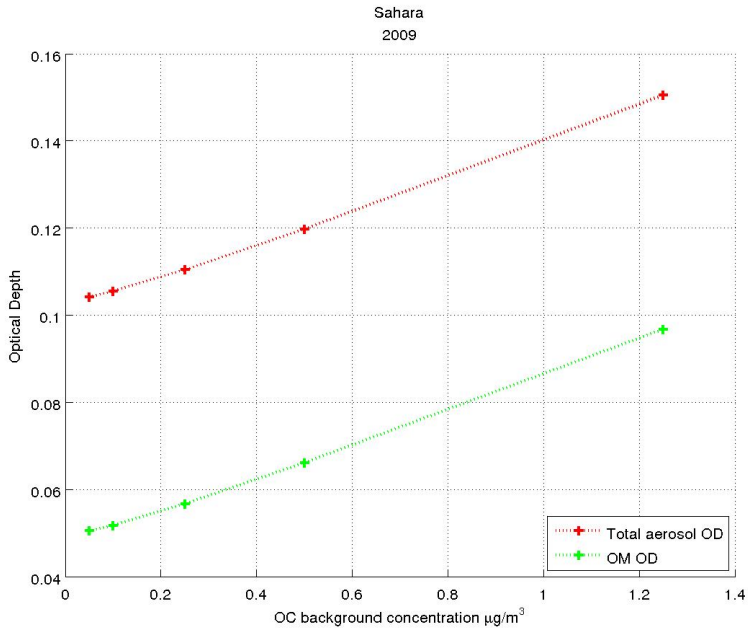


Figure B.2.1: *Relationship between the Organic Carbon background on the optical depth in Sahara for the year 2009 according to the Emep model.*

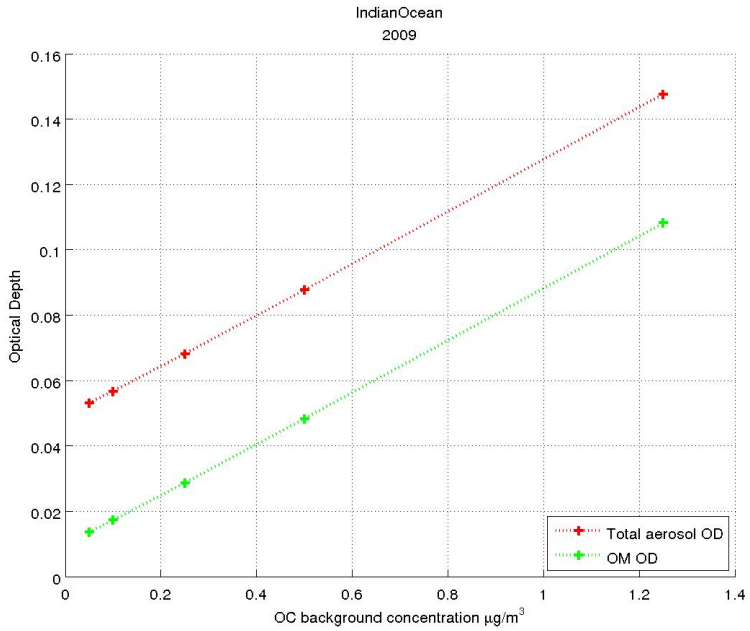


Figure B.2.2: *Relationship between the Organic Carbon background on the optical depth in the Indian Ocean for the year 2009 according to the Emep model.*

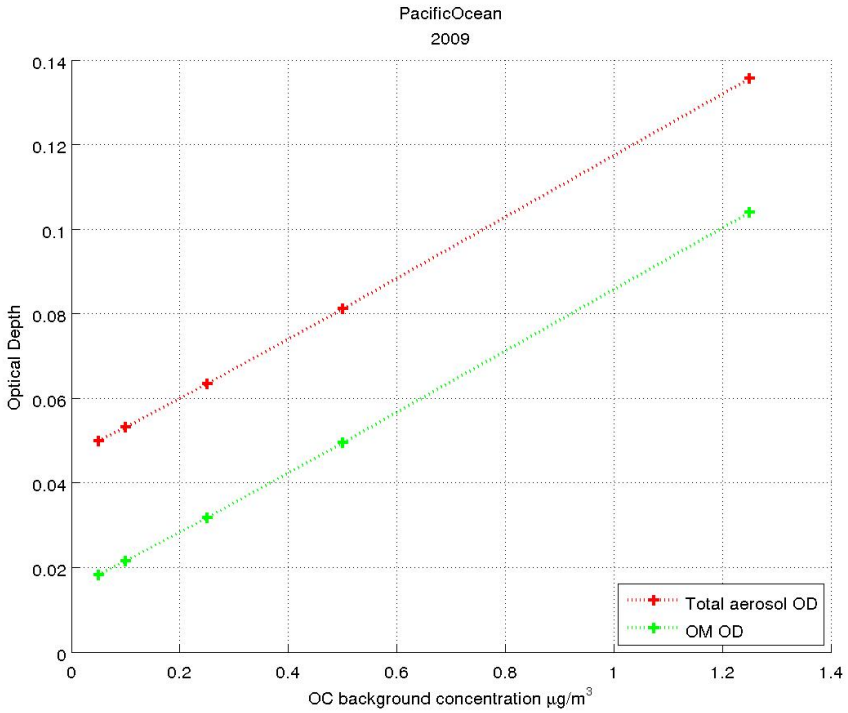


Figure B.2.3: *Relationship between the Organic Carbon background on the optical depth in the Pacific Ocean for the year 2009 according to the Emep model.*

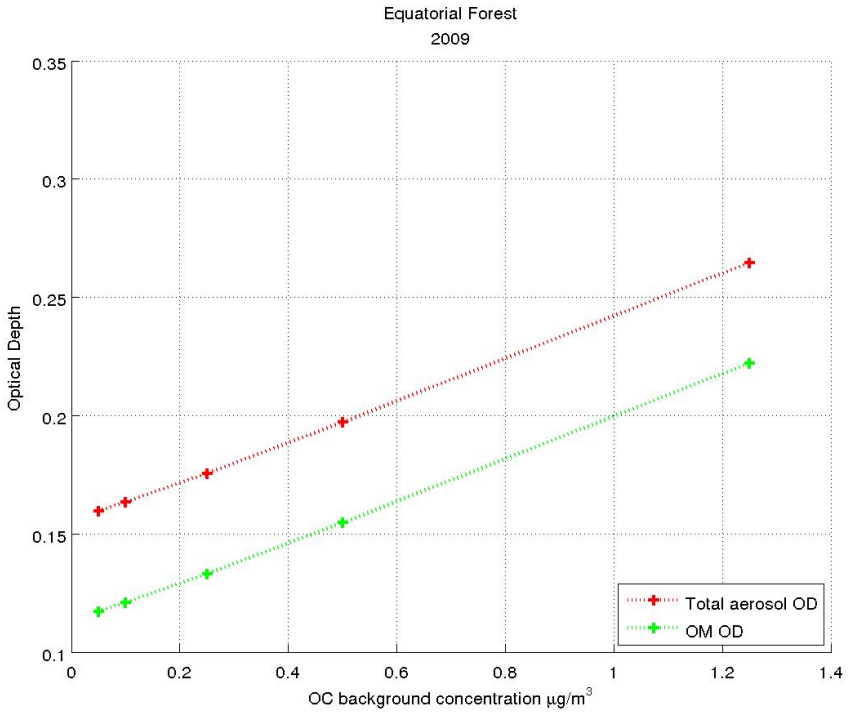


Figure B.2.4: *Relationship between the Organic Carbon background on the optical depth in Central Africa for the year 2009 according to the Emep model.*

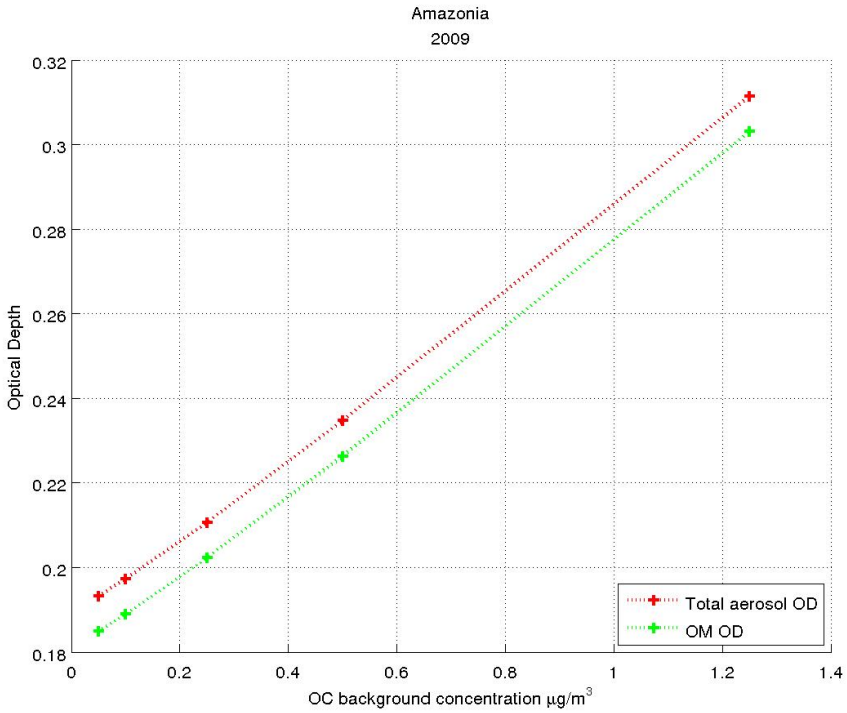


Figure B.2.5: *Relationship between the Organic Carbon background on the optical depth in Amazonia for the year 2009 according to the Emep model.*

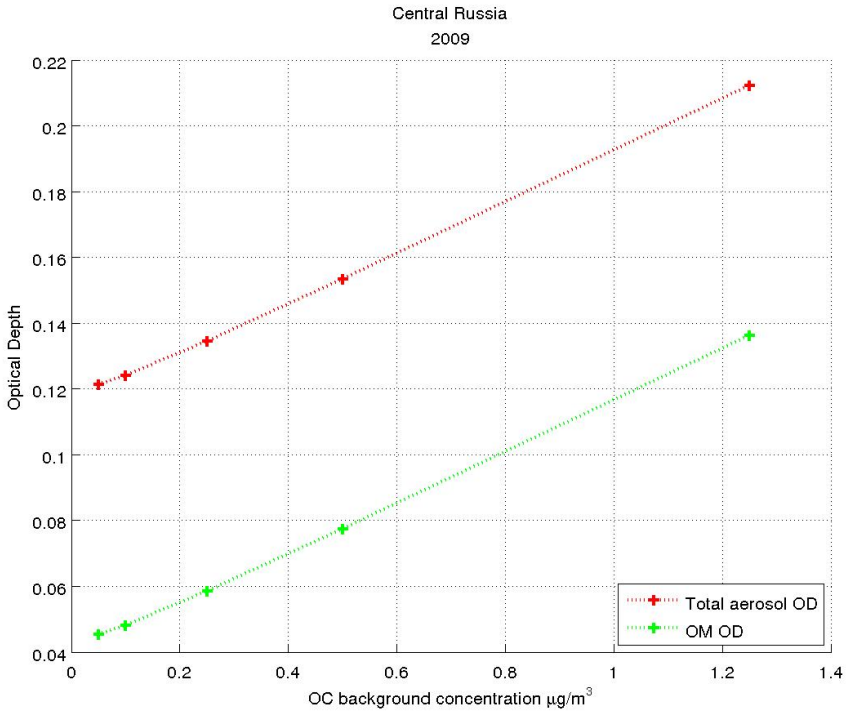


Figure B.2.6: *Relationship between the Organic Carbon background on the optical depth in Central Russia for the year 2009 according to the Emep model.*

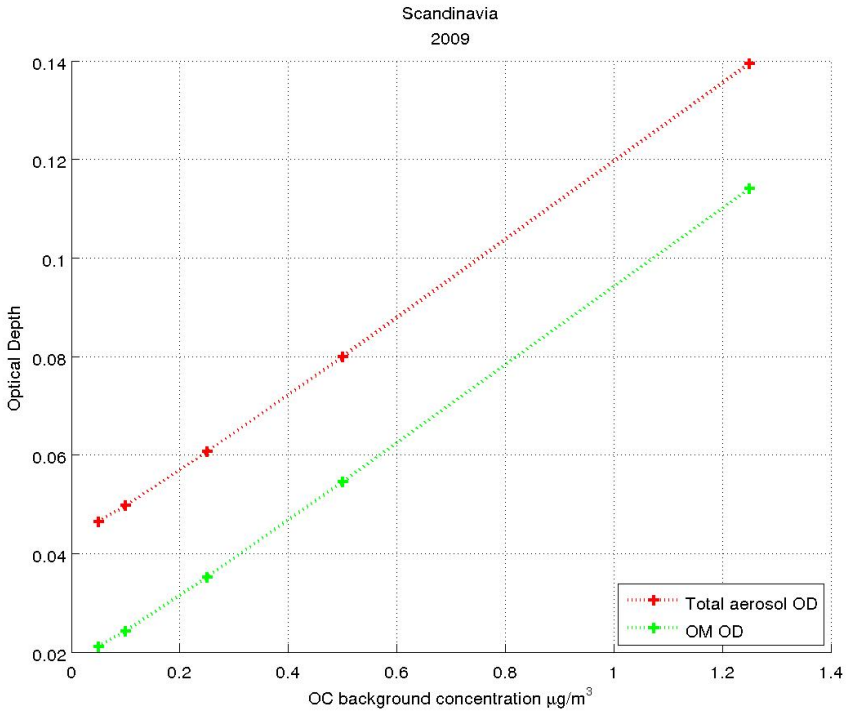


Figure B.2.7: *Relationship between the Organic Carbon background on the optical depth in Scandinavia for the year 2009 according to the Emep model.*

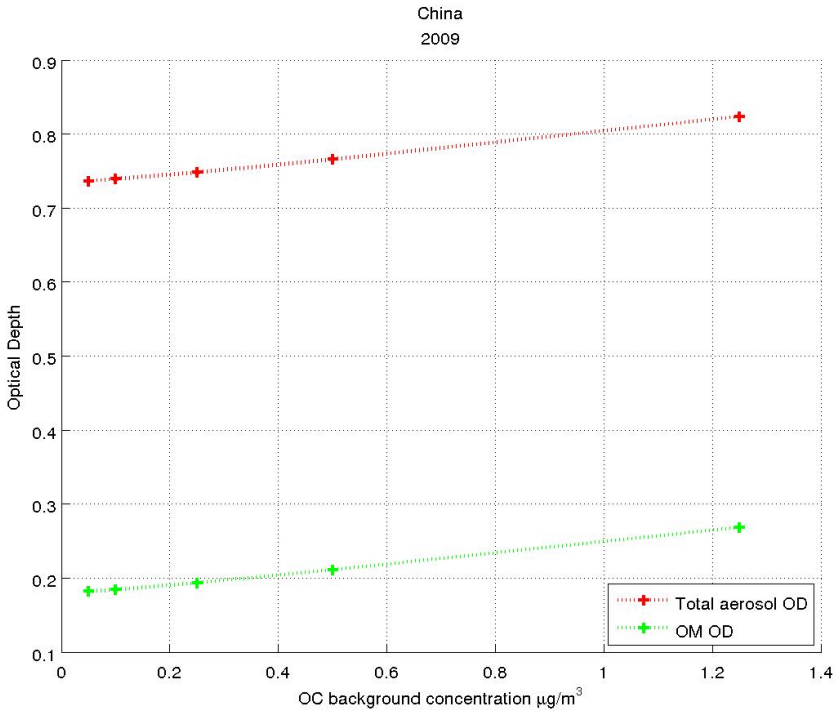


Figure B.2.8: *Relationship between the Organic Carbon background on the optical depth in China for the year 2009 according to the Emep model.*

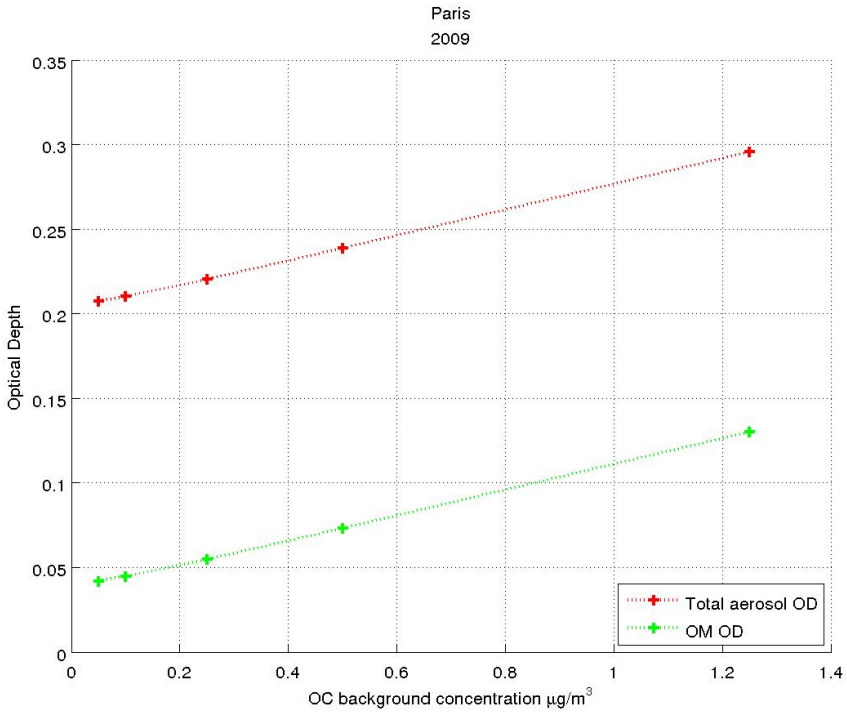


Figure B.2.9: *Relationship between the Organic Carbon background on the optical depth in Paris for the year 2009 according to the Emep model.*

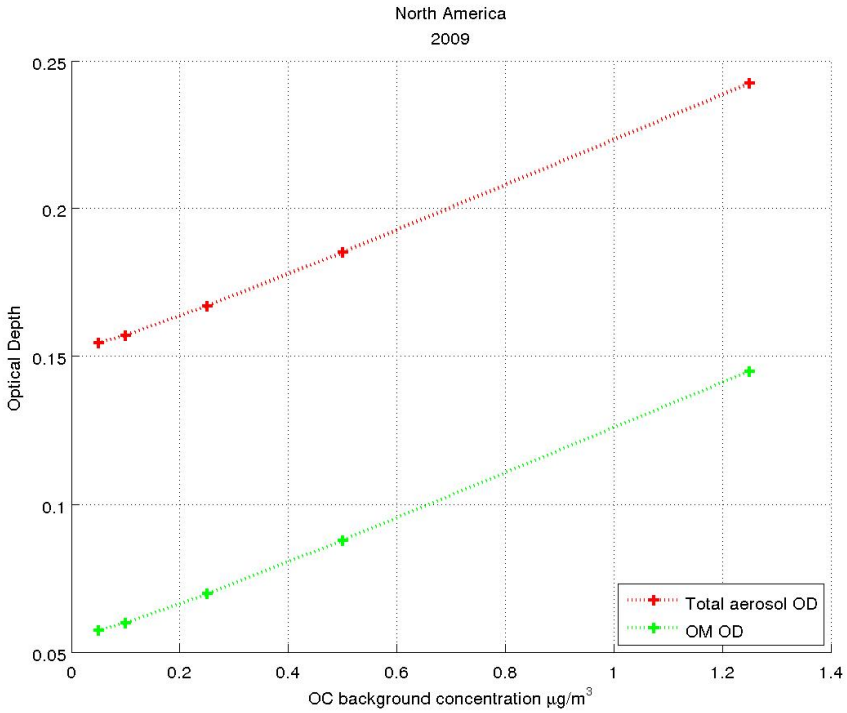


Figure B.2.10: *Relationship between the Organic Carbon background on the optical depth in North America for the year 2009 according to the Emep model.*

### B.2.2 Extinction Vertical Distribution

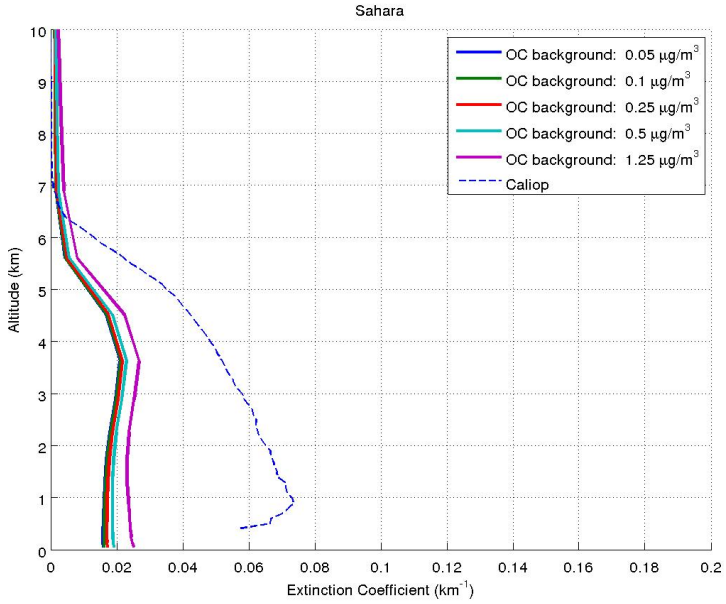


Figure B.2.11: *Vertical extinction coefficient profiles computed for five different Organic Carbon backgrounds and compared with the Caliop observation on a year basis in the Sahara.*

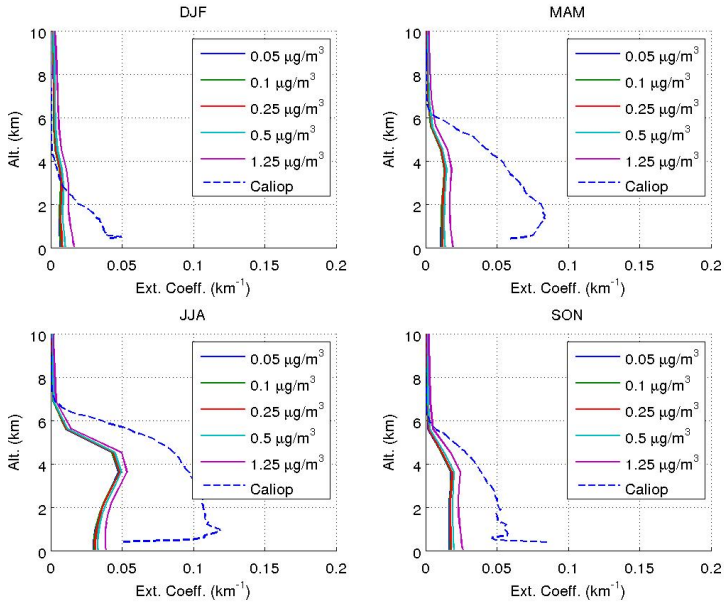


Figure B.2.12: *Vertical extinction coefficient profiles computed for five different Organic Carbon backgrounds and compared with the Caliop observation on a seasonal basis in the Sahara.*

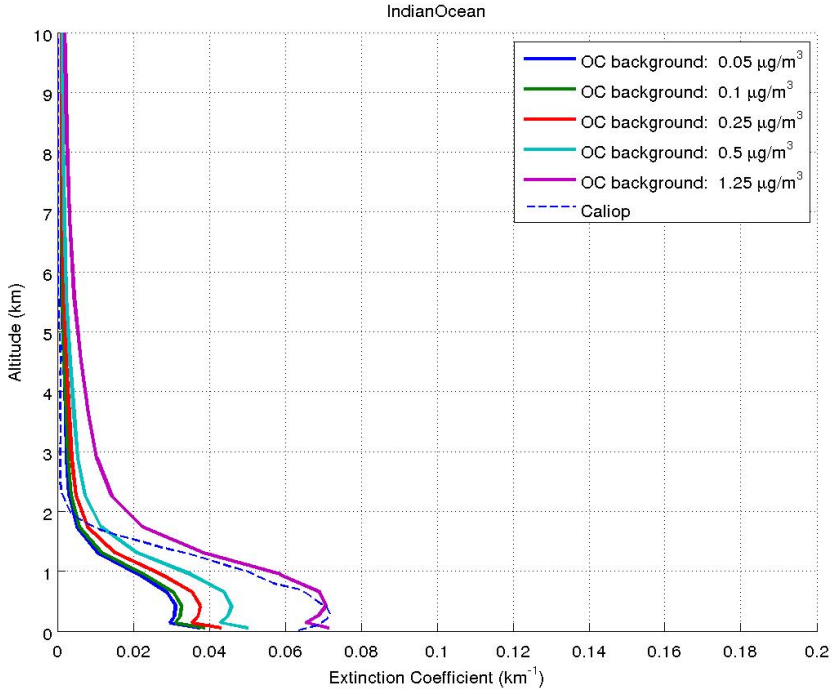


Figure B.2.13: *Vertical extinction coefficient profiles computed for five different Organic Carbon backgrounds and compared with the Caliop observation on a year basis in the Indian Ocean.*

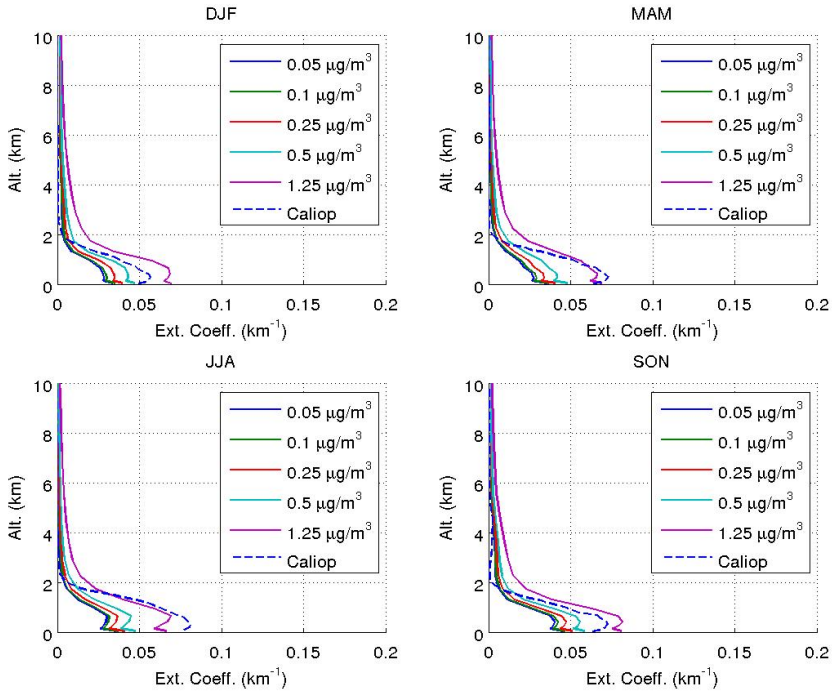


Figure B.2.14: *Vertical extinction coefficient profiles computed for five different Organic Carbon backgrounds and compared with the Caliop observation on a seasonal basis in the Indian Ocean.*

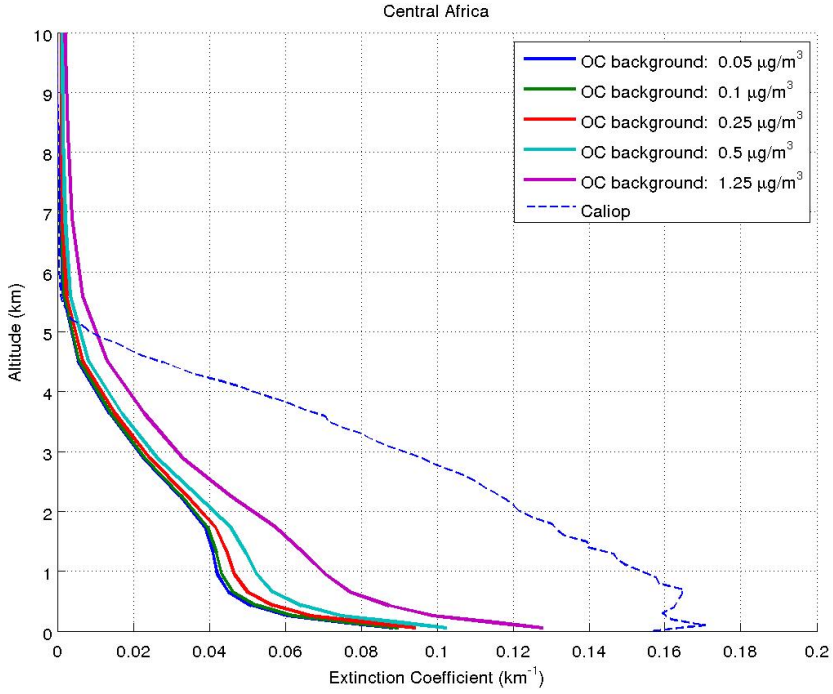


Figure B.2.15: *Vertical extinction coefficient profiles computed for five different Organic Carbon backgrounds and compared with the Caliop observation on a year basis in Central Africa.*

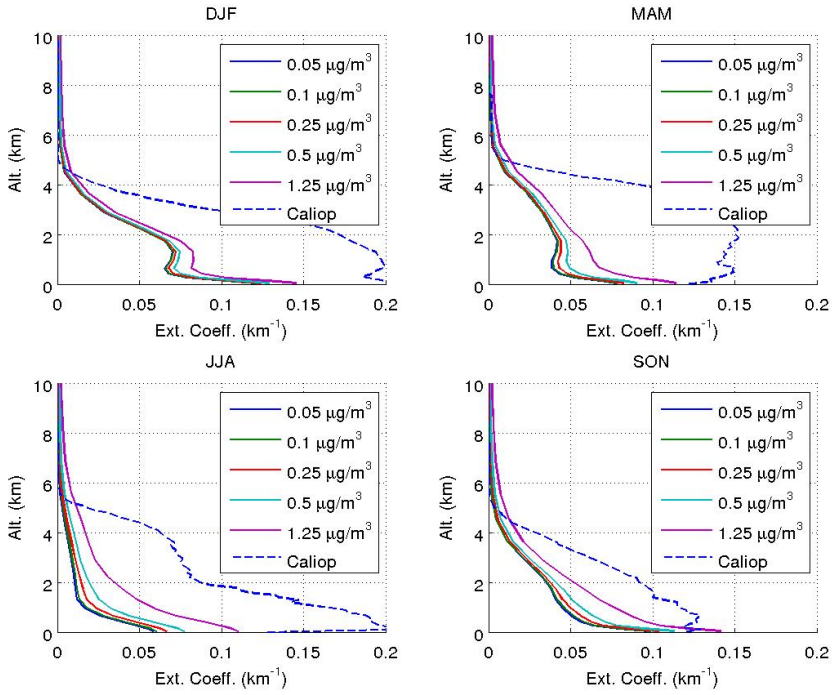


Figure B.2.16: *Vertical extinction coefficient profiles computed for five different Organic Carbon backgrounds and compared with the Caliop observation on a seasonal basis in Central Africa.*

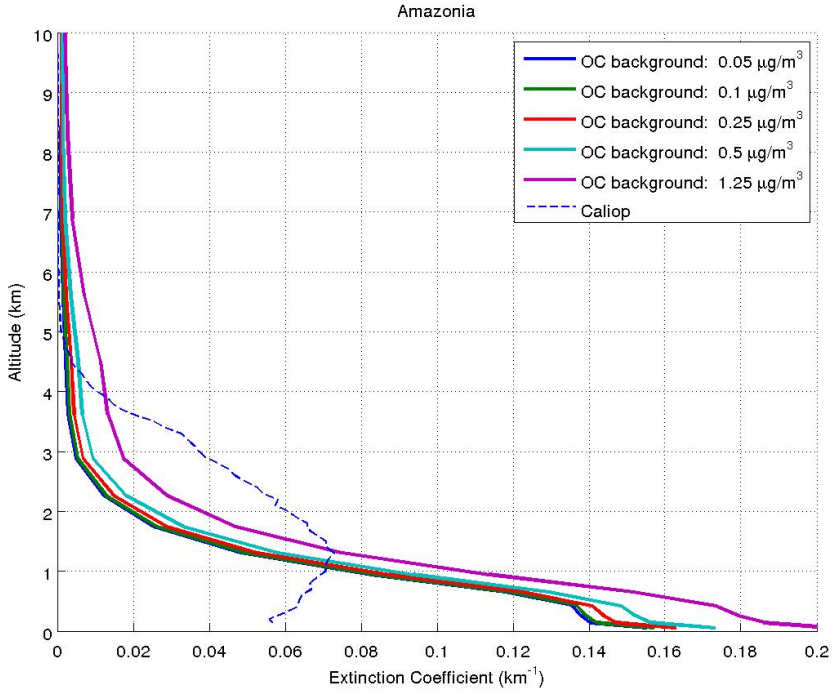


Figure B.2.17: *Vertical extinction coefficient profiles computed for five different Organic Carbon backgrounds and compared with the Caliop observation on a year basis in Amazonia.*

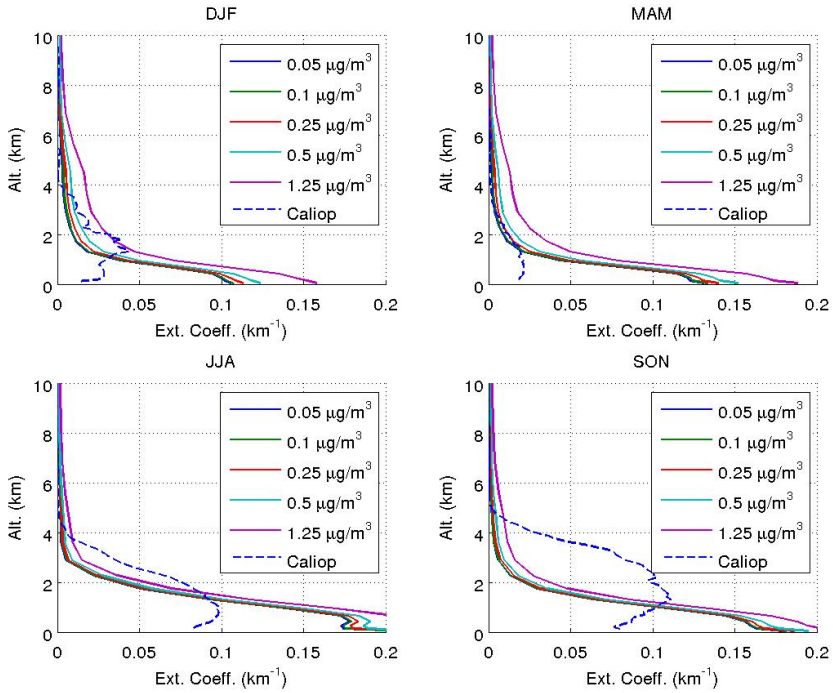


Figure B.2.18: *Vertical extinction coefficient profiles computed for five different Organic Carbon backgrounds and compared with the Caliop observation on a seasonal basis in Amazonia.*

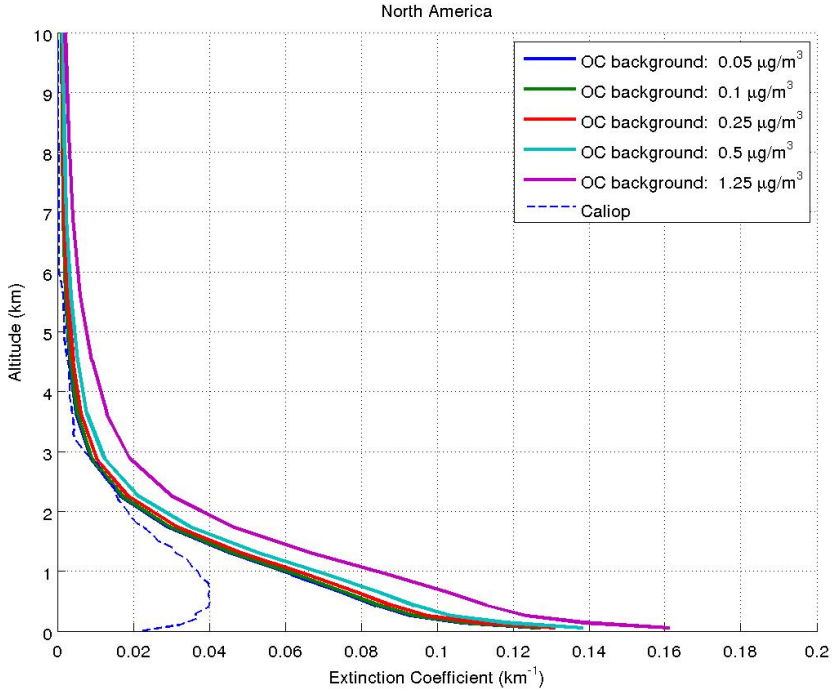


Figure B.2.19: *Vertical extinction coefficient profiles computed for five different Organic Carbon backgrounds and compared with the Caliop observation on a year basis in North America.*

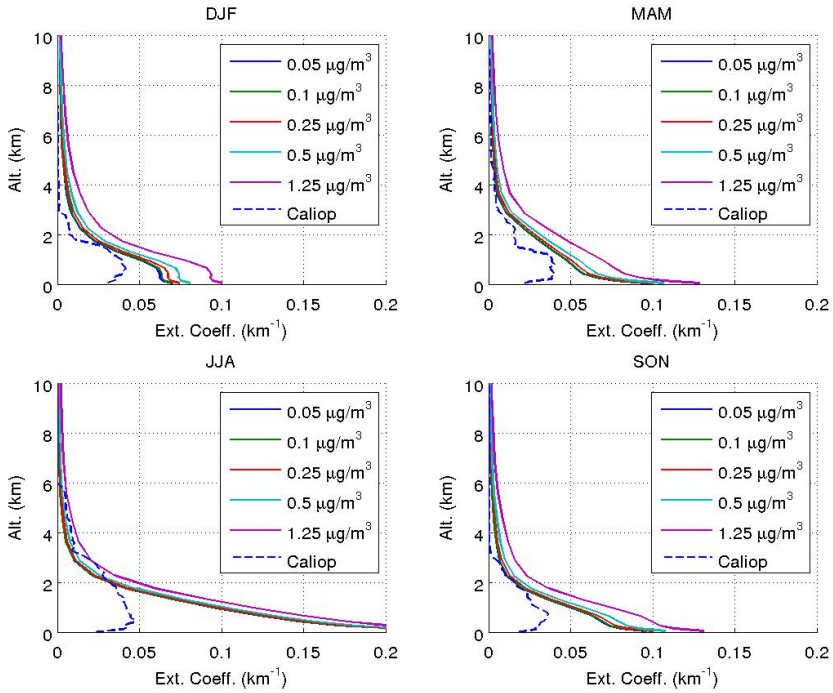


Figure B.2.20: *Vertical extinction coefficient profiles computed for five different Organic Carbon backgrounds and compared with the Caliop observation on a seasonal basis in North America.*

## B.3 EMEP model Sensitivity to the Scale Height

### B.3.1 Optical Depth

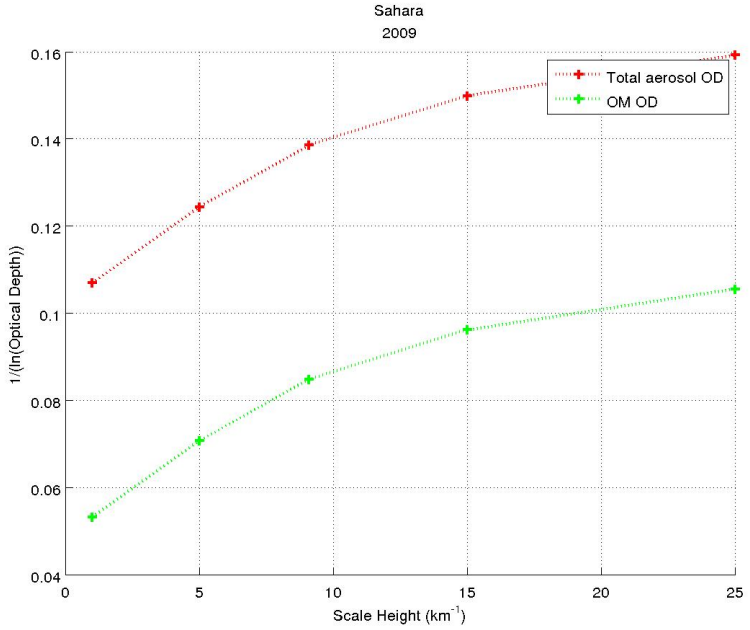


Figure B.3.1: *Relationship between the scale height on the optical depth in Sahara for the year 2009 according to the Emep model.*

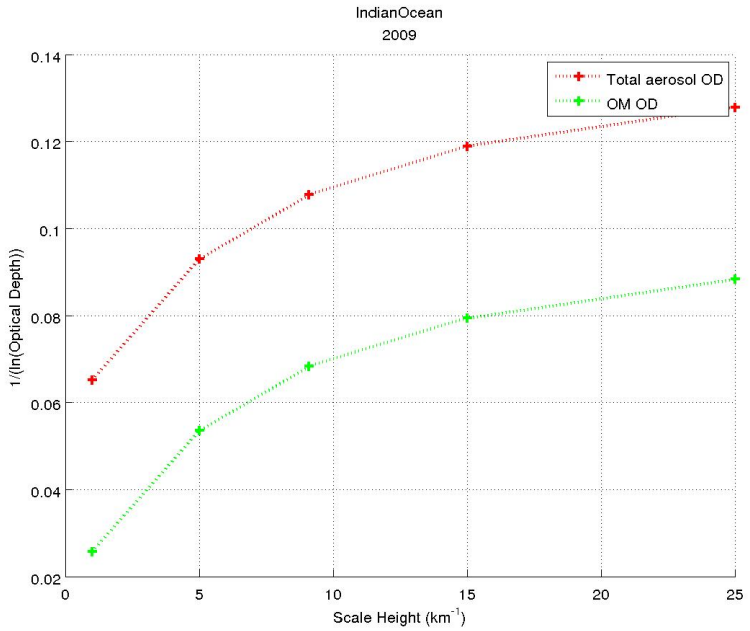


Figure B.3.2: *Relationship between the scale height on the optical depth in the Indian Ocean for the year 2009 according to the Emep model.*

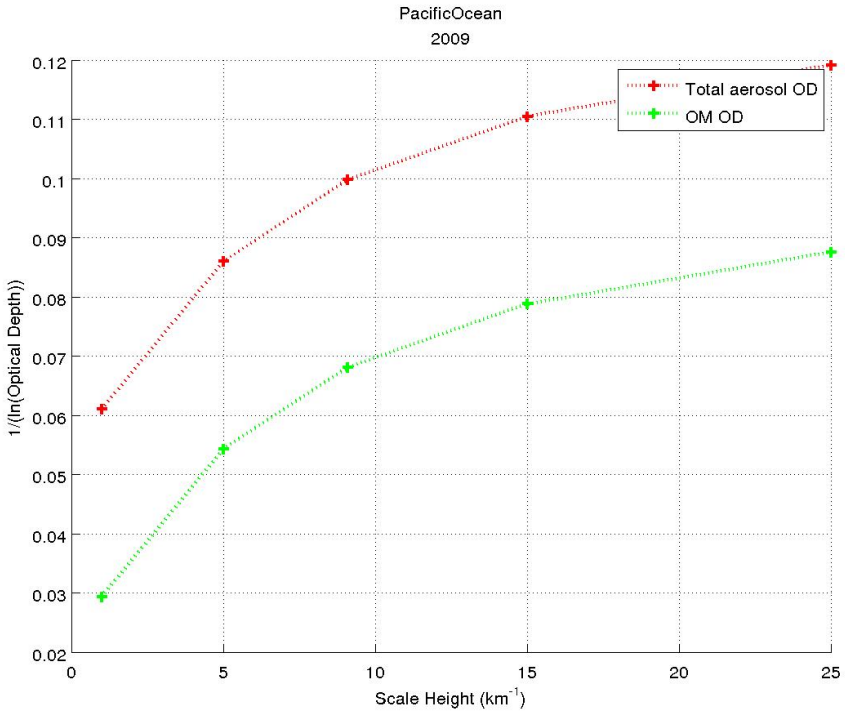


Figure B.3.3: *Relationship between the scale height on the optical depth in the Pacific Ocean for the year 2009 according to the Emep model.*

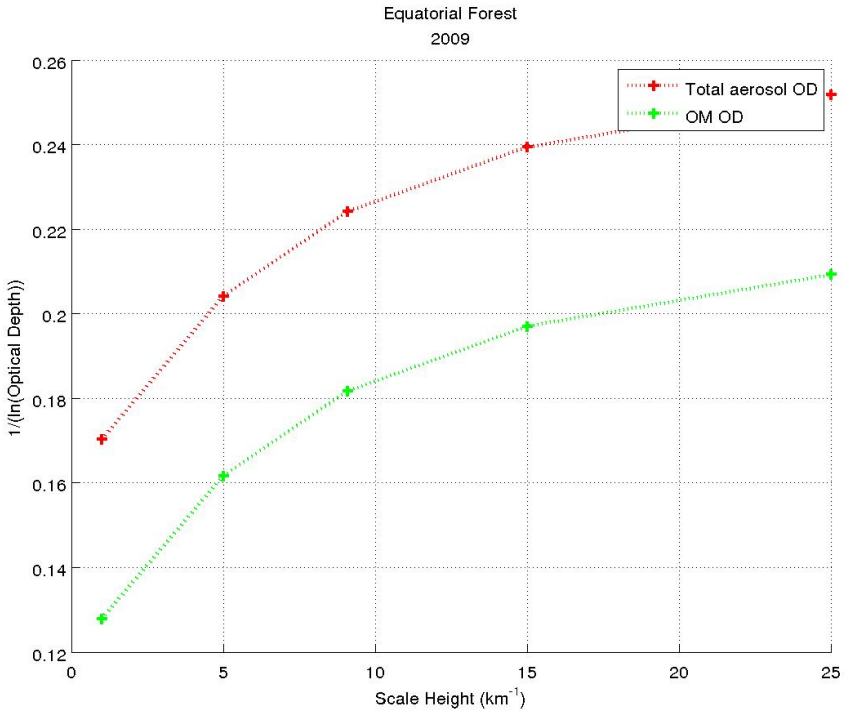


Figure B.3.4: *Relationship between the scale height on the optical depth in Central Africa for the year 2009 according to the Emep model.*

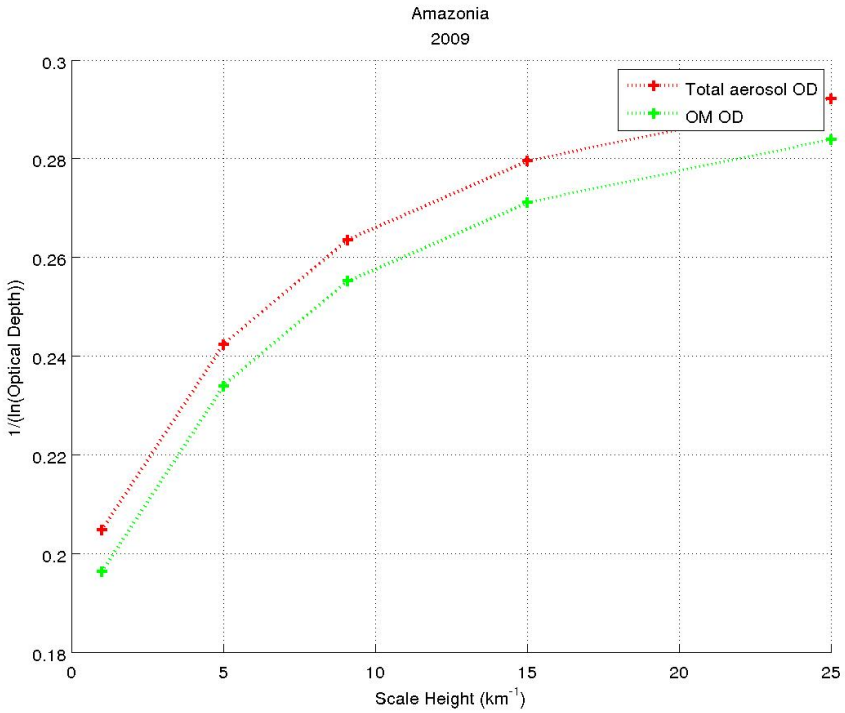


Figure B.3.5: *Relationship between the scale height on the optical depth in Amazonia for the year 2009 according to the Emep model.*

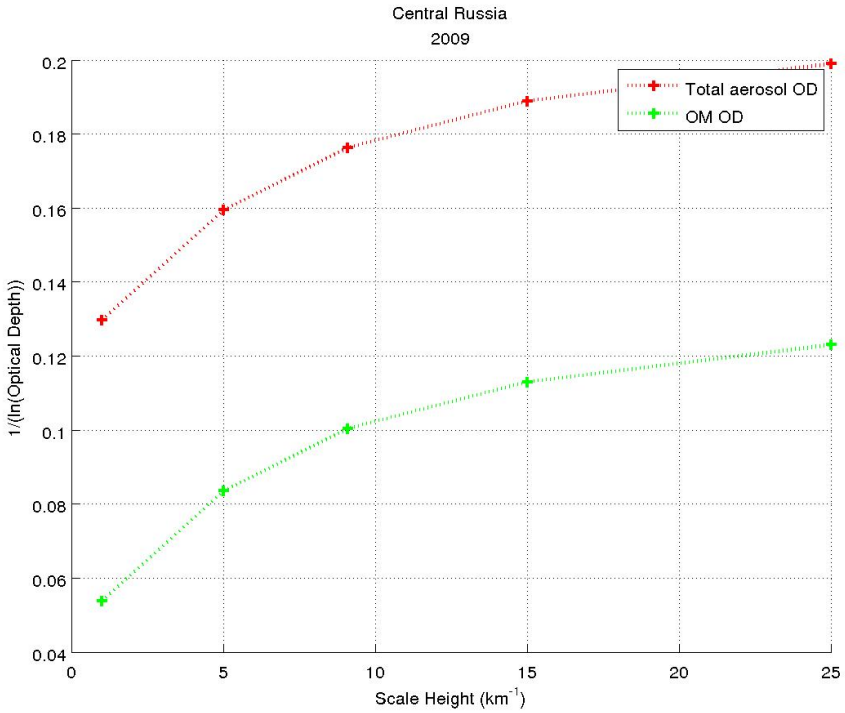


Figure B.3.6: *Relationship between the scale height on the optical depth in Central Russia for the year 2009 according to the Emep model.*

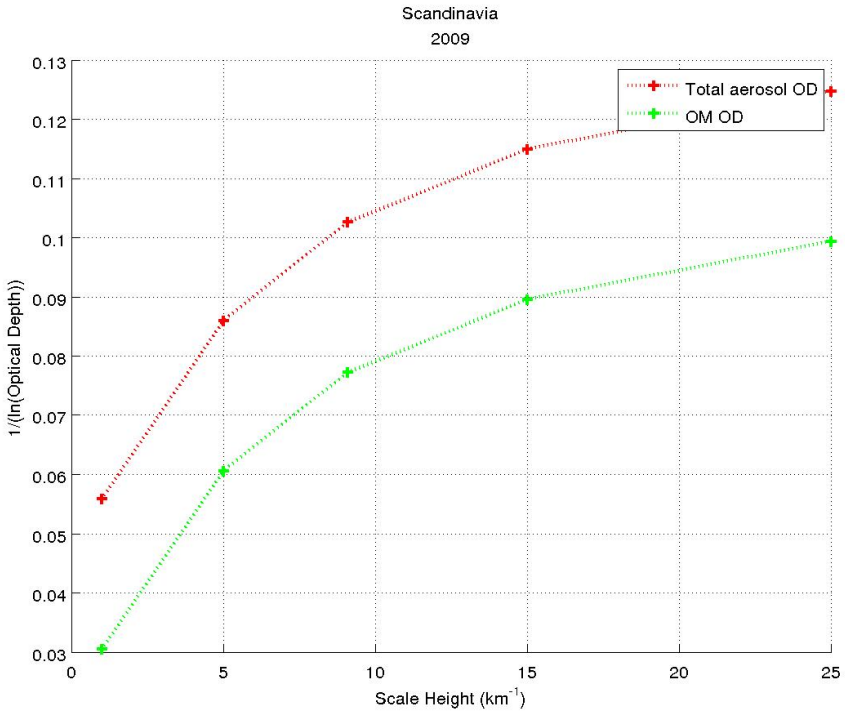


Figure B.3.7: *Relationship between the scale height on the optical depth in Scandinavia for the year 2009 according to the Emep model.*

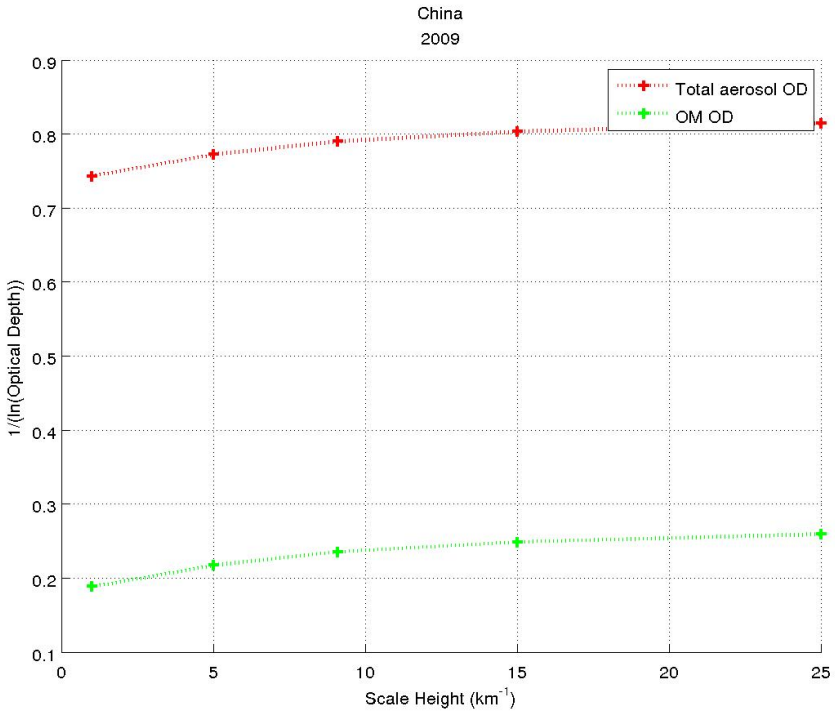


Figure B.3.8: *Relationship between the scale height on the optical depth in China for the year 2009 according to the Emep model.*

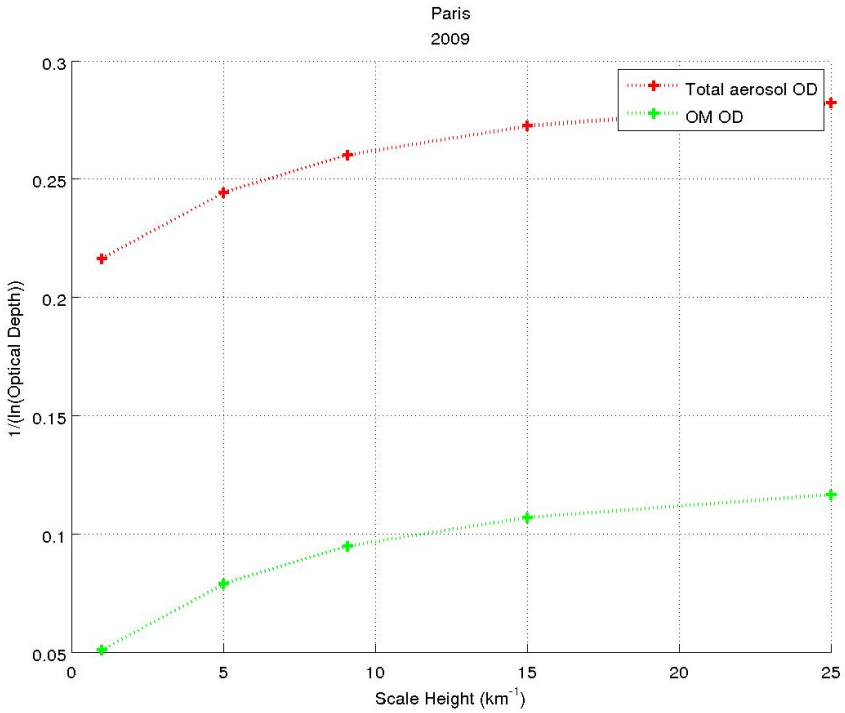


Figure B.3.9: *Relationship between the scale height on the optical depth in Paris for the year 2009 according to the Emep model.*

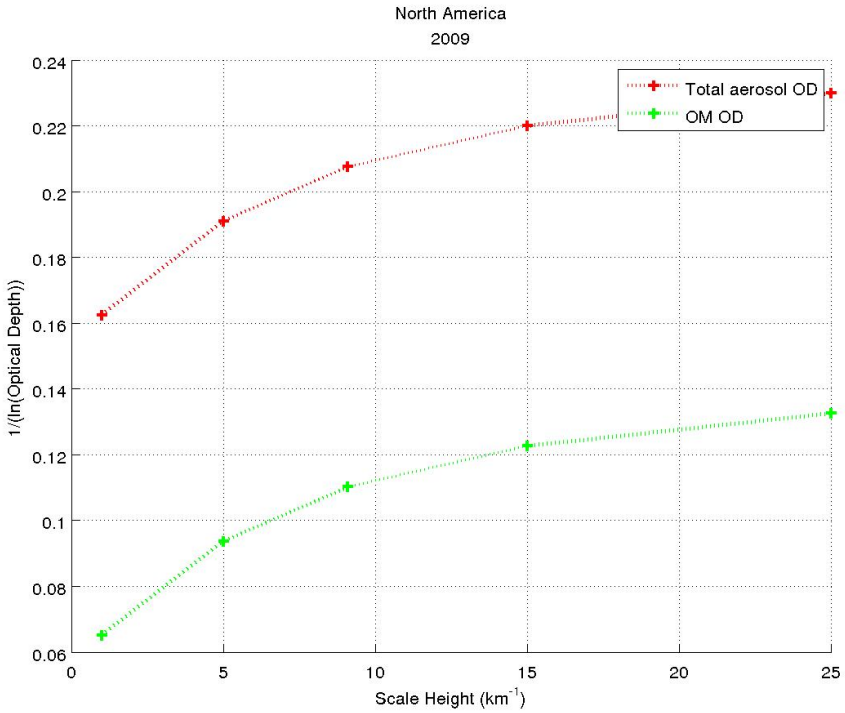


Figure B.3.10: *Relationship between the scale height on the optical depth in North America for the year 2009 according to the Emep model.*

### B.3.2 Extinction Vertical Distribution

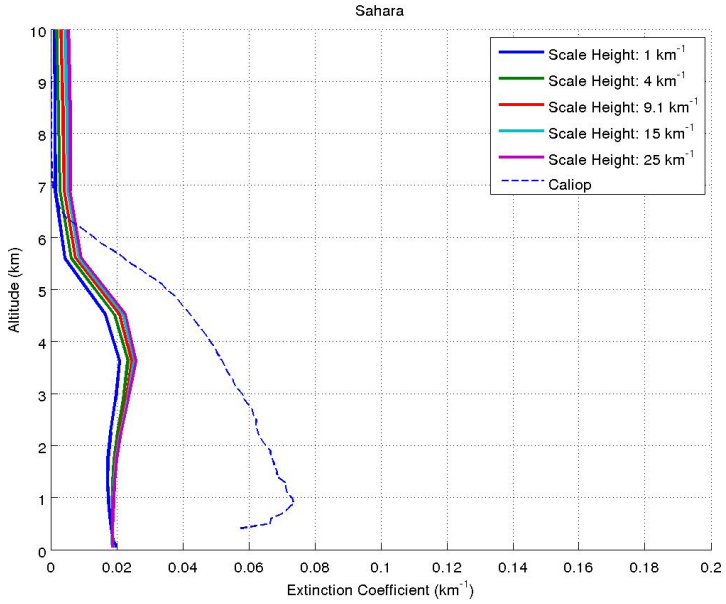


Figure B.3.11: *Vertical extinction coefficient profiles computed for five different scale heights and compared with the Caliop observation on a year basis in the Sahara.*

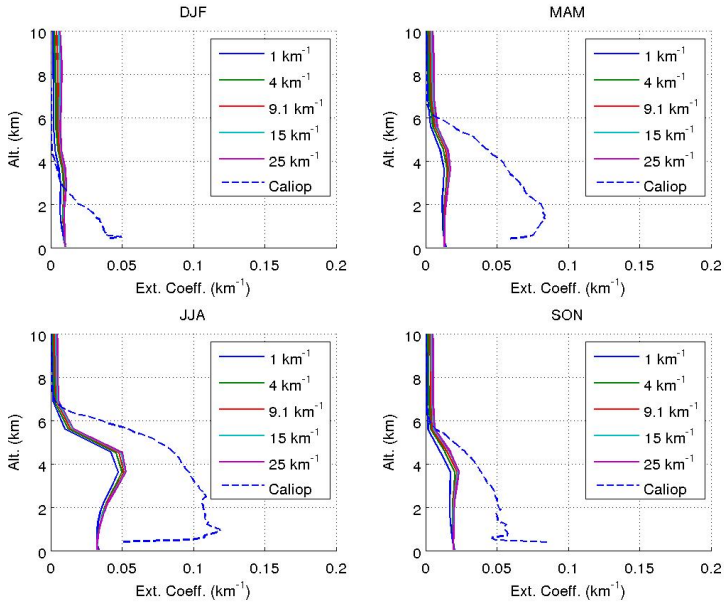


Figure B.3.12: *Vertical extinction coefficient profiles computed for five different scale heights and compared with the Caliop observation on a seasonal basis in the Sahara.*

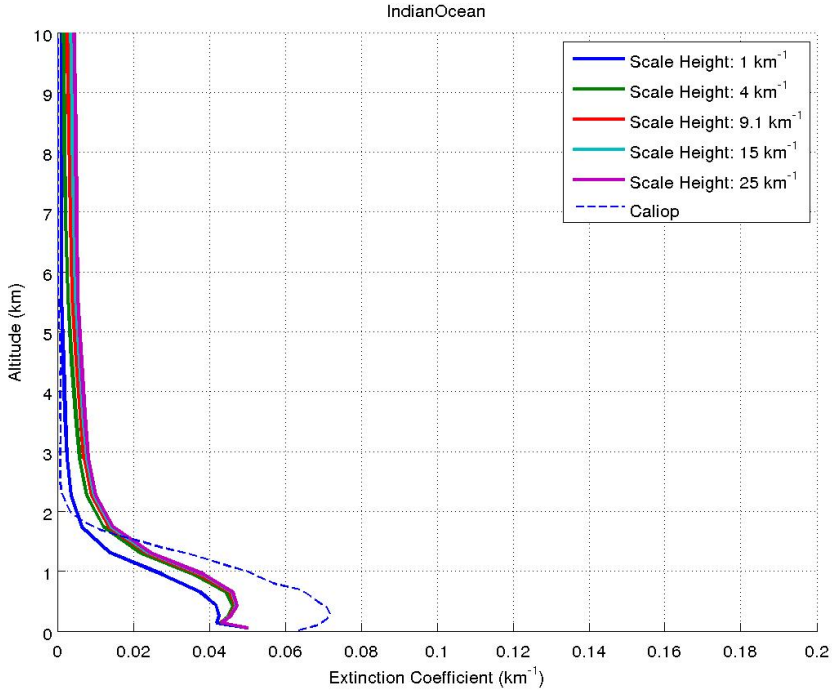


Figure B.3.13: *Vertical extinction coefficient profiles computed for five different scale heights and compared with the Caliop observation on a year basis in the Indian Ocean.*

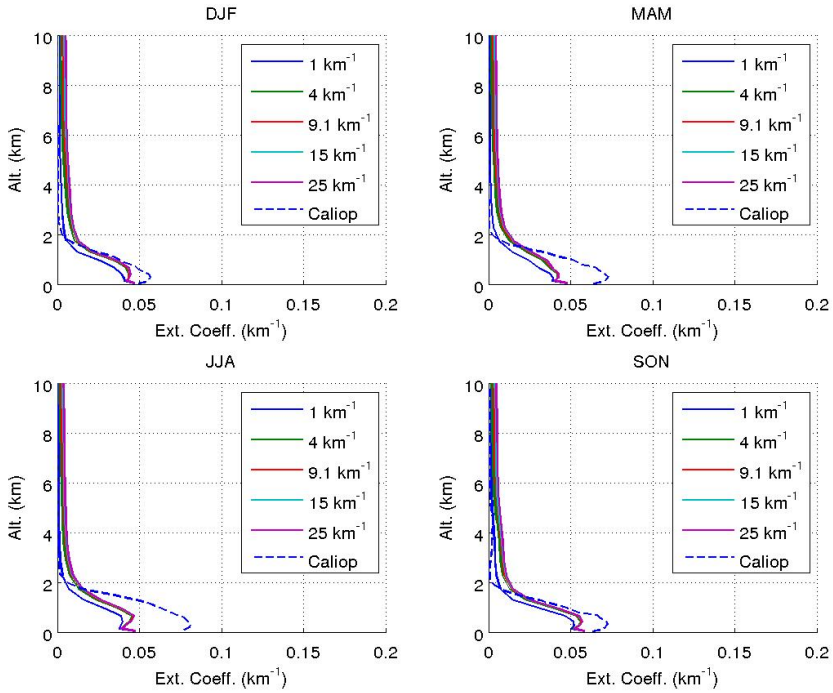


Figure B.3.14: *Vertical extinction coefficient profiles computed for five different scale heights and compared with the Caliop observation on a seasonal basis in the Indian Ocean.*

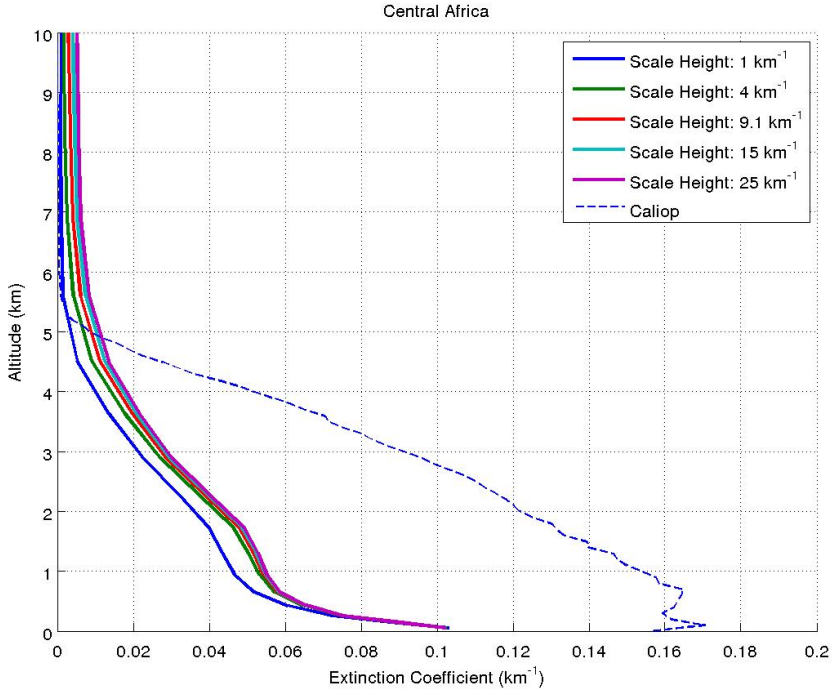


Figure B.3.15: *Vertical extinction coefficient profiles computed for five different scale heights and compared with the Caliop observation on a year basis in Central Africa.*

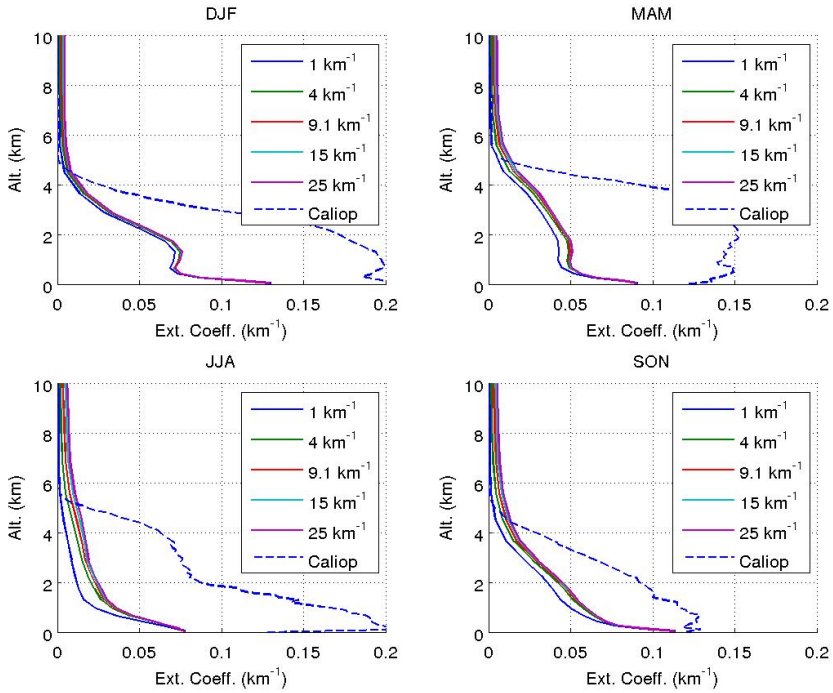


Figure B.3.16: *Vertical extinction coefficient profiles computed for five different scale heights and compared with the Caliop observation on a seasonal basis in Central Africa.*

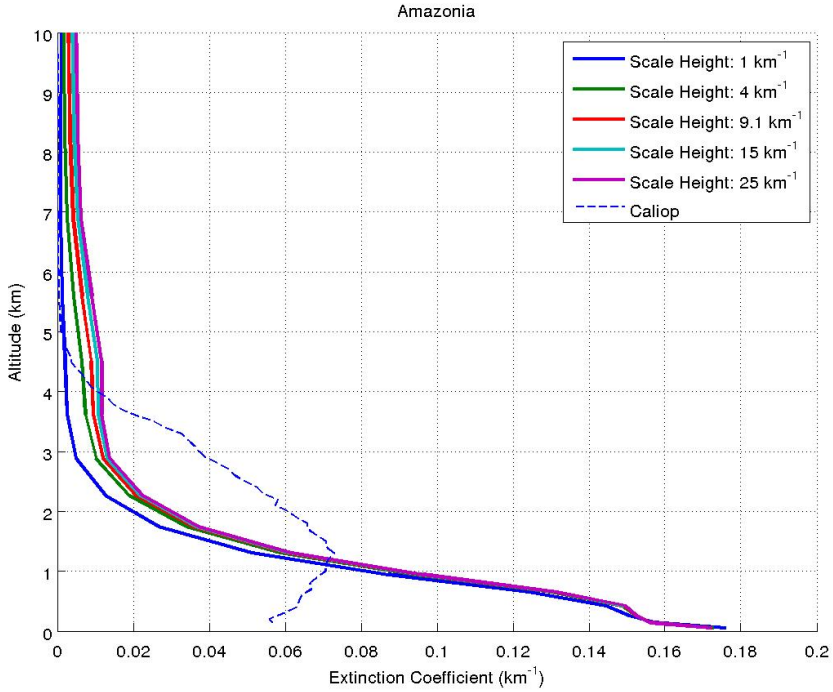


Figure B.3.17: *Vertical extinction coefficient profiles computed for five different scale heights and compared with the Caliop observation on a year basis in Amazonia.*

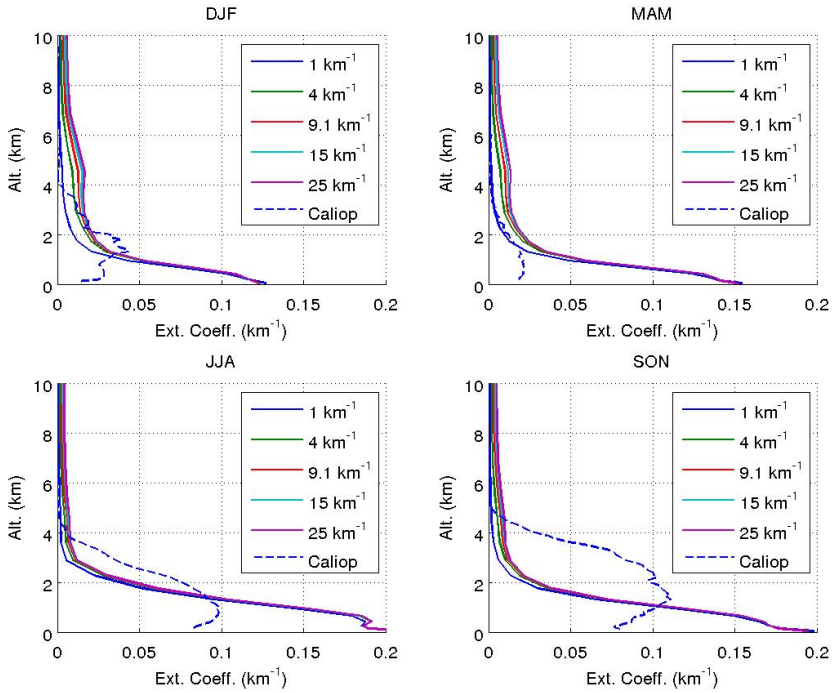


Figure B.3.18: *Vertical extinction coefficient profiles computed for five different scale heights and compared with the Caliop observation on a seasonal basis in Amazonia.*

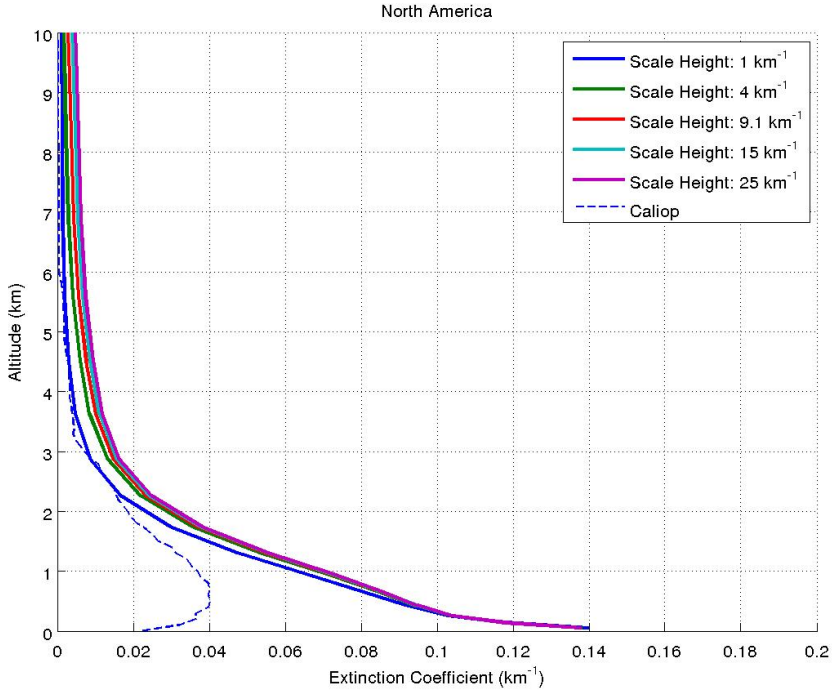


Figure B.3.19: *Vertical extinction coefficient profiles computed for five different scale heights and compared with the Caliop observation on a year basis in North America.*

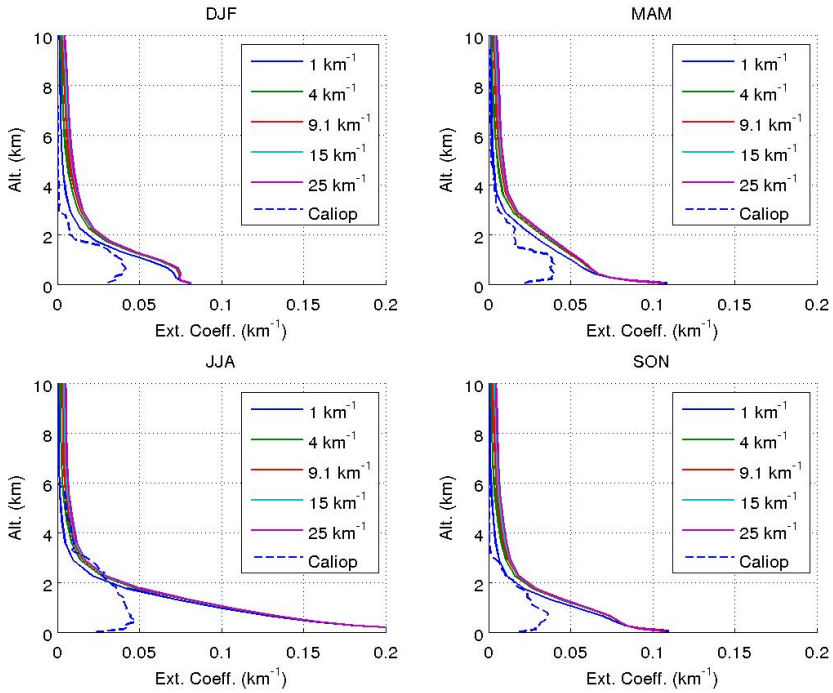


Figure B.3.20: *Vertical extinction coefficient profiles computed for five different scale heights and compared with the Caliop observation on a seasonal basis in North America.*

# C Appendix: MatLab codes.

## C.1 WorldMap.m

```
# function start
#
# clear;
# clc;
#
# ##### AREAS COORDINATES ----------------------------------------------------
#
# data = load('AOD_adjusted');
#
# A = isnan(data);
#
# for u = 1:length(A(:,1))
#     for v = 1:length(A(1,:))
#         if A(u,v) == 0
#             background(u,v) = 0.8;
#         else
#             background(u,v) = 1;
#         end
#     end
# end
#
# coor2 = load('Coordinates_3.txt');
# [coor] = coor_aerocom(coor2)
#
#
# ##### PLANISPHERE -----------------------------------------------------------
#
# landsea=netcdf.open('landsea_CALIOP3.nc', 'NC_NOWRITE');
# mask = netcdf.getVar(landsea, 0);
# lat = netcdf.getVar(landsea, 2);
# lon = netcdf.getVar(landsea, 1);
# netcdf.close(landsea);
#
# ##### REGION CREATION -------------------------------------------------------
#
# for i=1:1:length(coor(1,:))
#     for j=coor(1,i):1:coor(2,i)
#        for k=coor(3,i):1:coor(4,i)
#             background(j,k) = 0;
#         end
#     end
# end
#
# ##### PLOT FUNCTION ---------------------------------------------------------
#
# fig = figure;
# hold on;
# grid on;
# imagescnan(lon,lat, background)
# set(gca, 'XLim', [-180 180]);
# set(gca, 'YLim', [-90 90])
```

```
# contour(lon, lat, mask',1, 'b', 'LineWidth',2);
# colormap gray
# set(gca,'layer', 'top');
#
# saveas(fig, 'World_map_2.jpg');
#
# end
#
#
# ##### COORDINATES STANDARDIZATION ----------------------------------------
# (between the coordinates system used by Aerocom and the Geographical Reference System (GPS))
#
# function [coor] = coor_aerocom(coor2)
```

## C.2 SeasonalTrend.m

```
# function start
#
# clear;
# clc;
#
# ###-------------------------------------------------------------------------
# ###---- DEFINITION OF THE PARAMETERS -------------------------------------
# ###-------------------------------------------------------------------------
# c = 25; #Deviation from the mean
#
# ###-------------------------------------------------------------------------
# ###---- LOAD FILES -------------------------------------------------------
# ###-------------------------------------------------------------------------
#
# ###---- Coordinates of the selected areas --------------------------------
# coor_bis = load('Coordinates_real.txt');
# [coor] = change(coor_bis);
# [coor_aero] = change_aerocom(coor_bis);
# #[coor] = change(coor_bis)
# #coor_vd_bis = load('Coor_vd_1st_part.txt');
#
# ###---- AERONET data -----------------------------------------------------
# aeronet = load('aeronet_data.txt');
#
# ###---- CALIOP data ------------------------------------------------------
# for i=1:5
#     year = 2005 + i;
#     caliop_file = strcat('aerocom.CALIOP3.monthly.od550csaer.', num2str(year),'.nc');
#     caliop=netcdf.open(caliop_file, 'NC_NOWRITE');
#     AOD_caliop(i,:,:,:) = netcdf.getVar(caliop, 0);
#     netcdf.close(caliop);
# end
#
# ###---- EMEP data --------------------------------------------------------
# emep_file=netcdf.open('Reference.nc', 'NC_NOWRITE');
# [ndims,nvars,ngatts,unlimdimid] = netcdf.inq(emep_file);
# dimlen_new =[];
# for i=0:ndims-1
#    [dimname, dimlen] = netcdf.inqDim(emep_file,i);
```

```
#    dimlen_new = [dimlen_new; dimlen];
# end
# for i=0:nvars-1
#    [varname, xtype, dimids, numatts] = netcdf.inqVar(emep_file,i);
#    #---- Aerosol Optical Depth
#    if strcmp(num2str(varname), 'AOD') == 1
#        AOD_emep = netcdf.getVar(emep_file, i);
#    #---- Organic Matter Contribution
#    elseif strcmp(num2str(varname), 'AOD_OM') == 1
#        AOD_OM = netcdf.getVar(emep_file, i);
#    #---- Primary Organic Matter Contribution
#    elseif strcmp(num2str(varname), 'AOD_POM') == 1
#        AOD_POM = netcdf.getVar(emep_file, i);
#    #---- Extinction Coefficient
#    elseif strcmp(num2str(varname),'D3_ExtinCoef') == 1
#        EXT = netcdf.getVar(emep_file, i);
#    #---- Sigma Coordinates
#    elseif strcmp(num2str(varname), 'k') == 1
#        alt_e = netcdf.getVar(emep_file, i);
#    end
# end
# netcdf.close(emep_file);
#
# ###-------------------------------------------------------------------------
# ###     DATA PROCESSING - TEMPORAL EVOLUTION - OPTICAL DEPTH
# ###-------------------------------------------------------------------------
#
# for region = 1:length(coor)
#       [aeronet_data] = aeronet_load(region, aeronet);
#       [modis_data] = modis_load(coor, region);
#
#       [caliop_data] = process_caliop(AOD_caliop, coor_aero, region);
#       [emep_data] = process_emep(AOD_emep, coor_aero, region);
#       [om_data] = process_emep(AOD_OM+AOD_POM, coor_aero, region);
#
#       [td_aer] = trend(aeronet_data,c);
#       [td_modis] = trend(modis_data,c);
#       [td_caliop] = trend(caliop_data,c);
#
#       temporal_evolution(td_aer, td_modis, td_caliop, emep_data, om_data, region);
# end
# end
#
# ###-------------------------------------------------------------------------
# ### ------- DATA LOADING FUNCTIONS for each area (Aeronet & Modis) --------
# ###-------------------------------------------------------------------------
#
# function [aeronet_data] = aeronet_load(region, aeronet);
# for i=1:5
#     for j=1:12
#         aeronet_data(i,j) = aeronet((i-1)*12+j, region);
#     end
# end
# end
#
# function [modis_data] = modis_load(coor, region);
```

```
# for y = 1:5
#     year = 2005 + y;
#     for month=1:12
#         modis_file = strcat('modis_aod_', num2str(year),'_',num2str(month),'.txt');
#         modis = load(modis_file);
#
#         m = 0;
#         n = 0;
#         for i = coor(1,region):1:coor(2, region)
#             for j = coor(3, region):1:coor(4, region)
#                 if modis(i,j) < 0
#                     m = m;
#                     n = n;
#                 else
#                     m = m + modis(i,j);
#                     n = n + 1;
#                 end
#             end
#         end
#
#         if n == 0
#             modis_data(y,month) = NaN;
#         else
#             modis_data(y,month) = m/n;
#         end
#     end
# end
# end
#
# ###-------------------------------------------------------------------------
# ###---- STANDARDIZATION ------------------------------------------------
# ###-------------------------------------------------------------------------
#
# ###---- Coordinates Standardization ------------------------------------
# #(between the coordinates system used for the Aeronet, Modis and Caliop data and the Geographical
Reference System (GPS))
#
# function [coor] = change(coor2)
# for i=1:length(coor2(1,:))
#     if coor2(1,i) <= 0
#         coor(1,i) = 91 + abs(coor2(1,i));
#     else
#         coor(1,i) = 90 - coor2(1,i);
#     end
#     if coor2(2,i) <= 0
#         coor(2,i) = coor(1,i)+4;
#     else
#         coor(2,i) = coor(1,i)-4;
#     end
#     if coor2(3,i) <= 0
#         coor(3,i) = 180 + coor2(3,i);
#     else
#         coor(3,i) = 181 + coor2(3,i);
#     end
#     if coor2(4,i) <= 0
#         coor(4,i) = coor(3,i)-4;
```

```
#     else
#         coor(4,i) = coor(3,i) +4;
#     end
#
#     if coor(1,i) > coor(2,i)
#         a = coor(2,i);
#         coor(2,i) = coor(1,i);
#         coor(1,i) = a;
#     else
#     end
#     if coor(3,i) > coor(4,i)
#         b = coor(4,i);
#         coor(4,i) = coor(3,i);
#         coor(3,i) = b;
#     else
#     end
#
# end
# end
#
# #(between the coordinates system used by Aerocom and the Geographical Reference System (GPS))
#
# function [coor] = change_aerocom(coor2)
# for i=1:length(coor2(1,:))
#     if coor2(1,i) <= 0
#         coor(1,i) = 90 + (coor2(1,i));
#     else
#         coor(1,i) = 91 + coor2(1,i);
#     end
#     if coor2(2,i) < 0
#         coor(2,i) = coor(1,i)-4;
#     else
#         coor(2,i) = coor(1,i)+4;
#     end
#     if coor2(3,i) < 0
#         coor(3,i) = 180 + coor2(3,i);
#     else
#         coor(3,i) = 181 + coor2(3,i);
#     end
#     if coor2(4,i) < 0
#         coor(4,i) = coor(3,i)-4;
#     else
#         coor(4,i) = coor(3,i) +4;
#     end
#
#     if coor(1,i) > coor(2,i)
#         a = coor(2,i);
#         coor(2,i) = coor(1,i);
#         coor(1,i) = a;
#     else
#     end
#     if coor(3,i) > coor(4,i)
#         b = coor(4,i);
#         coor(4,i) = coor(3,i);
#         coor(3,i) = b;
#     else
```

```
#     end
#
# end
# end
#
# ###---- SEASONAL STANDARDIZATION ----------------------------------------
# #(Winter: December, January and February)
# #(Spring: March, April and May)
# #(Summer: June, July and August)
# #(Fall: September, October and November)
#
# function [data] = change_order(data_1)
# for k = 1:length(data_1(1,1,1,:))-1
#     data(:,:,:,k+1) = data_1(:,:,:,k);
# end
# data(:,:,:,1) = data_1(:,:,:,12);
# clear data_1;
# end
#
# ###---- DATA STANDARDIZATION --------------------------------------------
# #(Calculation of averaged data on a monthly basis with the same format)
#
# function [data] = process_caliop(AOD, coor, region)
# A = isnan(AOD);
# for k=1:5
#     for month=1:12
#         m = 0;
#         n = 0;
#         for j = coor(1,region):1:coor(2, region)
#             for i = coor(3, region):1:coor(4, region)
#                 if A(k,i,j,month) == 0 & AOD(k,i,j,month) < 3
#                     m = m + AOD(k,i,j,month);
#                     n = n + 1;
#                 else
#                 end
#             end
#         end
#
#         if n == 0
#             data(k,month) = NaN;
#         else
#             data(k,month) = m/n;
#         end
#
#     end
# end
#
# end
#
# function [data] = process_emep(AOD, coor, region)
# A = isnan(AOD);
# for month=1:12
#     m = 0;
#     n = 0;
#     for j = coor(1,region):1:coor(2, region)
#         for i = coor(3, region):1:coor(4, region)
```

```
#             if A(i,j,month) == 0 & AOD(i,j,month) < 3
#                 m = m + AOD(i,j,month);
#                 n = n + 1;
#             else
#             end
#         end
#     end
#
#     if n == 0
#         data(month) = NaN;
#     else
#         data(month) = m/n;
#     end
#
# end
# end
#
# ###-------------------------------------------------------------------------
# ###---- ALGORITHM calculating the seasonal trend from a set of data --------
# ###-------------------------------------------------------------------------
#
# function [td] = trend(data,c)
# [td] = average(data);
# n = 0;
#
# for i=1:length(data(:,1))
#     for j=1:length(data(1,:))
#         ec(i,j) = (data(i,j)-td(j))/(td(j));
#
#         if abs(ec(i,j)) > c/100
#             data(i,j) = NaN;
#             n = n + 1;
#         else
#         end
#
#     end
# end
#
# if n ~= 0
#     [td] = trend(data,c);
# else
# end
#
# end
#
# function [data_average] = average(data)
# D =isnan(data);
# for j=1:length(data(1,:))
#     m = 0;
#     n =0;
#     for i=1:length(data(:,1))
#         if D(i,j) == 0
#             m = m + data(i,j);
#             n = n + 1;
#         else
#         end
```

```
#     end
#
#     if n == 0
#         data_average(j) = NaN;
#     else
#         data_average(j) = m/n;
#     end
#
# end
# end
#
# ###-------------------------------------------------------------------------
# ###---- PLOT FUNCTION ------------------------------------------------------
# ###-------------------------------------------------------------------------
# function temporal_evolution(td_aer, td_modis, td_caliop, emep_data, om_data, region);;
# T = [0 1 2 3 4 5 6 7 8 9 10 11];
# region_name = {'Sahara' 'IndianOcean' 'PacificOcean' 'Equatorial Forest' 'Amazonia' 'Central
Russia' 'Scandinavia' 'China' 'Paris' 'North America'};
#
# fig_season = figure;
# hold on;
# plot( T, td_aer, T, td_modis, T, td_caliop, T, emep_data, 'LineWidth', 2);
# grid on;
# set(gca, 'XLim', [0 11]);
# set(gca, 'YLim', [0 0.5]);
# set(gca, 'XTick', 0:11, 'XTickLabel', {'J' 'F' 'M' 'A' 'M' 'J' 'J' 'A' 'S' 'O' 'N' 'D'});
# ylabel('Optical Depth ');
# title([region_name(region)]);
# legend('Aeronet', 'Modis', 'Caliop','Emep');
#
# A1 = char(region_name(region));
# formatSpec = '#s.jpg';
# saveas(fig_season, sprintf(formatSpec,A1));
#
# end
```

## C.3 OrganicAerosolStudy.m

```
# function start
#
# clear;
# clc;
#
# ###-------------------------------------------------------------------------
# ###---- INITIALIZATION OF THE PARAMETERS ----------------------------------
# ###-------------------------------------------------------------------------
# i_0 = 1;
# j_0 = 1;
# m = 1;
# n = 1;
# count = 0;
# c = 25;
# N = 0;
#
# ###-------------------------------------------------------------------------
```

```
# ###---- DATA LOADING ----------------------------------------------------
# ###----------------------------------------------------------------------
# [AOD_caliop, AOD_emep, AOD_OM, AOD_POM, AOD_SO4, AOD_NO3, AOD_NH4, AOD_EC, AOD_SS, AOD_DU, MODIS]
= loadfiles();
#
# landsea=netcdf.open('landsea_CALIOP3.nc', 'NC_NOWRITE');
# mask = netcdf.getVar(landsea, 0);
# lat = netcdf.getVar(landsea, 2);
# lon = netcdf.getVar(landsea, 1);
# netcdf.close(landsea);
#
# ###----------------------------------------------------------------------
# ###---- DATA PROCESSING -------------------------------------------------
# ###----------------------------------------------------------------------
#
# [data, dependency, share, N] = adjustement(AOD_caliop, AOD_emep, AOD_OM, AOD_POM, AOD_SO4, AOD_NO3,
 AOD_NH4, AOD_EC, AOD_SS, AOD_DU, MODIS, c)
# [yearly_data] = year_average(data);
# [yearly_share] = year_average(share);
# dlmwrite('AOD_adjusted', yearly_data);
# coherence = 100*N/(360*180/5/5)
#
# ###----------------------------------------------------------------------
# ###---- PLOT FUNCTIONS --------------------------------------------------
# ###----------------------------------------------------------------------
#
# fig_year_share = figure;
# hold on;
# imagescnan(lon,lat,yearly_share);
# axis([-180 180 -90 90]);
# caxis([0 1]);
# colorbar;
# contour(lon, lat, mask', 1, 'k','LineWidth', 2);
#
# saveas(fig_year_share, 'share_year_contribution.jpg');
#
# fig_year_share = figure;
# hold on;
# imagescnan(lon, lat, yearly_data);
# axis([-180 180 -90 90]);
# colorbar;
# contour(lon, lat, mask', 1, 'k','LineWidth', 2);
#
# saveas(fig_year_share, 'ODOA_year_contribution.jpg');
#
# end
#
# ###----------------------------------------------------------------------
# ###---- GENERAL FUNCTION FOR THE DATA PROCESSING ------------------------
# ###----------------------------------------------------------------------
#
# function [data, dependency, share, N] = adjustement(AOD_caliop, AOD_emep, AOD_OM, AOD_POM, AOD_SO4,
 AOD_NO3, AOD_NH4, AOD_EC, AOD_SS, AOD_DU, MODIS, c)
#
# ###---- Initialization of parameters ------------------------------------
# data = [];
```

```
# n = 0;
# N = 0;
#
# ###---- Definition of the 5x5 areas ----------------------------------
# for i=1:5:176
#     for j=1:5:356
#         coor(1) = i;
#         coor(2) = i + 4;
#         coor(3) = j;
#         coor(4) = j + 4;
#
# ###---- Algorithm processing for each area ---------------------------
#         [r, p, N, r_2]= unit_process(AOD_caliop, AOD_emep, AOD_OM, AOD_POM, AOD_SO4, AOD_NO3,
 AOD_NH4, AOD_EC, AOD_SS, AOD_DU, MODIS, coor,c, N);
#
# ###---- Adjustement of the coordinates -------------------------------
#         for u=coor(1):coor(2)
#             for v=coor(3):coor(4)
#                 dependency(180-u+1,v) = p;
#                 for k = 1:12
#                     data(180-u+1,v,k) = r(k);
#                     share(180-u+1,v,k) = r_2(k);
#                 end
#             end
#         end
#         N
#         n=n+1
#     end
# end
# end
#
# ###-------------------------------------------------------------------
# ###---- ALGORITHM ----------------------------------------------------
# ###-------------------------------------------------------------------
#
# function [r, p, N, r_2] = unit_process(AOD_caliop, AOD_emep, AOD_OM, AOD_POM, AOD_SO4, AOD_NO3,
 AOD_NH4, AOD_EC, AOD_SS, AOD_DU, MODIS, coor,c,N)
#
# ###---- Criterion of similarity between the Caliop and Modis data sets ----
# s = 5;
#
# ###---- Standardization of the format of the data --------------------
# [modis_data] = process_modis(MODIS, coor);
# [caliop_data] = process(AOD_caliop, coor);
#
# ###---- Computation of averages --------------------------------------
# [td_modis] = trend(modis_data,c);
# [td_caliop] = trend(caliop_data,c);
#
# [similarity_modis_caliop] = similarity(td_modis, td_caliop);
#
# if similarity_modis_caliop > s
#     Rmc = corr(td_modis', td_caliop', 'rows', 'complete');
#     if abs(Rmc) > 0.5
#         A = isnan(td_modis);
#         B = isnan(td_caliop);
```

```
#         for k=1:length(td_modis)
#             if A(k) == 0 & B(k) == 0
#                 satellite_data(k) = (td_modis(k)+td_caliop(k))/2;
#             elseif A(k) == 1 & B(k) == 0
#                 satellite_data(k) = td_caliop(k);
#             elseif A(k) == 0 & B(k) == 1
#                 satellite_data(k) = td_modis(k);
#             elseif A(k) == 1 & B(k) == 1
#                 satellite_data(k) = NaN;
#             end
#         end
#
#        [emep_data] = process_emep(AOD_emep, coor);
#        [similarity_emep_satellite] = similarity(satellite_data, emep_data);
#
#        if similarity_emep_satellite > s
#            Res = corr(emep_data', satellite_data','rows', 'complete');
#            if abs(Res) > 0.5
#                N = N + 1;
#
#                [om] = process_emep(AOD_OM+AOD_POM, coor);
#                [so4] = process_emep(AOD_SO4, coor);
#                [no3] = process_emep(AOD_NO3, coor);
#                [nh4] = process_emep(AOD_NH4, coor);
#                [ec] = process_emep(AOD_EC, coor);
#                [ss] = process_emep(AOD_SS, coor);
#                [du] = process_emep(AOD_DU, coor);
#
#                r_2 = ss./emep_data;  #--- Change Aerosols ------------
#                r = satellite_data.*r_2;
#
#                R(1) = abs(corr(emep_data', om','rows', 'complete'));
#                R(2) = abs(corr(emep_data', so4','rows', 'complete'));
#                R(3) = abs(corr(emep_data', no3','rows', 'complete'));
#                R(4) = abs(corr(emep_data', nh4','rows', 'complete'));
#                R(5) = abs(corr(emep_data', ec','rows', 'complete'));
#                R(6) = abs(corr(emep_data', ss','rows', 'complete'));
#                R(7) = abs(corr(emep_data', du','rows', 'complete'));
#                [value, ind] = max(R);
#
#                if value > 0.75
#                    p = ind;
#                else
#                    p = NaN;
#                end
#            else
#                [r, p, r_2] = nan();
#            end
#        else
#            [r, p, r_2] = nan();
#        end
#     else
#         [r, p, r_2] = nan();
#     end
# else
#     [r, p, r_2] = nan();
```

```
# end
# end
#
# ###-------------------------------------------------------------------------
# ###---- ANCILLARY FUNCTIONS ------------------------------------------------
# ###-------------------------------------------------------------------------
#
# function [data_average] = average(data)
#
# D =isnan(data);
#
# for j=1:length(data(1,:))
#     m = 0;
#     n =0;
#     for i=1:length(data(:,1))
#      if D(i,j) == 0
#          m = m + data(i,j);
#          n = n + 1;
#      else
#           end
#     end
#     if n == 0
#         data_average(j) = NaN;
#     else
#         data_average(j) = m/n;
#     end
# end
# end
#
# function [y_s] = year_average(share)
#
# A = isnan(share);
#
# for u = 1:length(share(:,1,1))
#     for v = 1:length(share(1,:,1))
#         m = 0;
#         n = 0;
#         for t = 1:length(share(1,1,:))
#             if A(u,v,t) == 0
#                 m = m + share(u,v,t);
#                 n = n + 1;
#             else
#             end
#         end
#         if n == 0
#             y_s(u,v) = NaN;
#         else
#             y_s(u,v) = m/n;
#         end
#     end
# end
# end
#
# function [similarity] = similarity(A,B)
#
# a = isnan(A);
```

```
# b = isnan(B);
#
# count = 0;
# count_2 = 0;
#
# for i=1:length(A)
#     if a(i) == 1 & b(i) == 1
#         count = count + 1;
#     elseif a(i) == 0 & b(i) == 1
#         count_2 = count_2 + 1;
#     elseif a(i) == 1 & b(i) == 0
#         count_2 = count_2 + 1;
#     end
# end
# similarity = length(A) - count - count_2;
# end
#
# function [td] = trend(data,c)
#
# [td] = average(data);
# n = 0;
#
# for i=1:length(data(:,1))
#     for j=1:length(data(1,:))
#         ec(i,j) = (data(i,j)-td(j))/(td(j));
#         if ec(i,j) > c/100
#             data(i,j) = NaN;
#             n = n + 1;
#         else
#         end
#     end
# end
# if n ~= 0
#     [td] = trend(data,c);
# else
# end
# end
#
# function [r, p, r_2] = nan();
#    for k = 1:12
#        r(k) = NaN;
#        p = NaN;
#        r_2(k) = NaN;
#    end
# end
#
# ###-------------------------------------------------------------------------
# ###---- Format Standardization Functions ---------------------------------
# ###-------------------------------------------------------------------------
#
# ###---- Modis Data Processing --------------------------------------------
# function [modis_data] = process_modis(MODIS, coor);
#
# for k = 1:5
#     for month = 1:12
#         m = 0;
```

```
#         n = 0;
#         for i = coor(1):1:coor(2)
#             for j = coor(3):1:coor(4)
#                 if MODIS(i,j,k,month) < 0
#                     m = m;
#                     n = n;
#                 else
#                     m = m + MODIS(i,j,k,month);
#                     n = n + 1;
#                 end
#             end
#         end
#
#         if n == 0
#             modis_data(k,month) = NaN;
#         else
#             modis_data(k,month) = m/n;
#         end
#     end
# end
# end
#
# ###---- Caliop Data Processing ------------------------------------------
# function [caliop_data] = process(AOD, coor2)
#
# [coor] = change(coor2);
#
# A = isnan(AOD);
#
# for k=1:5
#     for month=1:12
#         m = 0;
#         n = 0;
#         for j = coor(1):1:coor(2)
#             for i = coor(3):1:coor(4)
#                 if A(k,i,j,month) == 0 & AOD(k,i,j,month) < 3
#                     m = m + AOD(k,i,j,month);
#                     n = n + 1;
#                 else
#                 end
#             end
#         end
#
#         if n == 0
#             caliop_data(k,month) = NaN;
#         else
#             caliop_data(k,month) = m/n;
#         end
#
#     end
# end
#
# end
#
# ###---- Emep Data Processing --------------------------------------------
# function [emep_data] = process_emep(AOD, coor2)
```

```
#
# [coor] = change(coor2);
#
# A = isnan(AOD);
#
# for month=1:12
#     m = 0;
#     n = 0;
#     for j = coor(1):1:coor(2)
#         for i = coor(3):1:coor(4)
#             if A(i,j,month) == 0 & AOD(i,j,month) < 3
#                 m = m + AOD(i,j,month);
#                 n = n + 1;
#             else
#             end
#         end
#     end
#
#     if n == 0
#         emep_data(month) = NaN;
#     else
#         emep_data(month) = m/n;
#     end
#
# end
#
# end
#
# ###-------------------------------------------------------------------------
# ###---- STANDARDIZATION OF THE COORDINATES -------------------------------
# ###-------------------------------------------------------------------------
#
# #(between the coordinates system used by Aerocom and the Geographical Reference System (GPS))
# function [coor] = change_aerocom(coor2)
#
# for i=1:length(coor2(1,:))
#     if coor2(1,i) <= 0
#         coor(1,i) = 90 + (coor2(1,i));
#     else
#         coor(1,i) = 91 + coor2(1,i);
#     end
#     if coor2(2,i) < 0
#         coor(2,i) = coor(1,i)-4;
#     else
#         coor(2,i) = coor(1,i)+4;
#     end
#     if coor2(3,i) < 0
#         coor(3,i) = 180 + coor2(3,i);
#     else
#         coor(3,i) = 181 + coor2(3,i);
#     end
#     if coor2(4,i) < 0
#         coor(4,i) = coor(3,i)-4;
#     else
#         coor(4,i) = coor(3,i) +4;
#     end
```

```
#
#     if coor(1,i) > coor(2,i)
#         a = coor(2,i);
#         coor(2,i) = coor(1,i);
#         coor(1,i) = a;
#     else
#     end
#     if coor(3,i) > coor(4,i)
#         b = coor(4,i);
#         coor(4,i) = coor(3,i);
#         coor(3,i) = b;
#     else
#     end
# end
# end
#
# #(between the coordinates system used for the Aeronet, Modis and Caliop data and the Geographical
 Reference System (GPS))
# function [coor] = change(coor2)
# a = 180 - coor2(1) + 1;
# b = 180 - coor2(2) + 1;
# coor(1) = min(a,b);
# coor(2) = max(a,b);
# coor(3) = coor2(3);
# coor(4) = coor2(4);
# end
#
# ###-------------------------------------------------------------------------
# ###---- DATA LOADING FUNCTIONS -----------------------------------------
# ###-------------------------------------------------------------------------
#
# function [AOD_caliop, AOD_emep, AOD_OM, AOD_POM, AOD_SO4, AOD_NO3, AOD_NH4, AOD_EC, AOD_SS, AOD_DU,
 MODIS] = loadfiles();
#
# ###---- Modis Data -----------------------------------------------------
#
# for y = 1:5
#     year = 2005 + y;
#     for month=1:12
#         modis_file = strcat('modis_aod_', num2str(year),'_',num2str(month),'.txt');
#         modis = load(modis_file);
#         MODIS(:,:,y,month) = load(modis_file);
#     end
# end
#
# ###---- Caliop Data ----------------------------------------------------
#
# for i=1:5
#     year = 2005 + i;
#     caliop_file = strcat('aerocom.CALIOP3.monthly.od550csaer.', num2str(year),'.nc');
#     caliop=netcdf.open(caliop_file, 'NC_NOWRITE');
#     AOD_caliop(i,:,:,:) = netcdf.getVar(caliop, 0);
#     netcdf.close(caliop);
# end
#
# ###---- Emep Data ------------------------------------------------------
```

```
#
# emep_file=netcdf.open('Reference.nc', 'NC_NOWRITE');
# [ndims,nvars,ngatts,unlimdimid] = netcdf.inq(emep_file);
# dimlen_new =[];
#
# for i=0:ndims-1
#    [dimname, dimlen] = netcdf.inqDim(emep_file,i);
#    dimlen_new = [dimlen_new; dimlen];
# end
#
# for i=0:nvars-1
#    [varname, xtype, dimids, numatts] = netcdf.inqVar(emep_file,i);
#    if strcmp(num2str(varname), 'AOD') == 1
#        AOD_emep = netcdf.getVar(emep_file, i);
#    elseif strcmp(num2str(varname), 'AOD_OM') == 1
#        AOD_OM = netcdf.getVar(emep_file, i);
#    elseif strcmp(num2str(varname), 'AOD_POM') == 1
#        AOD_POM = netcdf.getVar(emep_file, i);
#    elseif strcmp(num2str(varname), 'AOD_SO4') == 1
#        AOD_SO4 = netcdf.getVar(emep_file, i);
#    elseif strcmp(num2str(varname), 'AOD_NO3') == 1
#        AOD_NO3 = netcdf.getVar(emep_file, i);
#    elseif strcmp(num2str(varname), 'AOD_NH4') == 1
#        AOD_NH4 = netcdf.getVar(emep_file, i);
#    elseif strcmp(num2str(varname), 'AOD_EC') == 1
#        AOD_EC = netcdf.getVar(emep_file, i);
#    elseif strcmp(num2str(varname), 'AOD_SS') == 1
#        AOD_SS = netcdf.getVar(emep_file, i);
#    elseif strcmp(num2str(varname), 'AOD_DU') == 1
#        AOD_DU = netcdf.getVar(emep_file, i);
#    end
# end
# netcdf.close(emep_file);
# end
```

## C.4 ExtinctionCoefficient.m

```
# function start
# clear;
# clc;
# ###-------------------------------------------------------------------------
# ###---- DATA LOADING FUNCTION ----------------------------------------------
# ###-------------------------------------------------------------------------
#
# ###---- Coordinates of the areas selected ----------------------------------
# coor = load('Coordinates_3.txt');
# #coor2 =change(coor);
# coor2 = change_aerocom(coor);
#
# ###---- Emep Data ----------------------------------------------------------
# file_id=netcdf.open('Reference.nc', 'NC_NOWRITE');
# [ndims,nvars,ngatts,unlimdimid] = netcdf.inq(file_id);
# dimlen_new =[];
# for i=0:ndims-1
```

```
#    [dimname, dimlen] = netcdf.inqDim(file_id,i);
#    dimlen_new = [dimlen_new; dimlen];
# end
#
# for i=0:nvars-1
#    [varname, xtype, dimids, numatts] = netcdf.inqVar(file_id,i);
#    if strcmp(num2str(varname), 'k') == 1
#        alt_m = netcdf.getVar(file_id, i);
#    elseif strcmp(num2str(varname), 'time') == 1
#        time = netcdf.getVar(file_id, i);
#    elseif strcmp(num2str(varname), 'D3_ExtinCoef') == 1
#        EXT = netcdf.getVar(file_id, i);
#   elseif strcmp(num2str(varname), 'D3_ext_OM') == 1
#        OM_EXT = netcdf.getVar(file_id, i);
#   elseif strcmp(num2str(varname), 'D3_ext_POM') == 1
#        POM_EXT = netcdf.getVar(file_id, i);
#    elseif strcmp(num2str(varname), 'AOD_OM') == 1
#        AOD_OM = netcdf.getVar(file_id, i);
#    elseif strcmp(num2str(varname), 'AOD_POM') == 1
#        AOD_POM = netcdf.getVar(file_id, i);
#    elseif strcmp(num2str(varname), 'AOD') == 1
#        AOD_emep = netcdf.getVar(file_id, i);
#    else
#    end
# end
# netcdf.close(file_id);
#
# ###-------------------------------------------------------------------------
# ###---- DATA PROCESSING ----------------------------------------------------
# ###-------------------------------------------------------------------------
# [emep_season, om_season, pom_season, caliop_season, alt] = oa_vertical_distribution(coor2, EXT,
 OM_EXT, POM_EXT, AOD_emep, AOD_OM, AOD_POM);
#
# ###-------------------------------------------------------------------------
# ###---- ALTITUDE STANDARDIZATION -------------------------------------------
# ###-------------------------------------------------------------------------
# alt_s = alt_standardization(alt_m);
# [caliop_season_alt] = altitude_transformation(caliop_season, alt, alt_s);
#
# ###-------------------------------------------------------------------------
# ###---- PLOT FUNCTION ------------------------------------------------------
# ###-------------------------------------------------------------------------
# # plot_seasonal_profile(alt_s, alt_s, (om_season+pom_season)./emep_season.*caliop_season_alt,
 caliop_season_alt,coor2);
# # end
#
# ###-------------------------------------------------------------------------
# ###---- DATA PROCESSING FUNCTION -------------------------------------------
# ###-------------------------------------------------------------------------
#
# ###---- Main Function ------------------------------------------------------
# function [emep_season, om_season, pom_season, caliop_season, alt] = oa_vertical_distribution(
coor2, EXT, OM_EXT, POM_EXT, AOD_emep, AOD_OM, AOD_POM)
# #---- Caliop data loading ------------------------------------------------
# for y=1:5
#      year = 2005 + y;
```

```
#     caliop_file = strcat('aerocom.CALIOP3.monthly.ec532cs3Daer.', num2str(year),'.nc');
#     file_ec_caliop=netcdf.open(caliop_file, 'NC_NOWRITE');
#
#     [ndims,nvars,ngatts,unlimdimid] = netcdf.inq(file_ec_caliop);
#     dimlen_new =[];
#     for i=0:ndims-1
#        [dimname, dimlen] = netcdf.inqDim(file_ec_caliop,i);
#        dimlen_new = [dimlen_new; dimlen];
#     end
#     #---- Caliop Altitude system loading ---------------------------------
#     for i=0:nvars-1
#        [varname, xtype, dimids, numatts] = netcdf.inqVar(file_ec_caliop,i);
#           if strcmp(num2str(varname), 'z') == 1
#               alt = netcdf.getVar(file_ec_caliop, i);
#           else
#           end
#     end
#         ec_caliop = netcdf.getVar(file_ec_caliop, 0);
#
#         #---- Data processing for each area ------------------------------
#         for u = 1:length(coor2)
#
#              i_s = coor2(1,u);
#  i_e = coor2(2,u);
#  j_s = coor2(3,u);
#  j_e = coor2(4,u);
#
#             [EXT_1] = change_order(EXT);
#             [ec_caliop_1] = change_order(ec_caliop);
#             [OM_EXT_1] = change_order(OM_EXT);
#             [POM_EXT_1] = change_order(POM_EXT);
#
#             [EXT_area_1, EXT_season_1, EXT_year_1] = mean_profile(EXT_1, i_s, i_e, j_s, j_e);
#                  emep_season(u,:,:) = EXT_season_1;
#             [OM_EXT_area_1, OM_EXT_season_1, OM_EXT_year_1] = mean_profile(OM_EXT_1, i_s, i_e,
 j_s, j_e);
#                  om_season(u,:,:) = OM_EXT_season_1;
#             [POM_EXT_area_1, POM_EXT_season_1, POM_EXT_year_1] = mean_profile(POM_EXT_1, i_s,
 i_e, j_s, j_e);
#                  pom_season(u,:,:) = POM_EXT_season_1;
#             [ec_caliop_area_1, ec_caliop_season_1, ec_caliop_year_1] = mean_profile( ec_caliop_1,
 i_s, i_e, j_s, j_e);
#                ec_caliop_season(y,u,:,:) = ec_caliop_season_1;
#           end
#         netcdf.close(file_ec_caliop);
#         display(strcat(caliop_file,' correctly loaded'))
# end
# [caliop_season] = average(ec_caliop_season);
# end
#
# ###---- Sub Functions ---------------------------------------------------
# function [data_area, data_season, data_year] = mean_profile(data, i_start, i_end, j_start,
 j_end);
#
# ###---- Monthly Basis ---------------------------------------------------
# A = isnan(data(:,:,:,:));
```

```
# for t=1:length(data(1,1,1,:))
#     for k=1:length(data(1,1,:,1))
#         m = 0;
#         n = 0;
#         for j=i_start:1:i_end
#             for i=j_start:1:j_end
#                 if A(i,j,k,t) == 0
#                    m = m + data(i,j,k,t);
#                    n = n + 1;
#                 else
#                 end
#             end
#         end
#         if n == 0
#             data_area(k,t) = NaN;
#         else
#             data_area(k,t) = m/n;
#         end
#     end
# end
#
# ###---- Yearly Basis ----------------------------------------------------
# B =isnan(data_area(:,:));
# for k = 1:length(data_area(:,1))
#     m = 0;
#     n = 0;
#     for t=1:12
#         if B(k,t) == 0
#             m = m + data_area(k,t);
#             n = n + 1;
#         else
#         end
#     end
#     if n==0
#         data_year(k) = NaN;
#     else
#         data_year(k) = m/n;
#     end
# end
#
# ###---- Seasonal Basis --------------------------------------------------
# for k = 1:length(data_area(:,1))
#     for i=1:4
#         m = 0;
#         n = 0;
#         for t = i*3-2:1:i*3
#             if B(k,t) == 0
#                 m = m + data_area(k,t);
#                 n = n + 1;
#             else
#             end
#         end
#         if n==0
#             data_season(k,i) = NaN;
#         else
#             data_season(k,i) = m/n;
```

```
#         end
#     end
# end
# end
#
# function [output] = average(input)
# A = isnan(input);
# if length(size(input)) == 4
#     for u=1:length(input(1,:,1,1))
#     for k=1:length(input(1,1,:,1))
#     for t=1:length(input(1,1,1,:))
#         m = 0;
#         n = 0;
#         for y = 1:length(input(:,1,1,1))
#                 if A(y,u,k,t) == 0
#                    m = m + input(y,u,k,t);
#                    n = n + 1;
#                 else
#                 end
#         end
#
#         if n == 0
#             output(u,k,t) = NaN;
#         else
#             output(u,k,t) = m/n;
#         end
#     end
#     end
#     end
# elseif length(size(input)) == 3
#     for u = 1:length(input(1,:,1))
#     for k=1:length(input(1,1,:))
#         m = 0;
#         n = 0;
#         for y = 1:length(input(:,1,1))
#                 if A(y,u,k) == 0
#                    m = m + input(y,u,k);
#                    n = n + 1;
#                 else
#                 end
#         end
#
#         if n == 0
#             output(u,k) = NaN;
#         else
#             output(u,k) = m/n;
#         end
#     end
#     end
# end
# end
#
# ###-------------------------------------------------------------------------
# ###---- STANDARDIZATION FUNCTIONS ------------------------------------------
# ###-------------------------------------------------------------------------
#
```

```
# ###---- Altitude ----------------------------------------------------------
# #(between the sigma coordinates used in the EMEP model and the corresponding elevation)
# function [alt_s] = alt_standardization(alt_m)
# for i=1:length(alt_m)
#     P_0 = 101.3;
#     P_t = 10.0;
#     P(i) = P_t + (P_0-P_t)*alt_m(i);
#     if P(i) > 22.632
#          t = 288.15/exp(-1.0/5.255876*log(P(i)/101.325));
#          alt_s(i) = (288.15-t)/6.5;
#     else
#          alt_s(i) = 11.0 + log( P(i)/22.632)/(-0.1576884);
#     end
# end
# end
#
# #(between the altitudes at which the altitude levels of the Emep model and the altitudes at
 which Caliop performs observations)
# function [caliop_season_alt] = altitude_transformation(caliop_season, alt, alt_s)
# a = length(caliop_season(:,1,1));
# c = length(caliop_season(1,1,:));
# b = length(alt_s);
# caliop_season_alt = zeros([a b c]);
# for i=1:length(alt_s)
#     i
#     [V, j] = min(abs(alt - alt_s(i)))
#     if alt_s(i) <= 10
#         alt_s(i)
#         for u = 1:length(caliop_season(:,1,1))
#             for t = 1:length(caliop_season(1,1,:))
#                 caliop_season_alt(u,i,t) = caliop_season(u,j,t);
#             end
#         end
#     else
#     end
# end
# end
#
# ###---- Coordinates -------------------------------------------------------
# function [coor] = change_aerocom(coor2)
# for i=1:length(coor2(1,:))
#     if coor2(1,i) <= 0
#         coor(1,i) = 90 + (coor2(1,i));
#     else
#         coor(1,i) = 91 + coor2(1,i);
#     end
#     if coor2(2,i) < 0
#         coor(2,i) = coor(1,i)-4;
#     else
#         coor(2,i) = coor(1,i)+4;
#     end
#     if coor2(3,i) < 0
#         coor(3,i) = 180 + coor2(3,i);
#     else
#         coor(3,i) = 181 + coor2(3,i);
#     end
```

```
#     if coor2(4,i) < 0
#         coor(4,i) = coor(3,i)-4;
#     else
#         coor(4,i) = coor(3,i) +4;
#     end
#
#     if coor(1,i) > coor(2,i)
#         a = coor(2,i);
#         coor(2,i) = coor(1,i);
#         coor(1,i) = a;
#     else
#     end
#     if coor(3,i) > coor(4,i)
#         b = coor(4,i);
#         coor(4,i) = coor(3,i);
#         coor(3,i) = b;
#     else
#     end
# end
# end
#
#
# ####---- Seasonal Standardization ----------------------------------------
# #(Winter: December, January and February)
# #(Spring: March, April and May)
# #(Summer: June, July and August)
# #(Fall: September, October and November)
# function [data] = change_order(data_1)
# for k = 1:length(data_1(1,1,1,:))-1
#     data(:,:,:,k+1) = data_1(:,:,:,k);
# end
# data(:,:,:,1) = data_1(:,:,:,12);
# end
#
# ###-----------------------------------------------------------------------
# ###---- PLOT FUNCTION ----------------------------------------------------
# ###-----------------------------------------------------------------------
#
# function plot_seasonal_profile(alt, alt_s, emep, caliop, coor2);
# for u = 1:length(coor2(1,:))
# region_name = {'Equatorial Africa' 'Indian Ocean' 'Pacific Ocean' 'Amazonia' 'SouthWest Europe'};
# fig_season = figure;
#     for i=1:4
#            subplot(2,2,i);
#            plot(emep(u,:,i), alt_s, caliop(u,:,i),alt,'LineWidth',2)
#            #plot(emep(:,i), alt_s, caliop(:,i),alt)
#            grid on;
#            legend( 'OA extinction', 'Total extinction');
#            xlabel('Extinction Coefficient (km^{-1})');
#            ylabel('Altitude (km)');
#            axis([0 0.2 0 10]);
#
#            if i==1
#                title(['DJF']);
#            elseif i==2
#                title(['MAM']);
```

```
#             elseif i==3
#                 title(['JJA']);
#             elseif i==4
#                 title(['SON']);
#             end
#     end
# A1 = char(region_name(u));
# formatSpec = 'Vertical_profile_#s_2009.jpg';
# saveas(fig_season, sprintf(formatSpec,A1));
# end
# end
```